

The background of the entire page is decorated with several overlapping, translucent bubbles of various sizes. The bubbles have a rainbow-like iridescence, with colors ranging from light blue and green to pink and purple. They are scattered across the white background, with some appearing in the top right and others in the bottom left and bottom right corners.

 **Carotid Artery**
Contrast Enhanced
Ultrasound

Luit ten Kate

Carotid Artery Contrast Enhanced Ultrasound

Luit ten Kate

ISBN 978-94-6169-475-1

CAROTID ARTERY CONTRAST ENHANCED ULTRASOUND

Contrast echo van de arteria carotis

Proefschrift

ter verkrijging van de graad van doctor aan de
Erasmus Universiteit Rotterdam

op gezag van de rector magnificus
Prof.dr H.A.P. Pols
en volgens besluit van het College voor Promoties.

De openbare verdediging zal plaatsvinden op
Woensdag 19 februari 2014 om 15.30 uur

door

Gerrit Luit ten Kate
geboren te Uithoorn



PROMOTIECOMMISSIE

Promotoren : Prof.dr. E.J.G. Sijbrands
Prof.dr.ir. A.F.W. van der Steen

Overige leden : Prof.dr. P.J. de Feyter
Prof.dr. A. van der Lugt
Prof.dr. M.J.A.P. Daemen

Copromotor : Dr. A.F.L. Schinkel

Financial support for the publication of this thesis was generously provided by Bracco Suisse SA

Financial support by the Dutch Heart Foundation for the publication of this thesis is gratefully acknowledged

This research was performed within the framework of CTMM, the Center for Translational Molecular Medicine (www.ctmm.nl), Eindhoven, The Netherlands, project Plaque-at-risk (PARISk) (grant 01C-202), and supported by a grant of the Dutch Heart Foundation (DHF 2008 T 94).

TABLE OF CONTENTS

Part I: Introduction: Current status of non-invasive imaging of atherosclerosis

| | | |
|-------------------|---|----|
| Chapter 1. | General introduction and aims | 9 |
| Chapter 2. | Non-invasive imaging of the vulnerable atherosclerotic plaque | 15 |
| Chapter 3. | Current status and future developments of contrast enhanced ultrasound of carotid atherosclerosis | 39 |

Part II: Contrast enhanced ultrasound for imaging atherosclerosis

| | | |
|-------------------|--|----|
| Chapter 4. | Assessment of subclinical atherosclerosis using contrast-enhanced ultrasound | 57 |
| Chapter 5. | Usefulness of contrast enhanced ultrasound for the detection of carotid plaque ulceration in patients with symptomatic carotid atherosclerosis | 71 |
| Chapter 6. | Carotid plaque burden as a measure of subclinical coronary artery disease in patients with heterozygous familial hypercholesterolemia | 85 |

Part III: Technical innovations in contrast enhanced ultrasound

| | | |
|-------------------|--|-----|
| Chapter 7. | Far-wall pseudoenhancement during contrast-enhanced ultrasound of the carotid arteries: clinical description and in vitro reproduction | 99 |
| Chapter 8. | Counter-propagating wave interaction for contrast-enhanced ultrasound imaging | 113 |
| Chapter 9. | Quantitative analysis of ultrasound contrast flow behaviour in carotid plaque neovasculature | 127 |

Part IV: Summary, Discussion and Perspectives

| | | |
|--------------------|--------------------------------------|-----|
| Chapter 10. | Summary, Discussion and Perspectives | 153 |
| | Nederlandse samenvatting | 163 |
| | Curriculum vitae | 169 |
| | Publications | 173 |
| | PhD portfolio | 177 |
| | Dankwoord | 179 |



PART I

INTRODUCTION:
CURRENT STATUS OF NON-INVASIVE
IMAGING OF ATHEROSCLEROSIS





Chapter 1

General introduction and aims



GENERAL INTRODUCTION

Despite advances in both primary and secondary prevention, cardiovascular disease remains one of the leading causes of morbidity and mortality in the Western world. An acute ischemic event, such as a transient ischemic attack (TIA) or stroke, is often the first manifestation of atherosclerosis in the carotid arteries. Previously the prediction of acute ischemic events focused on the presence of atherosclerotic plaque and the degree of stenosis it causes. However, acute ischemic events often result from the rupture of an atherosclerotic plaque that causes no significant stenosis.¹ Early identification of these rupture-prone plaques, otherwise known as vulnerable plaques, could allow for improvements in early intervention and selection of patients for more invasive treatment.

Comparison of carotid endarterectomy specimens of symptomatic and asymptomatic patients has identified several plaque characteristics that are important in predicting whether a carotid plaque will remain clinically silent or not.¹ Endarterectomy specimens of symptomatic patients were found to have a thinner fibrous cap, higher number of inflammatory cells, and a lipid-rich necrotic core more closely situated to the fibrous cap.²⁻⁴ Additionally, prospective follow-up studies have shown that the presence of plaque ulceration, intraplaque neovascularization and intraplaque hemorrhage are predictive markers of future cerebrovascular events.⁵⁻⁷ Non-invasive identification of vulnerable plaque characteristics could aid the prediction of cerebrovascular events and consequently treatment selection.

The last decades' major advances have been made with both non-invasive and catheter-based imaging techniques, for the evaluation of atherosclerosis.⁸ Techniques such as ultrasound, computed tomography (CT), magnetic resonance imaging (MRI), and intravascular ultrasound (IVUS) are readily available in clinical practice and have become central to the evaluation of patients with known or suspected vascular disease. Other newly developed techniques such as optical coherence tomography (OCT), spectroscopy, thermography and intravascular MRI are currently making their way into patient studies. These catheter-based techniques have shown promising histopathological correlation.⁹ However, their clinical value remains to be evaluated. The choice of imaging technique depends on patient characteristics and location of the artery under investigation. The superficial location and relative lack of motion in the carotid arteries does make them an attractive target for non-invasive imaging.

In clinical practice, ultrasound is still the most frequently used imaging modality for the evaluation of the carotid arteries, identification of atherosclerotic plaque and determination of its degree of stenosis. Additionally, ultrasound is the only non-invasive imaging modality with sufficient resolution to evaluate the thickness of the "non-diseased" vessel wall by measurement of the intima-media thickness (IMT). Carotid IMT is a well-accepted surrogate marker of atherosclerosis burden throughout the body.¹⁰ However, the addi-

tion of carotid IMT to traditional cardiovascular risk prediction models does not lead to a statistically significant increase in performance of those models.^{11, 12}

Thus far the studies investigating ultrasound for identification of vulnerable plaques have been limited and provided varying results. Several studies have attempted to predict plaque composition based on B-mode images, under the assumption that echolucent plaques contain more “soft” plaque components (lipids, intraplaque hemorrhage) and are thus more at risk for rupture.¹³⁻¹⁶ However results have been disappointing.

Recently, contrast-enhanced ultrasound (CEUS) has been introduced for the evaluation of carotid atherosclerosis and plaque vulnerability. Ultrasound contrast agents consist of gas microbubbles, stabilized with a phospholipid or protein shell. Microbubbles due to their size cannot leave the intravascular compartment, thus improving the delineation of the lumen-intima border. Additionally, the capability of ultrasound to detect individual microbubbles passing through the capillary system can be exploited to assess intraplaque neovascularization.¹⁷

AIMS OF THE THESIS

The **General aim** of this thesis is to show current applications and developments in carotid ultrasound imaging that keep it at the forefront of atherosclerosis imaging.

In **Part 1** we review the current knowledge on non-invasive imaging of the vulnerable plaque and use of CEUS for improving the ultrasound examination. In **Chapter 2** we aim to summarize the current status of vulnerable plaque imaging with non-invasive imaging techniques while in **Chapter 3** we focus on the use of specifically CEUS for the evaluation of vulnerable plaque features.

In **Part 2** we apply ultrasound techniques currently available for clinical practice in patients. In **Chapter 4 and Chapter 5** we investigate the addition of CEUS to improve the diagnostic accuracy of ultrasound examinations for the detection of subclinical atherosclerosis and assessment of plaque morphology. **Chapter 4** aims to show that the addition of CEUS improves the detection of plaques in patients with subclinical atherosclerosis. In **Chapter 5** we aim to improve the detection of ulcerations by adding CEUS to the ultrasound evaluation of patients with symptomatic cerebrovascular disease and a significant carotid artery stenosis. **Chapter 6** aims to show that carotid ultrasound measurements have an association with subclinical coronary artery disease and thus possibly provide a measure of atherosclerosis in less accessible locations.

In **Part 3** we will investigate new developments in contrast enhanced ultrasound that could find their way into clinical setting soon. **Chapter 7** aims to provide an insight in the problems with currently available CEUS equipment and show that technical development is necessary. In **Chapter 8** we aim to provide a possible solution to the problem provided in the previous chapter. **Chapter 9** aims to show developments in quantification software needed to provide reliable and reproducible measurements.

Finally **Part 4** summarizes our findings and discusses its clinical applications, as well as look forward to future developments in CEUS.

REFERENCES

1. Golledge J, Greenhalgh RM, Davies AH. The symptomatic carotid plaque. *Stroke*. 2000;31(3):774-81.
2. Hatsukami TS, Ferguson MS, Beach KW, Gordon D, Detmer P, Burns D, et al. Carotid plaque morphology and clinical events. *Stroke*. 1997;28(1):95-100.
3. Feeley TM, Leen EJ, Colgan MP, Moore DJ, Hourihane DO, Shanik GD. Histologic characteristics of carotid artery plaque. *J Vasc Surg*. 1991;13(5):719-24.
4. Seeger JM, Barratt E, Lawson GA, Klingman N. The relationship between carotid plaque composition, plaque morphology, and neurologic symptoms. *J Surg Res*. 1995;58(3):330-6.
5. Eliasziw M, Streifler JY, Fox AJ, Hachinski VC, Ferguson GG, Barnett HJ. Significance of plaque ulceration in symptomatic patients with high-grade carotid stenosis. *North American Symptomatic Carotid Endarterectomy Trial*. *Stroke*. 1994;25(2):304-8.
6. Handa N, Matsumoto M, Maeda H, Hougaku H, Kamada T. Ischemic stroke events and carotid atherosclerosis : Results of the Osaka Follow-up Study for Ultrasonographic Assessment of Carotid Atherosclerosis (the OSACA Study). *Stroke*. 1995;26(10):1781-6.
7. Hellings WE, Peeters W, Moll FL, Piers SRD, van Setten J, van der Spek PJ, et al. Composition of carotid atherosclerotic plaque is associated with cardiovascular outcome. A prognostic study. *Circulation*. 2010;121(17):1941-50.
8. de Korte CL, Hansen HHG, van der Steen AFW. Vascular ultrasound for atherosclerosis imaging. *Interface Focus*. 2011;1(4):565-75.
9. Schaar JA, Mastik F, Regar E, den Uil CA, Gijzen FJ, Wentzel JJ, et al. Current diagnostic modalities for vulnerable plaque detection. *Curr Pharm Des*. 2007;13(10):995-1001.
10. de Groot E, Jukema JW, Montauban van Swijndregt AD, Zwinderman AH, Ackerstaff RGA, van der Steen AFW, et al. B-mode ultrasound assessment of pravastatin treatment effect on carotid and femoral artery walls and Its correlations with coronary arteriographic findings: A report of the regression growth evaluation statin study (REGRESS). *J Am Coll Cardiol*. 1998;31(7):1561-7.
11. van den Oord SCH, Sijbrands EJG, ten Kate GL, van Klaveren D, van Domburg RT, van der Steen AFW, et al. Carotid intima-media thickness for cardiovascular risk assessment: Systematic review and meta-analysis. *Atherosclerosis*. 2013;228(1):1-11.
12. Lorenz MW, Schaefer C, Steinmetz H, Sitzer M. Is carotid intima media thickness useful for individual prediction of cardiovascular risk? Ten-year results from the Carotid Atherosclerosis Progression Study (CAPS). *Eur Heart J*. 2010;31(16):2041-8.
13. Bluth EI, Kay D, Merritt CR, Sullivan M, Farr G, Mills NL, et al. Sonographic characterization of carotid plaque: detection of hemorrhage. *AJR Am J Roentgenol*. 1986;146(5):1061-5.
14. Reilly LM, Lusby RJ, Hughes L, Ferrell LD, Stoney RJ, Ehrenfeld WK. Carotid plaque histology using real-time ultrasonography. Clinical and therapeutic implications. *Am J Surg*. 1983;146(2):188-93.
15. Grønholdt ML, Nordestgaard BG, Bentzon J, Wiebe BM, Zhou J, Falk E, et al. Macrophages are associated with lipid-rich carotid artery plaques, echolucency on B-mode imaging, and elevated plasma lipid levels. *J Vasc Surg*. 2002;35(1):137-45.
16. Droste DW, Karl M, Bohle RM, Kaps M. Comparison of ultrasonic and histopathological features of carotid artery stenosis. *Neurol Res*. 1997;19(4):380-4.
17. Feinstein SB. Contrast ultrasound imaging of the carotid artery vasa vasorum and atherosclerotic plaque neovascularization. *J Am Coll Cardiol*. 2006;48(2):236-43.



Chapter 2

Non-Invasive Imaging of the Vulnerable Atherosclerotic Plaque

Gerrit L. ten Kate, Eric J.G. Sijbrands, Daniel Staub, Blai Coll, Folkert
J. ten Cate, Steven B. Feinstein, Arend F.L. Schinkel

Curr Probl Cardiol. 2010; 35(11):556-591

ABSTRACT

Atherosclerosis is an inflammatory disease, complicated by progressively increasing atherosclerotic plaques that eventually may rupture. Plaque rupture is a major cause of cardiovascular events such as unstable angina, myocardial infarction and stroke. A number of non-invasive imaging techniques have been developed to evaluate the vascular wall in an attempt to identify so called vulnerable atherosclerotic plaques that are at prone to rupture. The purpose of the present review is to systematically investigate the accuracy of non-invasive imaging techniques in the identification of plaque components and morphological characteristics associated with plaque vulnerability, assessing their clinical and diagnostic value.

INTRODUCTION

Atherosclerosis is a progressive inflammatory disease of the arterial wall and the main cause of cardiovascular disease. Despite advances in both primary and secondary prevention, atherosclerotic cardiovascular disease remains one of the leading causes of morbidity and mortality in the Western world. In addition, the increasing number of individuals with known risk factors such as obesity and diabetes mellitus makes the management of atherosclerosis one of the main challenges in medicine for the foreseeable future.¹⁻⁶

Historically the burden of atherosclerosis was determined by means of angiographic measurement of stenosis and luminal diameter. However, it has become clear that plaque rupture and subsequent embolization of plaque particles as well as thrombosis, rather than stenosis, precipitates the majority of acute ischemic events. Plaques at risk of rupture and thrombosis have been defined as vulnerable plaques. Vulnerable plaques are histopathologically characterized by active inflammation, large lipid core, thin fibrous cap, intraplaque hemorrhage and neovascularization of the vasa vasorum.⁷⁻¹⁰ Vasa vasorum derived intraplaque neovascularization is an important feature in plaque development. The vasa vasorum are functional end arteries, present in the vessel wall of the aorta and large arteries, supplying the vessel wall with nutrients and removing waste products, thus sustaining plaque inflammation and growth. The neovessels are known to be of poor structural integrity which results in an increased risk for intraplaque hemorrhage and rupture.¹¹

Vulnerable plaque components are associated with a high degree of positive arterial remodeling, as a result of which up to 70% of ischemic events result from a plaque without significant stenosis on angiography.¹²⁻¹⁹ The last decades major advances have been made in the field of non-invasive imaging of vessel anatomy, arterial wall morphology, plaque composition and metabolic processes, allowing non-invasive evaluation of atherosclerotic plaque vulnerability.

The present review systematically investigates the accuracy of non-invasive imaging techniques in the identification of plaque components and morphological characteristics associated with plaque vulnerability. This review focuses on ultrasound, computed tomography (CT), and magnetic resonance imaging (MRI) of the carotid and coronary arteries, evaluating the advances made in the last 20 years.

METHODS

This systematic review analyzes all available studies on non-invasive imaging of atherosclerotic plaques from 1990 up to 2010. All studies were reviewed and considered

for inclusion in the systematic review if non-invasive imaging of the carotid arteries or coronary arteries in vivo human subjects was performed and the study used histology or intravascular ultrasound (IVUS) as a reference method. Studies with overlapping data were identified and only the most appropriate study was included. Studies that did not provide statistic data on correlations between techniques, or sufficient data to perform sensitivity and specificity calculations were excluded

The accuracy of each technique was determined by:

1. The correlations between plaque components determined by the non-invasive imaging technique and the reference standard (histology for carotid arteries and IVUS for coronary arteries)
2. The sensitivity and specificity of non-invasive imaging techniques in detecting plaque components.
3. Receiver operator curve characteristics when available.

The online MEDLINE database was searched using a search strategy containing a combination of the keywords: atherosclerosis, atherosclerotic plaque, CT, diagnostic use, MRI, non-invasive imaging, predictive value, plaque, plaque composition, plaque vulnerability, ultrasound, visualization, vulnerable plaque. Subsequent to the MEDLINE search, all articles meeting the inclusion criteria were identified. In addition a manual search of the reference lists of the identified manuscripts for relevant studies was performed. All relevant data on the outcome measures were extracted and where possible the sensitivity and specificity was calculated from the data provided. If an article reported more than one observer, the consensus interpretation was extracted. Where no consensus was reported, only the result from the first observer was used.

RESULTS

In total 62 studies were identified that met the inclusion criteria, including 23 studies investigating ultrasound, 18 CT, 18 MRI, 2 investigated both CT and ultrasound and 1 study investigated both MRI and ultrasound. The 50 studies on the carotid arteries used histology as reference method, while all 12 studies on the coronary arteries used IVUS for validation.

Ultrasound

High resolution vascular B-mode and Doppler ultrasound is widely available and has been shown to accurately depict a flow limiting stenosis in the carotid arteries.²⁰ Ultrasound in the clinical setting has a superior temporal and spatial resolution over other imaging modalities. However, transcutaneous ultrasound is limited to the evaluation of the superficial vascular system. Multiple ultrasound parameters that give an indication

of plaque characteristics and composition have been investigated (Table 1). The parameters echolucency, heterogeneity (combined echolucent and echogenic plaque) and border irregularity have been studied to identify their respective histological substrate and will be discussed one-by-one.

Table 1. Histological findings and the related findings with non-invasive imaging.

| Histology | Ultrasound | CT | MRI T1 Weighed | MRI T2 Weighed | MRI PD Weighed |
|------------------------|------------------------|------------------|-----------------------|-----------------------|-----------------------|
| Ulceration | Irregular border | Irregular border | Irregular border | Irregular border | Irregular border |
| Lipid core | Echolucent Homogenic | Hypodense | Very hyperintense | Hypointense | Hyperintense |
| Intraplaque hemorrhage | Echolucent Heterogenic | Hypodense | Age dependent | Age dependent | Age dependent |
| Fibrous plaque | Echogenic Homogenic | Isodense | Hyperintense | Hyperintense | Hyperintense |
| Calcifications | Echogenic Heterogenic | Hyperdense | Hypointense | Very hypointense | Very hypointense |
| Thrombus | Echolucent | Hypodense | Very hyperintense | Isointense | Hyperintense |
| Inflammation | Echolucent | | SPIO signal loss | SPIO signal loss | SPIO signal loss |
| Vasa vasorum | Contrast enhancement | | MRI signal increase | | |

CT, computed tomography; MRI, magnetic resonance imaging; PD, proton density; SPIO, super paramagnetic iron oxide

Border regularity

Eight studies investigated the detection of irregularities in the luminal border of the plaque. Six of these studies investigated the detection of plaque ulceration. Ulceration of a plaque exposes the thrombogenic interior of the plaque to the lumen and thus may precipitate clinical events. The European carotid plaque study group used B-mode ultrasound to detected plaque ulcerations with a sensitivity of 47% and a specificity of 63%.²¹ Five studies investigated the addition of Doppler techniques to B-mode ultrasound for the detection of ulcerations (Figure 1). The 5 studies showed a large variance in results, with a slight improvement in mean sensitivity (60%, range 38%-94%) and specificity (74%, range 33%-92%).²²⁻²⁶ Kagawa et al. demonstrated that border irregularities on B-mode ultrasound, rather than just ulceration could be detected with a high sensitivity (97%) and specificity (81%).²⁷ However, border irregularity is of unknown clinical value.

Two studies compared border regularity with the plaque composition. The presence of an irregular border on ultrasound was shown to predict an intraplaque hemorrhage with a sensitivity of 81% and specificity of 85%, while conversely heterogeneity and calcification on ultrasound had a poor predictive value for the presence of an ulceration.^{24, 28}

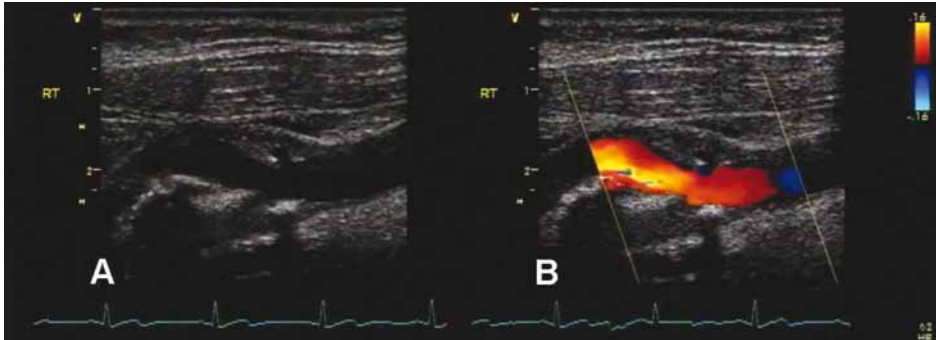


Figure 1. B-mode (A) and duplex (B) ultrasound images of the common carotid artery. An ulcerated atherosclerotic plaque can be observed at the origin of the internal carotid artery. The addition of color Doppler shows a clear improvement in the identification of the plaque border.

Echolucency

A total of 13 studies reported on the relation between echolucency and plaque composition. It has been shown that echolucent plaques contain significantly higher amounts of “soft” constituents (lipids, intraplaque hemorrhage), while echogenic plaques contain more fibrous tissue and calcifications.^{21, 25, 29-31} Widder et al. studied echolucency for the detection of plaque components and reported low sensitivities and specificities for the detection of intraplaque hemorrhage (sensitivity 34%, specificity 36%) and intraplaque hemorrhage with atheromatous debris (sensitivity 51%, specificity 68%).²²

To improve the detection of plaque components quantification of echolucency has been developed by means of grayscale median (GSM), pixel distribution analysis and integrated backscatter analysis. GSM measurements are made from digitized ultrasound images normalized to the GSM of blood (GSM 0-5) and adventitia (GSM 180-200). Subsequently, the echolucency in the region of interest is expressed in a 256 gray tone range with 0 is black and 255 is white. A strong correlation was found between the GSM and the amount of fibro-calcified tissue in the plaque. However, no correlation was found between the GSM and the lipid core size and only moderate correlations were found between the GSM and other tissue components.³²⁻³⁷ The use of GSM resulted in low sensitivities (range 40%-60%) for the detection of soft (GSM<35), combined (GSM 35-65) and calcified (GSM>65) plaques.³⁸ A plaque mapping system in 3 GSM ranges (GSM<50 = red, GSM 50-80 = yellow, GSM>80 = green), has been developed that may facilitate the detection of the lipid core in the plaque. The plaque mapping had a sensitivity of 84% and a specificity of 75% for localizing the lipid core.³⁹

Pixel distribution analysis uses GSM ranges from known tissue components (lipid: subcutaneous fat, muscle: biceps, fibrous tissue: iliotibial tract, calcification: bone, and hemorrhage: blood) to measure the percentage area of the plaque within each grayscale range. The use of pixel distribution analysis showed a better correlation with histology

than GSM. Unfortunately sensitivity and specificity calculations of this method have not been reported.⁴⁰

Integrated backscatter analysis is based on the unprocessed radiofrequency signal, measuring the reflected ultrasonic energy.^{41,42} It has been shown to detect soft, fibrous and calcified components. However, contradictory results have been reported differentiating individual soft components and the healthy vessel wall. This might be due to the discrepancies in the method used to calculate the backscatter value.⁴¹⁻⁴⁴ The use of integrated backscatter for the detection of various plaque components resulted in sensitivities ranging between 80% to 90% and specificities ranging between 78% to 91%. These results were obtained from both carotid and femoral arteries, making direct comparison with other studies difficult.^{43,45}

Echoluency has also been investigated for the evaluation of plaque inflammation; echolucent plaques were shown to have a significantly higher macrophage density in and a weak but statistically significant correlation to both grayscale median and mean.^{31,46}

Heterogeneity

The division of plaques in homogeneous and heterogeneous showed that heterogeneous plaques contain significantly more calcifications, while no difference in the amount of "soft" tissues was found.^{21,29,39} The evaluation of plaque heterogeneity improved the sensitivity (76%) and specificity (85%) for the detection of intraplaque hemorrhage over echoluency.²⁸ The evaluation of plaque heterogeneity predicted fibrous cap thickness (<80 μ m) and the location of the lipid core with sensitivities of 77% and 74% and specificities of 22% and 17% respectively.³⁹

Combined echoluency and heterogeneity scales

A number of scales combining echoluency and heterogeneity have been developed with the Gray-Weale scale as the most consistently used.⁴⁷ The use of these combined scores resulted in varying sensitivities ranging from 39% to 94% and specificities ranging from 57% to 80% for the detection of various components.^{25,48,49} The use of a more elaborate scale with 7 grades combining echoluency, heterogeneity and the surface regularity, showed only a slight improvement.⁵⁰ It has been proposed that the lack of accuracy is due to the large number of components investigated and the number of "soft" components identified by echoluency. The use of a score combining all "soft" components for the detection of "at risk" plaques was suggested as a strategy to increase the diagnostic accuracy.⁵⁰ This strategy resulted in a sensitivity of 75% and a specificity of 63% for the detection of at risk plaques (histologically defined as <70% fibrous tissue or calcification, with a lipid core or intraplaque hemorrhage).⁵¹

Vasa vasorum

Contrast-enhanced ultrasound uniquely visualizes the intraplaque microvascularisation. Ultrasound contrast agents consists of gas filled microbubbles, which are an obligatory intravascular contrast agent, small enough (1-5 μm) to pass through the capillary system. This has led to microbubbles being investigated for the visualization of the microvasculature in atherosclerotic plaques (Figure 2).^{52, 53} Coli et al. have shown that plaques with high contrasts enhancement have a significantly higher intraplaque vasa vasorum density, while in comparison, vasa vasorum density did not significantly differ between high and low grade stenotic plaques (stenosis >70%) or between echolucent and echogenic plaques. However, echolucent plaques had significantly higher degree of contrast enhancement compared with echogenic plaques.⁵⁴ Shah et al. found a strong correlation between contrast enhancement and CD-31 stained vasa vasorum in the plaque, indicating angiogenesis derived vasa vasorum, rather than pre-existing vasa vasorum.⁵⁵ Further studies are needed to determine the diagnostic accuracy of contrast-enhanced ultrasound for the detection of intraplaque neovascularisation.

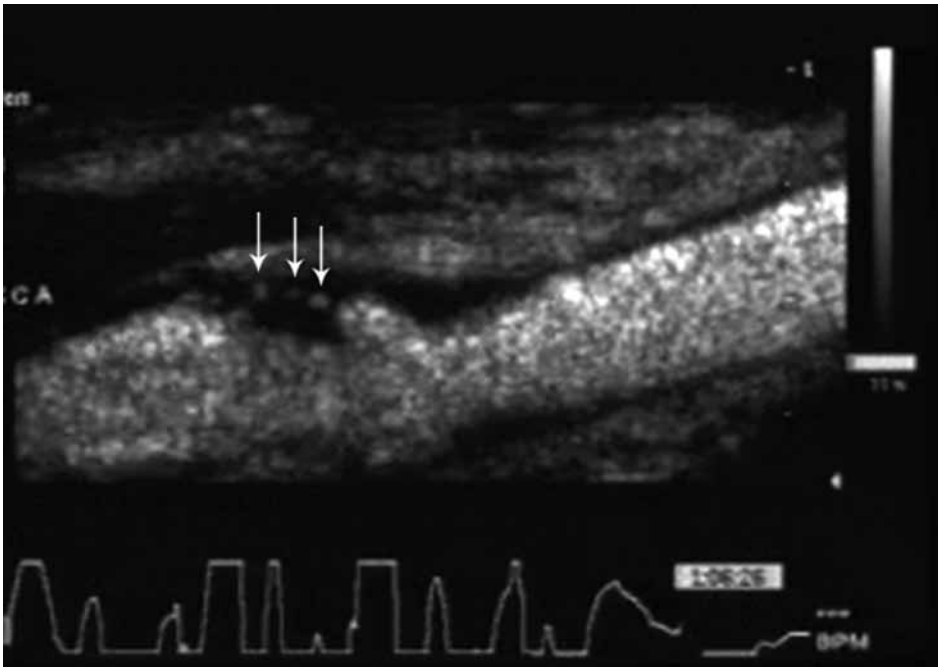


Figure 2. Contrast-enhanced ultrasound image of the common carotid artery with an ulcerated atherosclerotic plaque in the carotid bulb. Individual microbubbles can be seen in the plaque (arrows) indicating intraplaque vasa vasorum.

Summary

Hence, ultrasound can provide information about plaque components as lipid core, intraplaque hemorrhage, inflammation and vasa vasorum neovascularization that are related to plaque vulnerability. The use of ultrasound for the qualitative detection of border regularity, echolucency and heterogeneity is promising; however, the accuracy of ultrasound in detecting individual plaque components and characteristics shows a large variability.

Ultrasound has a relatively poor sensitivity (60%) for the detection of ulcerations, while the detection of irregular borders is more accurate (sensitivity 97%, specificity 81%). However, border irregularity is of uncertain clinical relevance. Remarkably, the presence of intraplaque haemorrhage is best predicted by an irregular plaque border (sensitivity 81%, specificity 85%) and a heterogenic plaque (sensitivity 76%, specificity 85%), rather than echolucency (sensitivity 34%, specificity 36%). The accuracy of visualizing other plaque components such as the lipid core or calcifications has not been investigated using qualitative techniques. The use of combined echolucency and heterogeneity scales, such as the Gray-Weale scale, may improve diagnostic accuracy and needs further development.

Two studies directly compared ultrasound with CT in the same patients. Saba et al. demonstrated that CT was more accurate than ultrasound for the detection of plaque ulceration (sensitivity 94% versus 38%, specificity 99% versus 92%).²⁶ Grønholdt et al. demonstrated that ultrasound GSM measurements correlated better with histology than CT density measurements for lipid and fibrous tissue content, and intraplaque hemorrhage.³⁶

The quantification of echolucency resulted in a clear improvement for the detection of various plaque components, with pixel distribution analysis and integrated backscatter analysis as significant adjuvant techniques. The use of microbubble contrast may improve the detection of ulcerations by enhancing the contrast between the lumen and the vessel wall.⁵⁶ The use of microbubble contrast shows a significant correlation with vasa vasorum neovascularization and might be an interesting new marker for plaque vulnerability.

It can be concluded that ultrasound can give an indication of plaque components. However, the sensitivity and specificity are limited and vary to a large extent, while the development of new quantitative techniques and contrast enhanced ultrasound show possibilities for the future.

Computed Tomography

Of the 20 studies investigating CT, 2 were made with single slice CT, 16 with multi slice CT, 1 with electron beam CT and 1 with dual source CT. CT has been shown to accurately depict stenosis in both the coronary and carotid arteries (Figure 3).^{20, 57-59} The use of CT



Figure 3. Multiplanar CT reconstruction (A) and conventional coronary angiogram (B) of the left anterior descending coronary artery showing the same lesions. Two fibro-lipidic plaques are observed proximally, causing no hemodynamically significant stenosis (thin arrows). A hemodynamically significant fibro-lipidic lesion is seen more distally (thick arrows).

for detecting the morphology and composition of the vessel wall has not been as clear. Identification of plaque composition has focused on density measurements (Table 1), expressed in Hounsfield units (HU), a value normalized to the density of water (0 HU).⁶⁰

Morphological measurements

Six studies investigated the correlation between CT and IVUS or histological measurements and showed a close correlation with vessel wall morphology both in the coronary and carotid arteries.⁶¹⁻⁶⁶ The receiver operator characteristics for coronary plaque symmetry and positive remodeling showed an area under the curve greater than 0.90.⁶⁷ Concomitant, excellent sensitivities and specificities have been found for the detection of plaque eccentricity (sensitivity 100%, specificity 100%) and positive remodeling (sensitivity 100%, specificity 90%). However, CT was less accurate for the detection of plaque disruption (sensitivity 57%, specificity 71%).⁶⁸ The introduction of multi slice CT did improve the detection of ulceration in the carotid arteries (single slice CT: sensitivity 60%, specificity 74%⁶⁹, multi slice CT: mean sensitivity 87% (range 50%-94%), mean specificity 98% (range 89%-99%).^{26, 70, 71} The detection of ulceration also depends on the method of reconstruction used, a combination of volume rendering and axial slides resulted in the best sensitivity (94%) and specificity (99%), while shaded surface display yielded a clearly inferior diagnostic accuracy (sensitivity 39%, specificity 88%).⁷²

Composition

Nine studies investigated the relation between density measurements and plaque composition, 5 of those studies investigated the carotid arteries and 4 the coronary arteries. The use of carotid CT has shown that the HU values found in calcified, fibrous and lipid plaques are significantly different, however with substantial overlap.^{66, 69, 73} The use of IVUS as reference standard for coronary plaques showed a similar pattern for calcified, echogenic and echolucent plaques.⁷⁴⁻⁷⁸

The correlation between single slice CT and histology is low with only calcification showing a weak correlation.³⁶ Multi slice CT markedly improved the measurements, showing a strong correlation for both calcification and fibrous tissue, while the correlation for lipid core size remained weak but was significant. The correlation with lipid core size improved after the exclusion of calcified plaques, suggesting that blooming artifacts by calcifications on CT hindered non-invasive plaque evaluation.⁶⁶ The use of the relatively new technique dual source CT showed similar correlations as conventional multi slice CT for calcified and fibrous plaques. Additionally, dual source CT was able to produce a strong correlation for lipid plaques without excluding calcified plaques.⁷⁹ There was no correlation between multi slice CT and IVUS for the amount of calcium or the amount of fibro-fatty tissue. A moderate correlation was found with both lipid core size and fibrous tissue.⁷⁸ The accuracy of CT in detecting calcifications has shown conflicting results. Oliver et al. found a sensitivity of 78% with a specificity of only 36%, while both Caussin et al. and Wintermark et al. found near perfect detection (Caussin: sensitivity 100%, specificity 93%, Wintermark: sensitivity 100%, specificity 100%). A possible explanation is that the decalcification during histological processing in the study of Oliver et al. resulted in a high number of false positive cases. The detection of soft components and fibrous tissue showed a more moderate sensitivity (range 62%-94%) and specificity (range 74%-100%).^{68, 70, 71}

Summary

Multi slice CT shows a close correlation in morphological measurements and is capable of demonstrating significant differences in densities for calcifications, fibrous tissue and the lipid core, however with substantial overlap. CT is capable of accurately detecting calcified plaques; however the detection of calcifications alone is not enough for the assessment of vulnerable plaques.^{63, 65, 80, 81} Due to technical limitations the soft tissue contrast of CT is low, resulting in a low correlation with soft components and only moderate accuracy.

Both histology and IVUS have been used as reference standard. The use of IVUS is controversial, since it is an imaging technique itself and therefore not a true reference standard as histology is. However, IVUS is an accepted method for evaluation of the coronary arteries, where histology cannot be obtained.

Magnetic resonance imaging

MRI angiograms are ever more used for the evaluation of carotid artery stenosis (Figure 4) and the development of MRI multiple contrast weightings allows for the identification of individual plaque components. In each contrast weighting individual plaque components show a different signal intensity, making differentiation possible (Table 1).^{59, 82, 83} Nineteen studies were included in this study. All MRI investigations were performed using 1.5 Tesla field strength imaging systems.

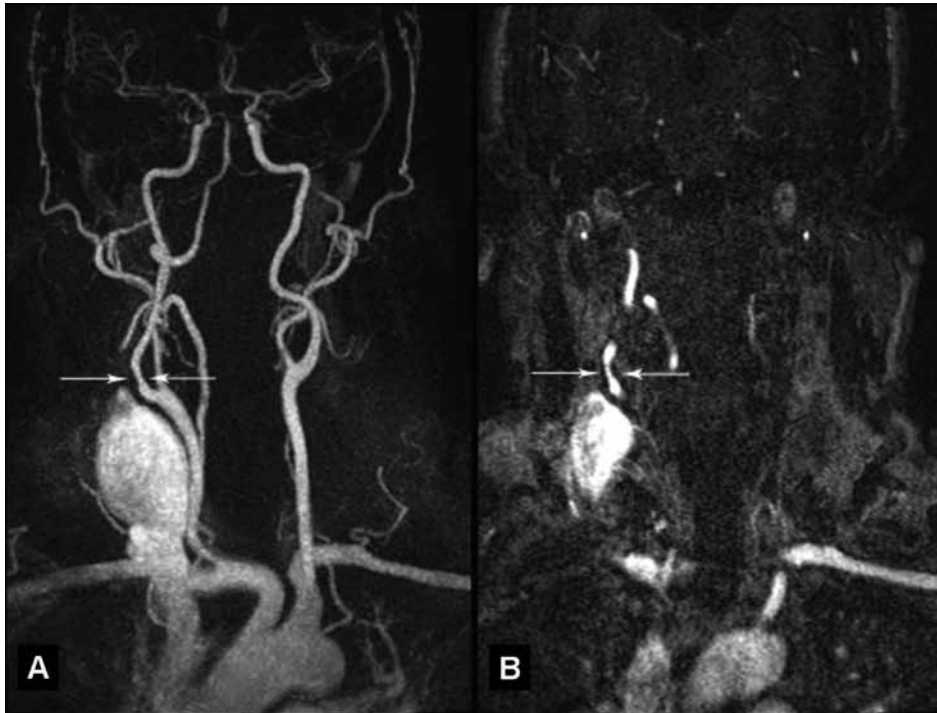


Figure 4. MRI angiographic reconstruction (A) and source image (B) of the carotid arteries. A carotid plaque can be observed at the origin of the right internal carotid artery (arrows).

Morphological measurements

Five studies have investigated the association between MRI and histological morphological measurements. Morphological measurements of the carotid vessel wall made with MRI showed a strong correlation with histology.^{84, 85} The visualization of fibrous cap status (thick intact, thin intact or ruptured) has also shown good agreement.⁸⁶ Consequently, unstable fibrous caps (ulcerated, fissured, disrupted or cap thickness $<0.25\text{mm}$) were detected with high sensitivity (81%) and specificity (90%).⁸⁷ Puppini et al. showed that ulceration alone was detected with a sensitivity of 100% and a specificity of 80%.⁸⁸

Composition

Ten studies have investigated the detection of plaque components. The use of MRI for the detection of the lipid core and intraplaque hemorrhage showed a strong correlation with histology.⁸⁴ Likewise the lipid core was detected with a mean sensitivity of 94% (range 91%-98%) and specificity of 79% (range 65%-100%)^{83, 85, 88}, while intraplaque hemorrhage was identified with a mean sensitivity of 88% (range 82%-96%) and specificity of 80% (range 74%-100%).^{85, 88-90} In addition, MRI was able to detect both the age of an intraplaque hemorrhage and the location with good sensitivity (88%) and specificity (98%).^{89, 90} Neither the combined detection of the lipid core and intraplaque hemorrhage (mean sensitivity 90% (range 85%-94%), mean specificity 95% (range 92%-100%)) or the quantification of signal intensity (sensitivity 76%, specificity 100%) was of added value.^{83, 88, 91}

The potential of MRI to detect calcifications has been questioned because of the lack of water in calcifications. In contrast to this assumption, a strong correlation was found and calcifications were detected with a mean sensitivity of 77% (range 76%-80%) and a specificity of 88% (range 86%-94%).^{85, 88}

The use of multiple contrast weightings improves the detection of plaque components. Watanabe et al. showed that using multiple contrast weightings (T1 and T2 weighted images) had a sensitivity of 96% and a specificity of 93% in the detection of soft plaque components.⁵¹ A clear improvement compared to Yoshida et al. (sensitivity 79%, specificity 84%), who used only the T1 weighted images to detect plaques containing more than 50% soft components.⁹²

Cai et al. compared a MRI adjusted American Heart Association (AHA) classification, a detailed numerical classification of the natural history and histology of plaques, with the histological determined AHA classification. High sensitivities (range 80%-84%) and specificities (range 90%-98%) were found for the detection of plaques with AHA classes III-VII.⁹³

Vasa vasorum

MRI in conjunction with gadolinium based contrast agents have been investigated for the detection of intraplaque vasa vasorum. A significantly stronger plaque enhancement was seen in plaques with vasa vasorum, resulting in a mean sensitivity of 76% (range 76%-83%) and specificity of 79% (range 75%-79%) for the detection of vasa vasorum.^{94, 95}

The use of a kinetic model for calculating the plaque fractional blood volume showed a strong correlation with the fractional vessel area on histology.⁹⁶ The calculation of the contrast transfer constant, showed significant correlations with intraplaque vasa vasorum and macrophages. No correlations were found between the contrast transfer constant and the necrotic core, calcifications and intraplaque hemorrhage.⁹⁷

Inflammation

The use MRI in conjunction with of super paramagnetic iron oxide particles has been investigated as a means of macrophage detection. Plaques with focal signal intensity loss after ultra small super paramagnetic iron oxide particle infusion were associated with an increased uptake of the iron oxide particles by CD-68 and MAC-378 stained macrophages, while plaques with diffuse signal intensity loss did not show such a correlation.⁹⁸ It was shown that a signal loss after small super paramagnetic iron oxide particles infusion predicted the presence of macrophages with a sensitivity of 63% and a specificity of 100%.⁹⁹

Summary

MRI multi-contrast imaging has a superior tissue contrast, capable of accurately detecting intraplaque hemorrhage (sensitivity 88%, specificity 80%), the lipid core (sensitivity 94%, specificity 79%) and calcifications (sensitivity 77%, specificity 88%) and MRI morphological measurements correlate closely with histology, allowing for accurate detection of the fibrous cap status. Watanabe et al. showed the superior tissue contrast of MRI in a direct comparative study between MRI and ultrasound in the same patients, demonstrating a higher accuracy for the detection of at risk plaques (sensitivity 96% versus 75%, specificity 93% versus 63%).⁵¹

The relatively long scan times of the current MRI systems results in a high number of motion artifacts. The development of high tesla MRI scanners, new coil technologies and pulse sequences will improve scan times, signal to noise ratio and spatial resolution. The use of intravenous contrast agents allows for the evaluation of intraplaque vasa vasorum and plaque inflammation. The development of computer controlled classifiers for the automated identification of plaque components might improve the accuracy of detection for some plaque components. Though these developments are in an early phase, an advantage of identification by computer controlled classifiers over human readers has been suggested for lipid components and therefore possibly improve the detection of vulnerable plaques.¹⁰⁰

DISCUSSION

The present review shows that identification of plaque components that are related to plaque vulnerability by means of non-invasive imaging is feasible. Each of the 3 non-invasive imaging techniques has its inherent advantages and disadvantages for the evaluation of vulnerable plaques (Table 2). The use of ultrasound has a high spatial and temporal resolution, is safe, low cost and readily available. However, the use of ultrasound is currently limited to the evaluation of the superficial vascular system. CT is increasingly

Table 2. Comparison of techniques for vulnerable plaque imaging

| Technique | Spatial resolution | Temporal resolution | Plaque morphology | Soft tissue contrast | Coronary imaging | Vasa vasorum imaging | Radiation | Contrast safety |
|------------|--------------------|---------------------|-------------------|----------------------|------------------|----------------------|-----------|-------------------|
| Ultrasound | µm | msec | + | ++ | - | + | - | Safe |
| CT | mm ³ | msec | +++ | + | + | - | + | Nephrotoxicity |
| MRI | mm ³ | sec | ++ | +++ | +/- | + | - | Systemic fibrosis |

CT, computed tomography; MRI, magnetic resonance imaging

used for non-invasive assessment of the coronary arteries. Plaque characterization using CT is currently limited by a poor soft tissue contrast, and moderate spatial resolution. Concerns exist about the dosage of ionizing radiation used in coronary imaging, though technical developments and the use of new imaging protocols have resulted in significant decrease in radiation doses. MRI shows the best discrimination in soft plaque components, but this technique has a relatively low spatial resolution and is contraindicated in patients with severe claustrophobia and implanted electronic devices.

Reviewing the available literature did not identify one superior imaging modality for detecting plaque components. This was in line with results from the 3 direct comparative studies using 2 imaging techniques in the same patients.^{26, 36, 51} The studies in the systematic review reported a varying accuracy for the detection of plaque components, which is partly caused by differences in study design. The studies evaluated different plaque components and used different definitions for each component. In all studies on carotid arteries histology was used as a reference method, while in the studies on the coronary arteries IVUS for validation. Histology is a superior reference standard over IVUS, although histological processing is also known to be subject to a high level of variability.¹⁰¹ The variability in histological processing may have resulted in an underestimation of accuracy and could partially explain the large variability in the diagnostic accuracy of the non-invasive carotid imaging techniques. Other factors that may have influenced the accuracy of the non-invasive imaging techniques were differences in patient selection and study protocols. Imaging systems from different manufacturers were used, and imaging settings and protocols varied. In the majority of the studies there was a time interval between non-invasive imaging and the collection of histology or IVUS. In that time-interval, natural progression of atherosclerosis and plaque rupture may have occurred. Finally, the studies discussed in this review were published over a time period of 20 years, and significant advances in medical therapy have been implemented in clinical practice over time.

Future strategies

Recently intraplaque vasa vasorum have been proposed as a marker of the vulnerable plaque. Both MRI and contrast-enhanced ultrasound are capable of identifying vasa

vasorum in the carotid arteries. Ultrasound has a number of advantages over MR. The use of gadolinium based contrast agents limits the clinical use of MRI, due to the risk of systemic fibrosis, while ultrasound contrast agents have been proven to be safe in large patient groups.^{102, 103} Additionally, the superior spatial resolution of ultrasound makes it capable of visualizing individual vasa vasorum (Figure 2). The clinical application and predictive value of contrast enhanced ultrasound for the detection of the vasa vasorum is still under investigation.

The development of molecular imaging might hold an important improvement for plaque characterization. Radionuclide imaging is readily used for molecular imaging in the field of cancer imaging. Currently, 3 studies have used radionuclide imaging for the evaluation of human atherosclerotic plaques and used histology as a reference standard. Manca et al. demonstrated a high diagnostic accuracy of scintigraphy using indium labeled platelets for the identification of carotid thrombus (sensitivity 89%, specificity 100%).¹⁰⁴ Tawakol et al. used 18F-fluorodeoxyglucose positron emission tomography to identify carotid plaque inflammation.¹⁰⁵ Annovazzi et al. evaluated 99mTc-interleukin-2 scintigraphy for the in vivo imaging of inflammation in vulnerable atherosclerotic plaques.¹⁰⁶ Ultrasound microbubble contrast agents are currently under development for molecular imaging, but in vivo human studies evaluating atherosclerosis are not yet available. MRI super paramagnetic iron oxide particle contrast has been successfully used for macrophage detection to study plaque inflammation, as discussed previously. These novel molecular imaging approaches will provide important information on function, which may be incremental to anatomical imaging for identification of the vulnerable atherosclerotic plaque.

The combination of detecting the degree of stenosis, plaque composition and the metabolic process may provide more insight in the development of atherosclerotic vascular disease, the identification of vulnerable plaques and the evaluation of its response to therapy.¹⁰⁷ The current non-invasive imaging modalities show promising results, however the studies lack standardized measurements. Consensus is needed on reproducible standards for measurements both in imaging and histology.

The benefit of carotid endarterectomy in high grade stenosis has been shown with large multi center trials, however the benefits of endarterectomy in patients with intermediate grade stenosis has been questioned.¹⁰⁸⁻¹¹⁰ The accurate identification of vulnerable plaques could have a role in the selection of therapy for patients with intermediate carotid stenosis. Prospective randomized studies are needed to assess the predictive value of non-invasive evaluation of plaque vulnerability in the selection of patients for invasive or medical interventions.

Coronary plaque imaging is a major challenge because of cardiac movement and the tortuous nature of the coronary arteries. CT is currently the only non-invasive imaging modality that combines the speed and resolution for visualizing individual plaques in

the coronary arteries. However, the suboptimal tissue contrast makes CT a less suited candidate for vulnerable plaque imaging. Due to technical limitations, non-invasive ultrasound is currently unable to image the coronary arteries, whether technological developments will allow for coronary imaging is uncertain. The relatively long MRI scan times and decreasing signal to noise ratios at distance from the radio frequency coil, result in insufficient detail for the evaluation of individual coronary plaques. However, technological developments in MRI are fast and ongoing and probably will allow for coronary plaque imaging in the future.

CONCLUSION

The results of this systematic review demonstrated that non-invasive imaging techniques are highly useful for the evaluation of the vulnerable atherosclerotic plaque. Ultrasound, CT and MRI each have their value in the assessment of different plaque components and characteristics. Visualization of plaque characteristic such as the lipid core, fibrous cap, and calcification can be used to estimate the risk of future plaque complications. Moreover, these techniques provide information on past plaque complications, such as intra plaque hemorrhage, plaque ulceration, rupture, and thrombosis. The development of non-invasive imaging techniques focusing on vasa vasorum and inflammation will further improve the identification of individuals at an increased risk of cardiovascular events and may guide therapeutic decisions.

REFERENCES

1. Fox R. Trends in cardiovascular mortality in Europe. *Circulation*. 1997;96(11):3817.
2. Sans S, Kesteloot H, Kromhout D. The burden of cardiovascular diseases mortality in Europe: Task Force of the European Society of Cardiology on Cardiovascular Mortality and Morbidity Statistics in Europe. *Eur Heart J*. 1997 8/2;18(8):1231-48.
3. Lusis AJ. Atherosclerosis. *Nature*. 2000;407(6801):233-41.
4. Levenson J, Skerrett P, Gaziano JM. Reducing the global burden of cardiovascular disease: The role of risk factors. *Prev Cardiol*. 2002;5(4):188-99.
5. Kastelein JJP, de Groot E. Ultrasound imaging techniques for the evaluation of cardiovascular therapies. *Eur Heart J*. 2008;29(7):849-58.
6. Ross R. The pathogenesis of atherosclerosis: a perspective for the 1990s. *Nature*. 1993;362(6423):801-9.
7. Falk E, Shah PK, Fuster V. Coronary plaque disruption. *Circulation*. 1995;92(3):657-71.
8. Naghavi M, Libby P, Falk E, Casscells SW, Litovsky S, Rumberger J, et al. From vulnerable plaque to vulnerable patient: A call for new definitions and risk assessment strategies: Part I. *Circulation*. 2003;108(14):1664-72.
9. Fleiner M, Kummer M, Mirlacher M, Sauter G, Cathomas G, Krapf R, et al. Arterial neovascularization and inflammation in vulnerable patients: Early and late signs of symptomatic atherosclerosis. *Circulation*. 2004;110(18):2843-50.
10. Fuster V, Moreno PR, Fayad ZA, Corti R, Badimon JJ. Atherothrombosis and high-risk plaque: Part I: Evolving concepts. *J Am Coll Cardiol*. 2005;46(6):937-54.
11. Ritman EL, Lerman A. The dynamic vasa vasorum. *Cardiovasc Res*. 2007;75(4):649-58.
12. Glagov S, Weisenberg E, Zarins CK, Stankunavicius R, Koletts GJ. Compensatory enlargement of human atherosclerotic coronary arteries. *N Engl J Med*. 1987;316(22):1371-5.
13. Little WC, Constantinescu M, Applegate RJ, Kutcher MA, Burrows MT, Kahl FR, et al. Can coronary angiography predict the site of a subsequent myocardial infarction in patients with mild-to-moderate coronary artery disease? *Circulation*. 1988;78(5 Pt 1):1157-66.
14. Giroud D, Li JM, Urban P, Meier B, Rutishauser W. Relation of the site of acute myocardial infarction to the most severe coronary arterial stenosis at prior angiography. *Am J Cardiol*. 1992;69(8):729-32.
15. Smits PC, Bos L, Quarles van Ufford MA, Eefting FD, Pasterkamp G, Borst C. Shrinkage of human coronary arteries is an important determinant of de novo atherosclerotic luminal stenosis: an in vivo intravascular ultrasound study. *Heart*. 1998;79(2):143-7.
16. Pasterkamp G, Schoneveld AH, van der Wal AC, Haudenschild CC, Clarijs RJ, Becker AE, et al. Relation of arterial geometry to luminal narrowing and histologic markers for plaque vulnerability: the remodeling paradox. *J Am Coll Cardiol*. 1998;32(3):655-62.
17. Schoenhagen P, Ziada KM, Kapadia SR, Crowe TD, Nissen SE, Tuzcu EM. Extent and direction of arterial remodeling in stable versus unstable coronary syndromes: an intravascular ultrasound study. *Circulation*. 2000;101(6):598-603.
18. Varnava AM, Mills PG, Davies MJ. Relationship between coronary artery remodeling and plaque vulnerability. *Circulation*. 2002;105(8):939-43.
19. Hardie AD, Kramer CM, Raghavan P, Baskurt E, Nandalur KR. The impact of expansive arterial remodeling on clinical presentation in carotid artery disease: a multidetector CT angiography study. *AJNR Am J Neuroradiol*. 2007;28(6):1067-70.

20. Wardlaw JM, Chappell FM, Best JJK, Wartolowska K, Berry E. Non-invasive imaging compared with intra-arterial angiography in the diagnosis of symptomatic carotid stenosis: A meta-analysis. *Lancet*. 2006;367(9521):1503-12.
21. European Carotid Plaque Study Group. Carotid artery plaque composition—relationship to clinical presentation and ultrasound B-mode imaging. *Eur J Vasc Endovasc Surg*. 1995;10(1):23-30.
22. Widder B, Paulat K, Hackspacher J, Hamann H, Hutschenreiter S, Kreutzer C, et al. Morphological characterization of carotid artery stenoses by ultrasound duplex scanning. *Ultrasound Med Biol*. 1990;16(4):349-54.
23. Comerota AJ, Katz ML, White JV, Grosh JD. The preoperative diagnosis of the ulcerated carotid atheroma. *J Vasc Surg*. 1990;11(4):505-10.
24. Sitzer M, Müller W, Rademacher J, Siebler M, Hort W, Kniemeyer HW, et al. Color-flow Doppler-assisted duplex imaging fails to detect ulceration in high-grade internal carotid artery stenosis. *J Vasc Surg*. 1996;23(3):461-5.
25. Kardoulas DG, Katsamouris AN, Gallis PT, Philippides TP, Anagnostakos NK, Gorgoyannis DS, et al. Ultrasonographic and histologic characteristics of symptom-free and symptomatic carotid plaque. *Cardiovasc Surg*. 1996;4(5):580-90.
26. Saba L, Caddeo G, Sanfilippo R, Montisci R, Mallarini G. CT and ultrasound in the study of ulcerated carotid plaque compared with surgical results: potentialities and advantages of multidetector row CT angiography. *AJNR Am J Neuroradiol*. 2007;28(6):1061-6.
27. Kagawa R, Moritake K, Shima T, Okada Y. Validity of B-mode ultrasonographic findings in patients undergoing carotid endarterectomy in comparison with angiographic and clinicopathologic features. *Stroke*. 1996;27(4):700-5.
28. AbuRahma AF, Kyer PD, Robinson PA, Hannay RS. The correlation of ultrasonic carotid plaque morphology and carotid plaque hemorrhage: clinical implications. *Surgery*. 1998;124(4):721-6.
29. Grønholdt ML, Wiebe BM, Laursen H, Nielsen TG, Schroeder TV, Sillesen H. Lipid-rich carotid artery plaques appear echolucent on ultrasound B-mode images and may be associated with intraplaque haemorrhage. *Eur J Vasc Endovasc Surg*. 1997;14(6):439-45.
30. Droste DW, Karl M, Bohle RM, Kaps M. Comparison of ultrasonic and histopathological features of carotid artery stenosis. *Neurol Res*. 1997;19(4):380-4.
31. Grønholdt ML, Nordestgaard BG, Bentzon J, Wiebe BM, Zhou J, Falk E, et al. Macrophages are associated with lipid-rich carotid artery plaques, echolucency on B-mode imaging, and elevated plasma lipid levels. *J Vasc Surg*. 2002;35(1):137-45.
32. El-Barghouty NM, Levine T, Ladvá S, Flanagan A, Nicolaidis A. Histological verification of computerized carotid plaque characterisation. *Eur J Vasc Endovasc Surg*. 1996;11(4):414-6.
33. Grønholdt ML, Nordestgaard BG, Wiebe BM, Wilhelm JE, Sillesen H. Echo-lucency of computerized ultrasound images of carotid atherosclerotic plaques are associated with increased levels of triglyceride-rich lipoproteins as well as increased plaque lipid content. *Circulation*. 1998;97(1):34-40.
34. Aly S, Bishop CC. An objective characterization of atherosclerotic lesion: an alternative method to identify unstable plaque. *Stroke*. 2000;31(8):1921-4.
35. Tegos TJ, Sohail M, Sabetai MM, Robless P, Akbar N, Pare G, et al. Echomorphologic and histopathologic characteristics of unstable carotid plaques. *AJNR Am J Neuroradiol*. 2000;21(10):1937-44.
36. Grønholdt ML, Wagner A, Wiebe BM, Hansen JU, Schroeder TV, Wilhelm JE, et al. Spiral computed tomographic imaging related to computerized ultrasonographic images of carotid plaque morphology and histology. *J Ultrasound Med*. 2001;20(5):451-8.

37. Ciulla M, Paliotti R, Ferrero S, Vandone P, Magrini F, Zanchetti A. Assessment of carotid plaque composition in hypertensive patients by ultrasonic tissue characterization: a validation study. *J Hypertens*. 2002;20(8):1589-96.
38. Denzel C, Fellner F, Wutke R, Bazler K, Müller KM, Lang W. Ultrasonographic analysis of arteriosclerotic plaques in the internal carotid artery. *Eur J Ultrasound*. 2003;16(3):161-7.
39. Sztajzel R, Momjian S, Momjian-Mayor I, Murith N, Djebaili K, Boissard G, et al. Stratified gray-scale median analysis and color mapping of the carotid plaque: correlation with endarterectomy specimen histology of 28 patients. *Stroke*. 2005;36(4):741-5.
40. Lal BK, Hobson RW, Hameed M, Pappas PJ, Padberg FT, Jamil Z, et al. Noninvasive identification of the unstable carotid plaque. *Ann Vasc Surg*. 2006;20(2):167-74.
41. Nagano K, Yamagami H, Tsukamoto Y, Nagatsuka K, Yasaka M, Nagata I, et al. Quantitative evaluation of carotid plaque echogenicity by integrated backscatter analysis: correlation with symptomatic history and histologic findings. *Cerebrovasc Dis*. 2008;26(6):578-83.
42. Urbani MP, Picano E, Parenti G, Mazzarisi A, Fiori L, Paterni M, et al. In vivo radiofrequency-based ultrasonic tissue characterization of the atherosclerotic plaque. *Stroke*. 1993;24(10):1507-12.
43. Kawasaki M, Takatsu H, Noda T, Ito Y, Kunishima A, Arai M, et al. Noninvasive quantitative tissue characterization and two-dimensional color-coded map of human atherosclerotic lesions using ultrasound integrated backscatter: comparison between histology and integrated backscatter images. *J Am Coll Cardiol*. 2001;38(2):486-92.
44. Waki H, Masuyama T, Mori H, Maeda T, Kitade K, Moriyasu K, et al. Ultrasonic tissue characterization of the atherosclerotic carotid artery: histological correlates or carotid integrated backscatter. *Circ J*. 2003;67(12):1013-6.
45. Noritomi T, Sigel B, Gahtan V, Swami V, Justin J, Feleppa E, et al. In vivo detection of carotid plaque thrombus by ultrasonic tissue characterization. *J Ultrasound Med*. 1997;16(2):107-11.
46. Puato M, Faggini E, Rattazzi M, Paterni M, Kozkov M, Palombo C, et al. In vivo noninvasive identification of cell composition of intimal lesions: a combined approach with ultrasonography and immunocytochemistry. *J Vasc Surg*. 2003;38(6):1390-5.
47. Gray-Weale AC, Graham JC, Burnett JR, Byrne K, Lusby RJ. Carotid artery atheroma: comparison of preoperative B-mode ultrasound appearance with carotid endarterectomy specimen pathology. *J Cardiovasc Surg*. 1988;29(6):676-81.
48. Feeley TM, Leen EJ, Colgan MP, Moore DJ, Hourihane DO, Shanik GD. Histologic characteristics of carotid artery plaque. *J Vasc Surg*. 1991;13(5):719-24.
49. Hatsukami TS, Thackray BD, Primozich JF, Ferguson MS, Burns DH, Beach KW, et al. Echolucent regions in carotid plaque: preliminary analysis comparing three-dimensional histologic reconstructions to sonographic findings. *Ultrasound Med Biol*. 1994;20(8):743-9.
50. Schulte-Altendorneburg G, Droste DW, Haas N, Kemény V, Nabavi DG, Füzesi L, et al. Preoperative B-mode ultrasound plaque appearance compared with carotid endarterectomy specimen histology. *Acta Neurol Scand*. 2000;101(3):188-94.
51. Watanabe Y, Nagayama M, Suga T, Yoshida K, Yamagata S, Okumura A, et al. Characterization of atherosclerotic plaque of carotid arteries with histopathological correlation: vascular wall MR imaging vs. color Doppler ultrasonography (US). *J Magn Reson Imaging*. 2008;28(2):478-85.
52. Feinstein SB. The powerful microbubble: from bench to bedside, from intravascular indicator to therapeutic delivery system, and beyond. *Am J Physiol Heart Circ Physiol*. 2004;287(2):H450-7.
53. Feinstein S, Coll B, Staub D, Adam D, Schinkel A, ten Cate F, et al. Contrast enhanced ultrasound imaging. *J Nucl Cardiol*. 2010;17(1):106-15.

54. Coli S, Magnoni M, Sangiorgi G, Marrocco-Trischitta MM, Melisurgo G, Mauriello A, et al. Contrast-enhanced ultrasound imaging of intraplaque neovascularization in carotid arteries: Correlation with histology and plaque echogenicity. *J Am Coll Cardiol*. 2008;52(3):223-30.
55. Shah F, Balan P, Weinberg M, Reddy V, Neems R, Feinstein M, et al. Contrast-enhanced ultrasound imaging of atherosclerotic carotid plaque neovascularization: A new surrogate marker of atherosclerosis? *Vasc Med*. 2007;12(4):291-7.
56. Kono Y, Pinnell SP, Sirlin CB, Sparks SR, Georgy B, Wong W, et al. Carotid arteries: Contrast-enhanced US angiography—Preliminary clinical experience. *Radiology*. 2004;230(2):561-8.
57. Cinat M, Lane CT, Pham H, Lee A, Wilson SE, Gordon I. Helical CT angiography in the preoperative evaluation of carotid artery stenosis. *J Vasc Surg*. 1998;28(2):290-300.
58. Randoux B, Marro B, Koskas F, Duyme M, Sahel M, Zouaoui A, et al. Carotid artery stenosis: prospective comparison of CT, three-dimensional gadolinium-enhanced MR, and conventional angiography. *Radiology*. 2001;220(1):179-85.
59. Fayad ZA, Fuster V, Nikolaou K, Becker C. Computed tomography and magnetic resonance imaging for noninvasive coronary angiography and plaque imaging: current and potential future concepts. *Circulation*. 2002;106(15):2026-34.
60. Hounsfield GN. Nobel Award address. Computed medical imaging. *Med Phys*. 1980;7(4):283-90.
61. Moselewski F, Ropers D, Pohle K, Hoffmann U, Ferencik M, Chan RC, et al. Comparison of measurement of cross-sectional coronary atherosclerotic plaque and vessel areas by 16-slice multidetector computed tomography versus intravascular ultrasound. *Am J Cardiol*. 2004;94(10):1294-7.
62. Achenbach S, Ropers D, Hoffmann U, MacNeill B, Baum U, Pohle K, et al. Assessment of coronary remodeling in stenotic and nonstenotic coronary atherosclerotic lesions by multidetector spiral computed tomography. *J Am Coll Cardiol*. 2004;43(5):842-7.
63. Achenbach S, Moselewski F, Ropers D, Ferencik M, Hoffmann U, MacNeill B, et al. Detection of calcified and noncalcified coronary atherosclerotic plaque by contrast-enhanced, submillimeter multidetector spiral computed tomography: A segment-based comparison with intravascular ultrasound. *Circulation*. 2004;109(1):14-7.
64. Imazeki T, Sato Y, Inoue F, Anazawa T, Tani S, Matsumoto N, et al. Evaluation of coronary artery remodeling in patients with acute coronary syndrome and stable angina by multislice computed tomography. *Circ J*. 2004;68(11):1045-50.
65. Leber AW, Becker A, Knez A, von Ziegler F, Sirol M, Nikolaou K, et al. Accuracy of 64-slice computed tomography to classify and quantify plaque volumes in the proximal coronary system: a comparative study using intravascular ultrasound. *J Am Coll Cardiol*. 2006;47(3):672-7.
66. de Weert TT, Ouhlous M, Meijering E, Zondervan PE, Hendriks JM, van Sambeek MRHM, et al. In vivo characterization and quantification of atherosclerotic carotid plaque components with multidetector computed tomography and histopathological correlation. *Arterioscler Thromb Vasc Biol*. 2006;26(10):2366-72.
67. Schoenhagen P, Tuzcu EM, Stillman AE, Moliterno DJ, Halliburton SS, Kuzmiak SA, et al. Non-invasive assessment of plaque morphology and remodeling in mildly stenotic coronary segments: comparison of 16-slice computed tomography and intravascular ultrasound. *Coron Artery Dis*. 2003;14(6):459-62.
68. Caussin C, Ohanessian A, Ghostine S, Jacq L, Lancelin B, Dambrin G, et al. Characterization of vulnerable nonstenotic plaque with 16-slice computed tomography compared with intravascular ultrasound. *Am J Cardiol*. 2004;94(1):99-104.

69. Walker LJ, Ismail A, McMeekin W, Lambert D, Mendelow AD, Birchall D. Computed tomography angiography for the evaluation of carotid atherosclerotic plaque: correlation with histopathology of endarterectomy specimens. *Stroke*. 2002;33(4):977-81.
70. Oliver TB, Lammie GA, Wright AR, Wardlaw J, Patel SG, Peek R, et al. Atherosclerotic plaque at the carotid bifurcation: CT angiographic appearance with histopathologic correlation. *AJNR Am J Neuroradiol*. 1999;20(5):897-901.
71. Wintermark M, Jawadi SS, Rapp JH, Tihan T, Tong E, Glidden DV, et al. High-resolution CT imaging of carotid artery atherosclerotic plaques. *AJNR Am J Neuroradiol*. 2008;29(5):875-82.
72. Saba L, Caddeo G, Sanfilippo R, Montisci R, Mallarini G. Efficacy and sensitivity of axial scans and different reconstruction methods in the study of the ulcerated carotid plaque using multidetector-row CT angiography: comparison with surgical results. *AJNR Am J Neuroradiol*. 2007;28(4):716-23.
73. Estes JM, Quist WC, Lo Gerfo FW, Costello P. Noninvasive characterization of plaque morphology using helical computed tomography. *J Cardiovasc Surg*. 1998;39(5):527-34.
74. Schroeder S, Kopp AF, Baumbach A, Meisner C, Kuettner A, Georg C, et al. Noninvasive detection and evaluation of atherosclerotic coronary plaques with multislice computed tomography. *J Am Coll Cardiol*. 2001;37(5):1430-5.
75. Pohle K, Achenbach S, Macneill B, Ropers D, Ferencik M, Moselewski F, et al. Characterization of non-calcified coronary atherosclerotic plaque by multi-detector row CT: comparison to IVUS. *Atherosclerosis*. 2007;190(1):174-80.
76. Iriart X, Brunot S, Coste P, Montaudon M, Dos-Santos P, Leroux L, et al. Early characterization of atherosclerotic coronary plaques with multidetector computed tomography in patients with acute coronary syndrome: a comparative study with intravascular ultrasound. *Eur Radiol*. 2007;17(10):2581-8.
77. Motoyama S, Kondo T, Anno H, Sugiura A, Ito Y, Mori K, et al. Atherosclerotic plaque characterization by 0.5-mm-slice multislice computed tomographic imaging. *Circ J*. 2007;71(3):363-6.
78. Choi BJ, Kang DK, Tahk SJ, Choi SY, Yoon MH, Lim HS, et al. Comparison of 64-slice multidetector computed tomography with spectral analysis of intravascular ultrasound backscatter signals for characterizations of noncalcified coronary arterial plaques. *Am J Cardiol*. 2008;102(8):988-93.
79. Das M, Braunschweig T, Mühlenbruch G, Mahnken A, Krings T, Langer S, et al. Carotid plaque analysis: comparison of dual-source computed tomography (CT) findings and histopathological correlation. *Eur J Vasc Endovasc Surg*. 2009;38:14-9.
80. Baumgart D, Schmermund A, Goerge G, Haude M, Ge J, Adamzik M, et al. Comparison of electron beam computed tomography with intracoronary ultrasound and coronary angiography for detection of coronary atherosclerosis. *J Am Coll Cardiol*. 1997;30(1):57-64.
81. Leber AW, Knez A, Becker A, Becker C, von Ziegler F, Nikolaou K, et al. Accuracy of multidetector spiral computed tomography in identifying and differentiating the composition of coronary atherosclerotic plaques: a comparative study with intracoronary ultrasound. *J Am Coll Cardiol*. 2004;43(7):1241-7.
82. Fayad ZA. The assessment of the vulnerable atherosclerotic plaque using MR imaging: a brief review. *Int J Cardiovasc Imaging*. 2001;17(3):165-77.
83. Yuan C, Mitsumori LM, Ferguson MS, Polissar NL, Echelard D, Ortiz G, et al. In vivo accuracy of multispectral magnetic resonance imaging for identifying lipid-rich necrotic cores and intraplaque hemorrhage in advanced human carotid plaques. *Circulation*. 2001;104(17):2051-6.
84. Cai J, Hatsukami TS, Ferguson MS, Kerwin WS, Saam T, Chu B, et al. In vivo quantitative measurement of intact fibrous cap and lipid-rich necrotic core size in atherosclerotic carotid plaque:

- comparison of high-resolution, contrast-enhanced magnetic resonance imaging and histology. *Circulation*. 2005;112(22):3437-44.
85. Saam T, Ferguson MS, Yarnykh VL, Takaya N, Xu D, Polissar NL, et al. Quantitative Evaluation of Carotid Plaque Composition by In Vivo MRI. *Arterioscler Thromb Vasc Biol*. 2005;25(1):234-9.
 86. Hatsukami TS, Ross R, Polissar NL, Yuan C. Visualization of fibrous cap thickness and rupture in human atherosclerotic carotid plaque in vivo with high-resolution magnetic resonance imaging. *Circulation*. 2000;102(9):959-64.
 87. Mitsumori LM, Hatsukami TS, Ferguson MS, Kerwin WS, Cai J, Yuan C. In vivo accuracy of multi-sequence MR imaging for identifying unstable fibrous caps in advanced human carotid plaques. *J Magn Reson Imaging*. 2003;17(4):410-20.
 88. Puppini G, Furlan F, Cirota N, Veraldi G, Piubello Q, Montemezzi S, et al. Characterisation of carotid atherosclerotic plaque: comparison between magnetic resonance imaging and histology. *Radiol Med*. 2006;111(7):921-30.
 89. Kampschulte A, Ferguson MS, Kerwin WS, Polissar NL, Chu B, Saam T, et al. Differentiation of intraplaque versus juxtaluminal hemorrhage/thrombus in advanced human carotid atherosclerotic lesions by in vivo magnetic resonance imaging. *Circulation*. 2004;110(20):3239-44.
 90. Chu B, Kampschulte A, Ferguson MS, Kerwin WS, Yarnykh VL, O'Brien KD, et al. Hemorrhage in the atherosclerotic carotid plaque: a high-resolution MRI study. *Stroke*. 2004;35(5):1079-84.
 91. Cappendijk VC, Cleutjens KBJM, Kessels AGH, Heeneman S, Schurink GWH, Welten RJTJ, et al. Assessment of human atherosclerotic carotid plaque components with multisequence MR imaging: initial experience. *Radiology*. 2005;234(2):487-92.
 92. Yoshida K, Narumi O, Chin M, Inoue K, Tabuchi T, Oda K, et al. Characterization of carotid atherosclerosis and detection of soft plaque with use of black-blood MR imaging. *AJNR Am J Neuroradiol*. 2008;29(5):868-74.
 93. Cai JM, Hatsukami TS, Ferguson MS, Small R, Polissar NL, Yuan C. Classification of human carotid atherosclerotic lesions with in vivo multicontrast magnetic resonance imaging. *Circulation*. 2002;106(11):1368-73.
 94. Yuan C, Kerwin WS, Ferguson MS, Polissar N, Zhang S, Cai J, et al. Contrast-enhanced high resolution MRI for atherosclerotic carotid artery tissue characterization. *J Magn Reson Imaging*. 2002;15(1):62-7.
 95. Kawahara I, Morikawa M, Honda M, Kitagawa N, Tsutsumi K, Nagata I, et al. High-resolution magnetic resonance imaging using gadolinium-based contrast agent for atherosclerotic carotid plaque. *Surg Neurol*. 2007;68(1):60-5.
 96. Kerwin W, Hooker A, Spilker M, Vicini P, Ferguson M, Hatsukami T, et al. Quantitative magnetic resonance imaging analysis of neovasculature volume in carotid atherosclerotic plaque. *Circulation*. 2003;107(6):851-6.
 97. Kerwin WS, Oikawa M, Yuan C, Jarvik GP, Hatsukami TS. MR imaging of adventitial vasa vasorum in carotid atherosclerosis. *Magn Reson Med*. 2008;59(3):507-14.
 98. Trivedi RA, Mallawarachi C, U-King-Im JM, Graves MJ, Horsley J, Goddard MJ, et al. Identifying inflamed carotid plaques using in vivo USPIO-enhanced MR imaging to label plaque macrophages. *Arterioscler Thromb Vasc Biol*. 2006;26(7):1601-6.
 99. Kawahara I, Nakamoto M, Kitagawa N, Tsutsumi K, Nagata I, Morikawa M, et al. Potential of magnetic resonance plaque imaging using superparamagnetic particles of iron oxide for the detection of carotid plaque. *Neurol Med Chir (Tokyo)*. 2008;48(4):157-61.

100. Hofman JMA, Branderhorst WJ, ten Eikelder HMM, Cappendijk VC, Heeneman S, Kooi ME, et al. Quantification of atherosclerotic plaque components using in vivo MRI and supervised classifiers. *Magn Reson Med*. 2006;55(4):790-9.
101. Lovett JK, Redgrave JNE, Rothwell PM. A critical appraisal of the performance, reporting, and interpretation of studies comparing carotid plaque imaging with histology. *Stroke*. 2005;36(5):1091-7.
102. Issa N, Poggio ED, Fatica RA, Patel R, Ruggieri PM, Heyka RJ. Nephrogenic systemic fibrosis and its association with gadolinium exposure during MRI. *Cleve Clin J Med*. 2008 February 2008;75(2):95-111.
103. Wei K, Mulvagh SL, Carson L, Davidoff R, Gabriel R, Grimm RA, et al. The safety of deFinity and Optison for ultrasound image enhancement: a retrospective analysis of 78,383 administered contrast doses. *J Am Soc Echocardiogr*. 2008;21(11):1202-6.
104. Manca G, Parenti G, Bellina R, Boni G, Grosso M, Bernini W, et al. 111In platelet scintigraphy for the noninvasive detection of carotid plaque thrombosis. *Stroke*. 2001;32(3):719-27.
105. Tawakol A, Migrino RQ, Bashian GG, Bedri S, Vermylen D, Cury RC, et al. In vivo 18F-fluorodeoxyglucose positron emission tomography imaging provides a noninvasive measure of carotid plaque inflammation in patients. *J Am Coll Cardiol*. 2006;48(9):1818-24.
106. Annovazzi A, Bonanno E, Arca M, D'Alessandria C, Marcoccia A, Spagnoli LG, et al. 99mTc-interleukin-2 scintigraphy for the in vivo imaging of vulnerable atherosclerotic plaques. *Eur J Nucl Med Mol Imaging*. 2006;33(2):117-26.
107. Fayad ZA, Fuster V. Clinical imaging of the high-risk or vulnerable atherosclerotic plaque. *Circ Res*. 2001;89(4):305-16.
108. North American Symptomatic Carotid Endarterectomy Trial Collaborators. Beneficial effect of carotid endarterectomy in symptomatic patients with high-grade carotid stenosis. *N Engl J Med*. 1991;325(7):445-53.
109. Executive Committee for the Asymptomatic Carotid Atherosclerosis Study. Endarterectomy for asymptomatic carotid artery stenosis. *JAMA*. 1995;273(18):1421-8.
110. European Carotid Surgery Trial. Randomised trial of endarterectomy for recently symptomatic carotid stenosis: final results of the MRC European Carotid Surgery Trial (ECST). *Lancet*. 1998;351(9113):1379-87.
111. Carrascosa PM, Capuñay CM, Garcia-Merletti P, Carrascosa J, Garcia MF. Characterization of coronary atherosclerotic plaques by multidetector computed tomography. *Am J Cardiol*. 2006;97(5):598-602.
112. Moody AR, Murphy RE, Morgan PS, Martel AL, Delay GS, Allder S, et al. Characterization of complicated carotid plaque with magnetic resonance direct thrombus imaging in patients with cerebral ischemia. *Circulation*. 2003;107(24):3047-52.



Chapter 3

Current Status and Future Developments of Contrast Enhanced Ultrasound of Carotid Atherosclerosis

Gerrit L. ten Kate, Stijn C.H. van den Oord, Eric J.G. Sijbrands, Aad van der Lugt, Nico de Jong, Johan G. Bosch, Antonius F.W. van der Steen, Arend F.L. Schinkel

J Vasc Surg. 2013; 57(2):539-546



ABSTRACT

B-mode and Doppler ultrasound are commonly used for the evaluation of atherosclerosis in the carotid arteries. Recently, contrast-enhanced ultrasound (CEUS) has been introduced as a technique to improve the detection of carotid atherosclerosis and evaluate the presence of intraplaque neovascularization, which is considered a marker of plaque vulnerability. The present review focuses on the role of CEUS for the assessment of atherosclerosis and plaque instability. Currently available literature and future developments with CEUS are discussed.

INTRODUCTION

According to the current guidelines,¹ carotid endarterectomy is highly beneficial in patients at average or low surgical risk who experience nondisabling ischemic stroke or transient ischemic cerebral symptoms and a >70% stenosis present in the ipsilateral internal carotid artery. Carotid endarterectomy in patients with a high-grade stenosis but asymptomatic for cerebrovascular disease and in those with a 50% to 69% stenosis may be beneficial, but the benefit-to-risk ratio decreases and more individualized management decisions must be made.¹ A risk stratification method distinguishing patients with stable carotid plaque from those with unstable plaque could improve selection of patients for carotid surgery.

The concept of the vulnerable atherosclerotic plaque was first described for coronary artery disease and relates to plaques with a thin fibrous cap covering a large lipid necrotic core, and active inflammation, characteristics that make the plaque at increased risk of rupture.² Intraplaque neovascularization is a novel marker of plaque vulnerability.^{2,3} The intraplaque neovessels are leaky due to increased gap junctions, thus serving as a port of entry for inflammatory cells, lipids, and even red blood cells, which contributes to plaque growth. Moreover, the neovessels are at increased risk for rupture, causing intraplaque hemorrhage and subsequent rapid progression to symptomatic disease. The presence of neovascularization in carotid plaques has been associated with symptomatic cerebrovascular disease.⁴

B-mode and Doppler ultrasound are widely available and are frequently used for evaluation of atherosclerosis in the carotid arteries.¹ Recently, contrast-enhanced ultrasound (CEUS) has been introduced for the evaluation of carotid atherosclerosis and plaque vulnerability by identifying the presence of intraplaque neovascularization.⁵⁻¹⁹ The present review provides a brief overview of the commonly used ultrasound techniques for the evaluation of carotid atherosclerosis and subsequently focuses on the role of CEUS for the assessment of carotid atherosclerosis and plaque instability. The promising results of the initial CEUS studies in humans are discussed. Additionally, quantification of CEUS images and future developments, including molecular imaging are discussed.

METHODS

Study design

This review included all available original studies reporting the use of transcutaneous CEUS for the evaluation of carotid atherosclerosis, in particular intraplaque neovascularization. Review articles and animal studies were excluded.

Literature search and data extraction

The online MEDLINE database was searched for literature in June 2012 using PubMed (National Center for Biotechnology Information, U.S. National Library of Medicine, Bethesda, Md). The search strategy was “carotid,” “contrast-enhanced,” and “ultrasound.” No time restriction for publication date was used. All titles and abstracts of the articles were evaluated. After exclusion based on the title and abstract, full articles were evaluated, and articles meeting the inclusion criteria were identified. In addition, a manual search of the reference lists of the identified studies was performed, and references were evaluated. Selected studies were reviewed and relevant patient characteristics and CEUS findings were registered. Extracted parameters were the number of included patients, age, gender, studied population, degree of stenosis, proportion of symptomatic patients, use of quantification of CEUS, and whether histology was used as a reference method.

Statistical analysis

Statistical analysis was performed using Microsoft Excel 2010 (Microsoft Corporation, Redmond, Wash) and SPSS version 15.0 (SPSS, Chicago, Ill). Continuous variables were reported as mean. Categorical variables were summarized as percentages. From the pooled data, summary estimates were calculated.

RESULTS

B-mode ultrasound scan

Based on the B-mode images, an evaluation can be made whether the plaque is predominantly echolucent, echogenic, or mixed (heterogenic).²⁰ Echolucent plaques are thought to consist of soft plaque components (lipids, intraplaque hemorrhage), whereas echogenic plaques contain more hard components (fibrous tissue, calcifications).²¹ Consequently, echolucent plaques are considered to be more at risk of rupture and thrombus formation. Hence, standard B-mode ultrasound scan measures can be used to improve prediction of cerebrovascular events and thus possibly refine the selection for carotid endarterectomy.

Contrast-enhanced ultrasound: Current status

CEUS is an enhanced form of ultrasound scan using intravenous administration of a microbubble contrast agent. The contrast agent is an intraluminal tracer and can be used to obtain angiography-like images of the carotid arteries. Ultrasound scan contrast agents were introduced in clinical practice in the early 1990s. The currently approved and used agents include SonoVue (Bracco SpA, Milan, Italy), Optison (GE Healthcare, Princeton,

NJ), Definity (Lantheus Medical Imaging, N. Billerica, Mass), and Levovist (Schering AG, Berlin, Germany). The contrast agents consist of microbubbles (approximately 1-8 μm), generally filled with a perfluorinated gas that has a low solubility, and stabilized with a phospholipid or protein shell to improve circulation time. Microbubble contrast agents are intravascular tracers that, because of their size, cannot leave the intravascular compartment. The microbubble shell is eliminated from the body through the reticuloendothelial system when the gas is exhaled. Contraindications for microbubble contrast agents are unstable angina, acute cardiac failure, acute endocarditis, known right-to-left shunts, and known allergy for microbubble contrast agents. Microbubble contrast agents have been administered in millions of patients and are safe; side effects are extremely rare.²²

For clinical application, microbubble contrast agents have been registered for tissue perfusion imaging and cardiac chamber border enhancement. None of the contrast agents has been registered for imaging of carotid intraplaque neovascularization. However, the 2011 updated guideline on nonhepatic applications of CEUS by the European Federation of Societies for Ultrasound in Medicine and Biology, recommends the use of CEUS for the differentiation between total carotid occlusion and residual flow in tight stenosis, the improvement of lumen delineation in technically difficult carotid arteries, and for the evaluation of carotid plaque neovascularization.²³ Previous studies by Ferrer et al.²⁴ and Droste et al.²⁵ have demonstrated that CEUS has a high diagnostic accuracy for the detection of carotid artery occlusion and assessment of carotid artery stenosis. These studies have demonstrated that CEUS findings were in good agreement with the results from digital subtraction angiography and/or surgery, and also in patients with poor nonenhanced examination conditions.

Most commercially available ultrasound systems provide specific pulse sequences (eg, amplitude modulation or pulse inversion) that retrieve nonlinearities at low acoustic power, which are only exhibited by microbubbles.²⁶ These techniques enable the suppression of tissue in the image and allow the specific identification of individual microbubbles. Microbubble contrast agents enhance the arterial lumen, improving the delineation of the lumen, and consequently the detection of atherosclerotic plaques and vessel wall irregularities (Figure 1).^{18, 27} The capability of ultrasound scans to detect individual microbubbles passing through the capillary system allows direct visualization of intraplaque neovascularization. Because the microbubbles are strict intravascular tracers, their presence in plaque represents the presence of an intraplaque neovessel (Figure 1 and 2). The identification of individual neovessels cannot be matched by any of the currently available imaging modalities (eg, magnetic resonance imaging is capable of making estimations about the amount of intraplaque vascularization based on contrast diffusion²⁸). This has been supported by *in vivo* studies in animal models of

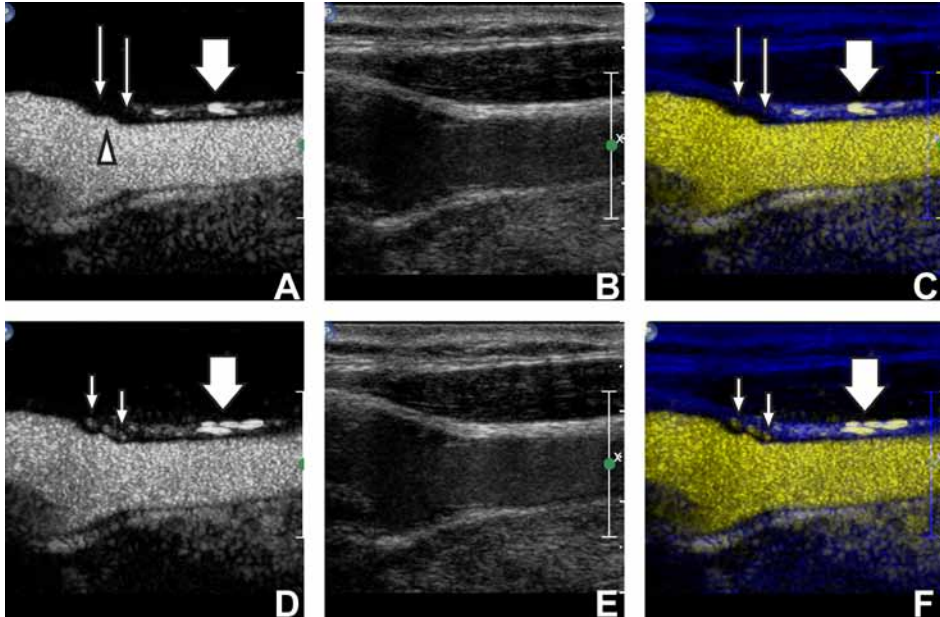


Figure 1. Evaluation of vascular wall irregularities and intraplaque neovascularization by contrast-enhanced ultrasound (CEUS). Carotid artery ultrasound scan performed in the side-by-side contrast mode, acquiring the contrast only images (A and D) and B-mode images (B and E) at the same time. C and F, present an overlay image of both the contrast (yellow) and the B-mode (blue) images, allowing for better delineation of the plaque. In the contrast-enhanced image (A) a small noncalcified plaque of 1.5 mm thick is present in the near wall, proximally to the carotid bifurcation (long thin arrows), which is barely noticeable on the B-mode image (B). In the overlay image (C), a void can be observed between the lumen contrast and vessel wall. The luminal plaque surface appears irregular and is probably ulcerated (arrowhead). The bright regions outside the vessel lumen (thick arrows) are saturation artifacts caused by high scattering regions and are constantly present during the examination. Lower panels: approximately 10 seconds after contrast has reached the carotid lumen, the contrast microbubbles have entered the atherosclerotic plaque indicating intraplaque neovascularization (D and F, small arrows). (Images acquired with a Philips iU22 ultrasound system with a L9-3 probe, SonoVue contrast agent injected intravenously in boluses of 0.5 to 1.0 mL).

atherosclerosis, showing an increase in plaque echogeneity after contrast infusion and confirming the presence of neovascularization with histology.²⁹

How to perform CEUS

Carotid CEUS can be relatively straightforward, implemented in the routine carotid ultrasound scan acquisition protocol. After a patient has been referred for a clinically indicated carotid ultrasound examination, informed consent should be obtained for the off-label use of the microbubble contrast agent.³⁰ Subsequently, a peripheral venous access catheter is placed. After acquisition of the standard carotid ultrasound scan images, the contrast presets of the ultrasound system are selected. These contrast presets

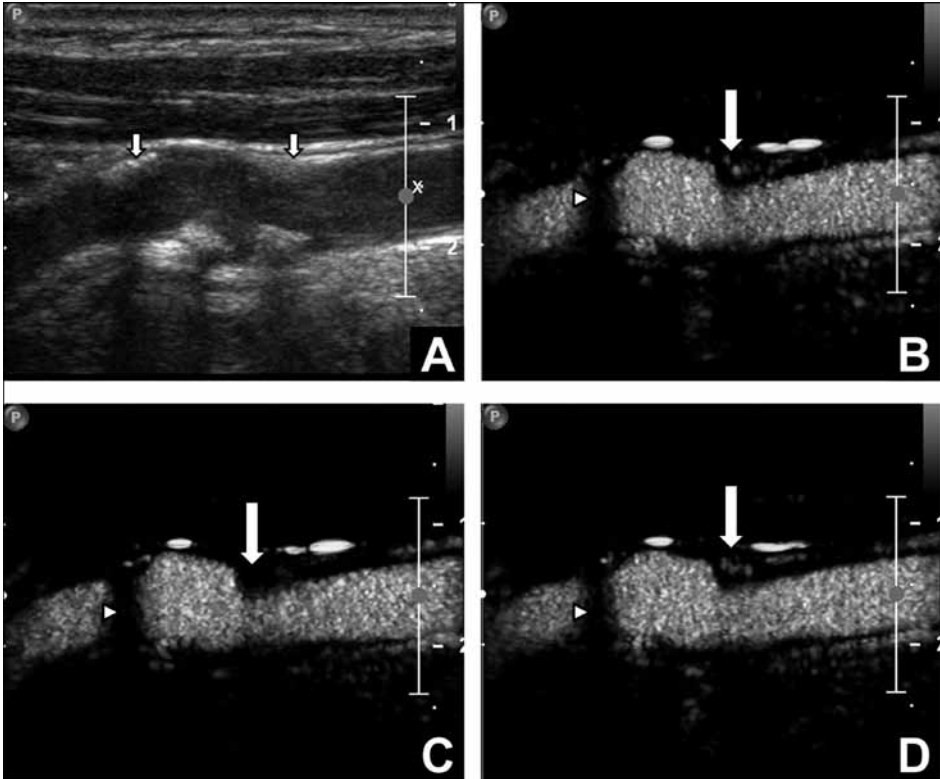


Figure 2. Identification of intraplaque neovascularization by contrast-enhanced ultrasound (CEUS) scan. Carotid artery B-mode ultrasound (A), and CEUS (B-D) acquired at three consecutive time points. Atherosclerotic plaques are present (small arrows) in the proximal part and distal part of the bulb. The distal plaque contains a calcification, identifiable by the shadowing (B-D: arrowheads). The highly enhanced regions (B-D) on the left and right side of the arrow are saturation artifacts. Panel (B) was acquired 0.5 seconds before a high mechanical index flash to destroy the contrast given. Contrast enhancement can be observed in the plaque (large arrow). Panel (C) was acquired 1.5 seconds after the flash, the intraluminal contrast has been replenished quickly, while the plaque enhancement has disappeared (large arrow). Panel (D) was acquired 6 seconds after the flash and shows the contrast microbubbles in the plaque (large arrow) indicating the presence of intraplaque neovascularization (image acquisition described in Figure 1 legend).

are available in nearly all currently used vascular ultrasound systems. The presets use an ultrasound pulse sequence with a low mechanical index to avoid destruction of the microbubbles. After injection of contrast agent followed by a saline flush, high quality CEUS images can be obtained. After a few minutes, the contrast is eliminated, the ultrasound signal intensity becomes weaker, and administration of the contrast agent can be repeated.

Assessment of intraplaque neovascularization with CEUS

The literature search yielded 163 articles (Figure 3). After review, exclusion, and cross-referencing, a total of 15 observational studies were included in the review. These 15 studies included a total of 802 patients (69% men, mean age 66 years). The majority of the patients were asymptomatic for transient ischemic attack (TIA) or stroke (88%). Feinstein⁵ was the first to report on the role of CEUS of the carotid arteries in humans to identify the vasa vasorum *in vivo*. In his 2006 review on carotid ultrasound, a case report was presented demonstrating the identification of the vasa vasorum by CEUS and regression of the vasa vasorum 8 months after initiation of statin therapy. In this report, a visual qualitative evaluation of the vasa vasorum was provided and, although no histologic conformation was performed, this initial report led the way for others

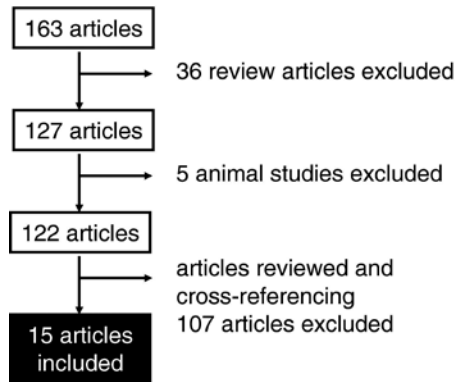


Figure 3. Flow chart of the literature search and study selection. The initial search yielded 163 eligible studies, of which 36 review articles and 5 animal studies were excluded. The remaining 122 studies were evaluated, and after cross-referencing, a total of 15 articles were included in the review.

Six studies, including a total of 95 patients, provided histologic validation of the CEUS images by carotid endarterectomy; a summary of these studies is provided in Table 1. It was shown that plaque with a higher amount of contrast enhancement had a significantly increased density of small diameter (20-30 μm) microvessels in the corresponding region on histology.^{8, 13} No association has been found between plaque echolucency and vessel density.⁸ Histologic staining for specific vascular (CD31, CD34, hemosiderin, and von Willebrand factor) and angiogenic markers (vascular endothelial growth factor) showed a correlation between intraplaque contrast enhancement and the amount of staining.^{7, 13, 19} Thus, contrast enhancement was shown to correlate with the presence and degree of intraplaque neovascularization. A major limitation of the currently available studies on the relation between CEUS findings and histologic examination of the plaques after surgery is the poor description of the diagnostic accuracy of CEUS for the

Table 1. Summary of the studies comparing carotid intraplaque neovascularization on contrast-enhanced ultrasound (CEUS) scan with histopathological analysis of the plaque after surgery

| Author | Year | Cases with histology | Histologic findings |
|-------------------------------|------|----------------------|--|
| Vicenzini et al. ⁶ | 2007 | 1 | Histology confirmed the CEUS findings |
| Shah et al. ⁷ | 2007 | 17 | Spearman rank correlation of 0.68 between CEUS and histology |
| Coli et al. ⁸ | 2008 | 17 | Good correlation between CEUS and histology |
| Giannoni et al. ¹³ | 2009 | 9 | Histology confirmed the presence of vascularization in all symptomatic plaque consistent with the presence of contrast-enhancement on CEUS |
| Shalhoub et al. ¹⁷ | 2011 | 29 | Significant correlation between late phase CEUS and CD68 immunopositivity ($r = .466$; $P = .011$) |
| Hoogi et al. ¹⁹ | 2011 | 22 | Intraplaque neovascularization on CEUS correlated well with histopathology ($r^2 = .79$; $P < .01$) |
| Summary estimate | | 95 | |

CEUS, Contrast-enhanced ultrasound scan.

assessment of intraplaque neovascularization. Authors of future studies on this topic are encouraged to report at least a cross tabulation of the CEUS findings and histology results, with the sensitivity and specificity of the test, and a measure of statistical uncertainty. Moreover, it should be clear how indeterminate, or missing results, and outliers were handled.

Several B-mode ultrasound scan-derived plaque characteristics have been investigated in association with contrast enhancement. The degree of stenosis and maximum plaque thickness have a weak correlation with the degree of contrast enhancement.¹⁶ Characterizing the plaques by their echolucency has shown that the majority of plaques characterized as soft or mixed plaques contained vascularization (94% and 73%, respectively), whereas hard and calcified plaques seem to lack vascularization.^{6, 9, 18} Histologic studies are needed to confirm these findings, because calcification in hard plaques may hinder the CEUS evaluation of intraplaque neovascularization due to acoustic shadowing, leading to false-negative results. The echogenicity was shown to have an inverse but weak correlation to plaque vascularization ($P = -.199$, $P < .001$).¹⁶ Vicenzini et al.⁶ identified plaque with an ulceration in the luminal border, and observed that every ulceration had an intraplaque vessel present underneath the ulceration. The clinical relevance of this observation deserves further investigation.

Magnoni et al.¹⁰ combined contrast ultrasound scan with B-flow imaging to evaluate the presence of adventitial vasa vasorum in atherosclerotic (stenosis >50%) and healthy (intima-media thickness <1.0 mm) vessels of patients matched for gender, age, and clinical features. B-flow imaging is a non-Doppler technique that provides information on blood flow during gray scale ultrasound scan by displaying flowing intravascular

echo-signals. It differs from power Doppler imaging, a technique using the Doppler effect, which is a shift in the frequency of the reflected ultrasound from that of the initial ultrasound pulse. A peri-adventitial B-flow signal was detected in all patients. However, the thickness of the B-flow signal was significantly higher in patients with carotid atherosclerosis (1.10 ± 0.11 mm vs 0.80 ± 0.06 mm; $P < .0001$).¹⁰

Four studies evaluated the difference in contrast enhancement between patients symptomatic and asymptomatic for cardiovascular diseases. Patients with cerebrovascular symptoms (TIA or stroke) were shown to have significantly higher contrast enhancement compared to asymptomatic patients with a similar plaque thickness (13.9 ± 6.4 dB vs 8.8 ± 5.2 dB; $P < .001$).^{12, 13} Staub et al.¹⁴ investigated the association between CEUS findings and cardiovascular disease (peripheral artery disease, coronary artery disease, myocardial infarction, or cerebrovascular disease, including TIA and stroke) and events (myocardial infarction, TIA, or stroke). It was shown that the presence of an intraluminal plaque was significantly associated with cardiovascular disease (odds ratio, 4.7; 95% confidence interval, 1.6-13.8), whereas intraplaque neovascularization was associated with a history of cardiovascular events (odds ratio, 4.0; 95% confidence interval, 1.3-12.6). These findings support the concept that intraplaque neovascularization is a sign of plaque vulnerability.¹⁴ Prospective follow-up studies have been initiated to further elucidate this issue.

Owen et al.¹⁵ investigated the *in vivo* value of late phase-contrast enhancement (6 minutes after contrast injection) as a marker for damaged endothelium and plaque inflammation. *In vitro* studies have demonstrated that untargeted microbubbles are both phagocytosed by monocytes and directly adhere to damaged endothelium.^{31, 32} The retention of microbubbles in a plaque might thus indicate the presence of inflammatory cells adhering to the vessel wall and endothelial damage. Owen et al.¹⁵ reported a significant increase in contrast enhancement 6 minutes after contrast injection in symptomatic patients, compared to asymptomatic patients. Hence, late phase-contrast enhancement might have the potential to identify plaque inflammation and endothelial damage *in vivo*. In a second study, it was shown that late phase enhancement correlates with biological features of inflammation and angiogenesis on histology.¹⁷

Quantification

Quantification methods to analyze ultrasound images are under development to further improve the accuracy of interpretation and to decrease inter-reader variation. The majority of the previously discussed studies used a qualitative scale to visually score the presence and amount of intraplaque neovascularization.^{6-8, 12-14} These scales are easily implemented and already show significant differences in contrast enhancement between symptomatic and asymptomatic patient groups.¹²⁻¹⁴ Quantitative measurement

of the contrast enhancement should further improve the reproducibility and observer variability.

Most quantitative techniques currently used are based on the evaluation of signal intensity increase after contrast infusion and show significant differences between symptomatic and asymptomatic patient groups.^{11, 12, 15} However, the accuracy and reproducibility of these methods need further evaluation. The use of B-flow imaging as proposed by Magnoni et al.¹⁰ is an interesting technique to quantitatively evaluate the adventitial vasa vasorum in the vessel wall. Histopathological studies have demonstrated that intraplaque neovascularization sprouts from these adventitial vasa vasorum. Clearly, further studies are desired to evaluate the exact role of B-flow imaging for this purpose.

Hoogi et al.¹⁹ showed promising results with a more sophisticated quantification technique. They calculated the ratio of the neovascularized plaque area to the total plaque area and reconstructed different routes microbubbles travel through the plaque with an automated algorithm. A highly significant relationship was found between the neovascularization to plaque area ratio on CEUS and histology ($R^2 = .7905$; $P < .01$), making this a promising tool for quantification of neovascularization.

Limitations of CEUS

The current commercially available ultrasound systems are equipped with 2D transducers for carotid imaging. The use of 2D data is subject to operator dependency and out of plane probe motion. Several producers of ultrasound equipment are currently developing vascular 3D matrix probes. The implementation of 3D CEUS will allow acquisition of full volume information of carotid lumen and plaque, including intraplaque neovascularization (Figure 4). The 3D carotid ultrasound scan will probably also improve interobserver and intraobserver variability.

A recently recognized limitation of CEUS is the pseudoenhancement artifact.³³ This artifact is caused by nonlinear propagation of ultrasound waves through the microbubble contrast agent, leading to pseudoenhancement visible in the far wall (the vessel wall furthest from the probe) at locations where no contrast agent is present. Misidentification of pseudoenhancement may lead to false-positive results. New ultrasound pulse sequences are being developed to suppress the pseudoenhancement artifact and are expected to become commercially available in the near future.

Future developments in CEUS

Developments in targeted contrast agents present a prospective for molecular CEUS imaging of intraplaque neovascularization. By using molecular imaging, one would be able to not only identify the presence of intraplaque neovascularization but also evaluate the angiogenic activity in the plaque. Studies using targeted microbubbles have shown the possibility to identify cellular adhesion molecules and receptors associated

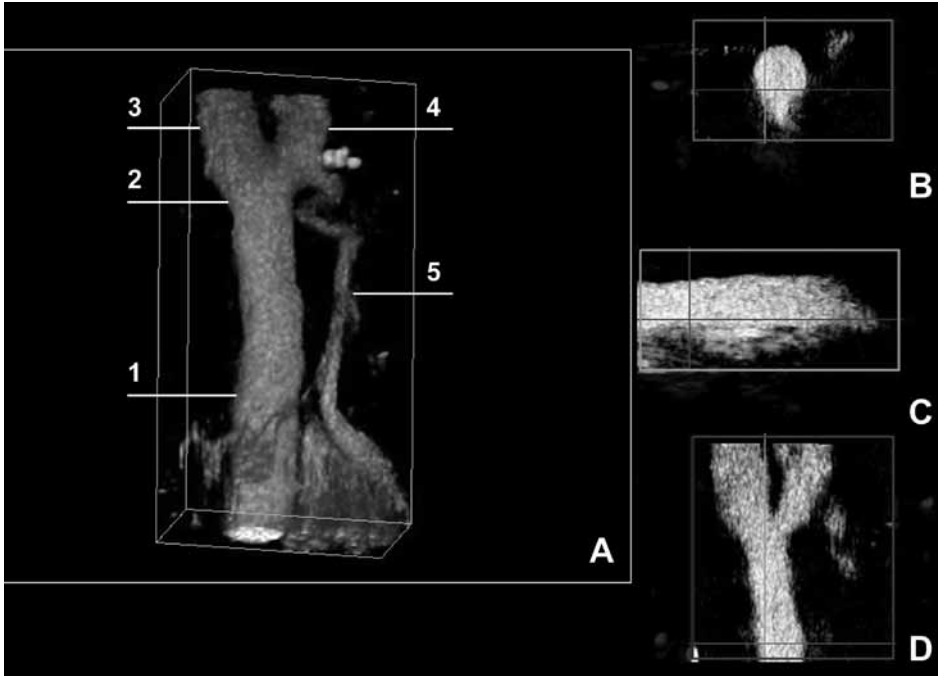


Figure 4. Contrast-enhanced 3D ultrasound scan using volume rendering (A) and multiplanar reconstruction demonstrating the transversal (B), sagittal (C), and coronal plane (D), reconstructed from a freehand sweep of the carotid artery (QLAB; Philips Healthcare, Best, The Netherlands). The volume rendering image shows the common carotid artery, (1) carotid bifurcation, (2) proximal internal, (3) and external carotid artery. (4) The superior thyroid artery (5) branches from the external carotid artery and descends to the thyroid gland.

with angiogenesis in atherosclerotic animal models.³⁴ The first human study evaluating vascular endothelial growth factor receptor targeted microbubbles has recently been performed in patients with prostate cancer, showing promising results for identification of active angiogenesis (<http://clinicaltrials.gov>; study no: NCT01253213).³⁵

CONCLUSIONS

CEUS can be relatively easily incorporated into a standard carotid ultrasound protocol to improve the evaluation of plaque morphology and assess intraplaque neovascularization. Identification of an unstable vascularized carotid plaque using CEUS could refine the selection of patients considered for carotid endarterectomy.

REFERENCES

1. American College of Cardiology Foundation/American Heart Association Task Force, American Stroke Association; American Association of Neuroscience Nurses, American Association of Neurological Surgeons, American College of Radiology, American Society of Neuroradiology, Congress of Neurological Surgeons, et al. ASA/ACCF/AHA/AANN/AANS/ACR/ASNR/CNS/SAIP/SCAI/SIR/SNIS/SVM/SVS guideline on the management of patients with extracranial carotid and vertebral artery disease: executive summary. *J NeuroIntervent Sur.* 2011;3(2):100-30.
2. Schaar JA, Muller JE, Falk E, Virmani R, Fuster V, Serruys PW, et al. Terminology for high-risk and vulnerable coronary artery plaques. *Eur Heart J.* 2004;25(12):1077-82.
3. Virmani R, Kolodgie FD, Burke AP, Finn AV, Gold HK, Tulenko TN, et al. Atherosclerotic plaque progression and vulnerability to rupture: angiogenesis as a source of intraplaque hemorrhage. *Arterioscler Thromb Vasc Biol.* 2005;25(10):2054-61.
4. McCarthy MJ, Loftus IM, Thompson MM, Jones L, London NJ, Bell PR, et al. Angiogenesis and the atherosclerotic carotid plaque: An association between symptomatology and plaque morphology. *J Vasc Surg.* 1999;30(2):261-8.
5. Feinstein SB. Contrast ultrasound imaging of the carotid artery vasa vasorum and atherosclerotic plaque neovascularization. *J Am Coll Cardiol.* 2006;48(2):236-43.
6. Vicenzini E, Giannoni MF, Puccinelli F, Ricciardi MC, Altieri M, Di Piero V, et al. Detection of carotid adventitial vasa vasorum and plaque vascularization with ultrasound cadence contrast pulse sequencing technique and echo-contrast agent. *Stroke.* 2007;38(10):2841-3.
7. Shah F, Balan P, Weinberg M, Reddy V, Neems R, Feinstein M, et al. Contrast-enhanced ultrasound imaging of atherosclerotic carotid plaque neovascularization: A new surrogate marker of atherosclerosis? *Vasc Med.* 2007;12(4):291-7.
8. Coli S, Magnoni M, Sangiorgi G, Marrocco-Trischitta MM, Melisurgo G, Mauriello A, et al. Contrast-enhanced ultrasound imaging of intraplaque neovascularization in carotid arteries: Correlation with histology and plaque echogenicity. *J Am Coll Cardiol.* 2008;52(3):223-30.
9. Huang PT, Huang FG, Zou CP, Sun HY, Tian XQ, Yang Y, et al. Contrast-enhanced sonographic characteristics of neovascularization in carotid atherosclerotic plaques. *J Clin Ultrasound.* 2008;36(6):346-51.
10. Magnoni M, Coli S, Marrocco-Trischitta MM, Melisurgo G, De Dominicis D, Cianflone D, et al. Contrast-enhanced ultrasound imaging of periadventitial vasa vasorum in human carotid arteries. *Eur J Echocardiogr.* 2009;10(2):260-4.
11. Papaioannou TG, Vavuranakis M, Androulakis A, Lazaros G, Kakadiaris I, Vlaseros I, et al. In-vivo imaging of carotid plaque neoangiogenesis with contrast-enhanced harmonic ultrasound (letter). *Int J Cardiol.* 2009;134(3):e110-2.
12. Xiong L, Deng YB, Zhu Y, Liu YN, Bi XJ. Correlation of carotid plaque neovascularization detected by using contrast-enhanced US with clinical symptoms. *Radiology.* 2009;251(2):583-9.
13. Giannoni MF, Vicenzini E, Citone M, Ricciardi MC, Irace L, Laurito A, et al. Contrast carotid ultrasound for the detection of unstable plaques with neoangiogenesis: A pilot study. *Eur J Vasc Endovasc Surg.* 2009;37(6):722-7.
14. Staub D, Patel MB, Tibrewala A, Ludden D, Johnson M, Espinosa P, et al. Vasa vasorum and plaque neovascularization on contrast-enhanced carotid ultrasound imaging correlates with cardiovascular disease and past cardiovascular events. *Stroke.* 2010;41(1):41-7.

15. Owen DR, Shalhoub J, Miller S, Gauthier T, Doryforou O, Davies AH, et al. Inflammation withing carotid atherosclerotic plaque: Assessment with late-phase contrast enhanced US. *Radiology*. 2010;255(2):638-44.
16. Staub D, Partovi S, Schinkel AFL, Coll B, Uthoff H, Aschwanden M, et al. Correlation of Carotid Artery Atherosclerotic Lesion Echogenicity and Severity at Standard US with Intraplaque Neovascularization Detected at Contrast-enhanced US. *Radiology*. 2011;258(2):618-26.
17. Shalhoub J, Monaco C, Owen DRJ, Gauthier T, Thapar A, Leen ELS, et al. Late-phase contrast-enhanced ultrasound reflects biological features of instability in human carotid atherosclerosis. *Stroke*. 2011;42(12):3634-46.
18. Clevert DA, Sommer WH, Helck A, Saam T, Reiser M. Improved carotid atherosclerotic plaques imaging with contrast-enhanced ultrasound (CEUS). *Clin Hemorheol Microcirc*. 2011;48(1):141-8.
19. Hoogi A, Adam D, Hoffman A, Kerner H, Reisner S, Gaitini D. Carotid plaque vulnerability: Quantification of neovascularization on contrast-enhanced ultrasound with histopathologic correlation. *AJR Am J Roentgenol*. 2011;196(2):431-6.
20. Bluth EI, Kay D, Merritt CR, Sullivan M, Farr G, Mills NL, et al. Sonographic characterization of carotid plaque: detection of hemorrhage. *AJR Am J Roentgenol*. 1986;146(5):1061-5.
21. Grønholdt ML, Nordestgaard BG, Bentzon J, Wiebe BM, Zhou J, Falk E, et al. Macrophages are associated with lipid-rich carotid artery plaques, echolucency on B-mode imaging, and elevated plasma lipid levels. *J Vasc Surg*. 2002;35(1):137-45.
22. Main ML, Ryan AC, Davis TE, Albano MP, Kusnetzky LL, Hibberd M. Acute Mortality in Hospitalized Patients Undergoing Echocardiography With and Without an Ultrasound Contrast Agent (Multi-center Registry Results in 4,300,966 Consecutive Patients). *Am J Cardiol*. 2008;102(12):1742-6.
23. Piscaglia F, Nolsøe C, Dietrich CF, Cosgrove DO, Gilja OH, Bachmann Nielsen M, et al. The EFSUMB guidelines and recommendations on the clinical practice of contrast enhanced ultrasound (CEUS): Update 2011 on non-hepatic applications. *Ultraschall Med*. 2012;33(1):33-59.
24. Ferrer JME, Samsó JJ, Serrando JR, Valenzuela VF, Montoya SB, Docampo MM. Use of ultrasound contrast in the diagnosis of carotid artery occlusion. *J Vasc Surg*. 2000;31(4):736-41.
25. Droste DW, Jürgens R, Nabavi DG, Schuierer G, Weber S, Ringelstein EB. Echocontrast-Enhanced Ultrasound of Extracranial Internal Carotid Artery High-Grade Stenosis and Occlusion. *Stroke*. 1999;30(11):2302-6.
26. Powers J, Averkiou M, Bruce M. Principles of cerebral ultrasound contrast imaging. *Cerebrovasc Dis*. 2009;27(Suppl. 2):14-24.
27. Sirlin CB, Lee YZ, Girard MS, Peterson TM, Steinbach GC, Baker KG, et al. Contrast-enhanced B-mode US angiography in the assessment of experimental in vivo and in vitro atherosclerotic disease. *Acad Radiol*. 2001;8(2):162-72.
28. Kerwin WS, Oikawa M, Yuan C, Jarvik GP, Hatsukami TS. MR imaging of adventitial vasa vasorum in carotid atherosclerosis. *Magn Reson Med*. 2008;59(3):507-14.
29. Schinkel AFL, Krueger CG, Tellez A, Granada JF, Reed JD, Hall A, et al. Contrast-enhanced ultrasound for imaging vasa vasorum: Comparison with histopathology in a swine model of atherosclerosis. *Eur J Echocardiogr*. 2010;11(8):659-64.
30. Feinstein SB, Coll B, Staub D, Adam D, Schinkel AF, ten Cate FJ, et al. Contrast enhanced ultrasound imaging. *J Nucl Cardiol*. 2010;17(1):106-15.
31. Lindner JR, Dayton PA, Coggins MP, Ley K, Song J, Ferrara K, et al. Noninvasive imaging of inflammation by ultrasound detection of phagocytosed microbubbles. *Circulation*. 2000;102(5):531-8.

32. Tsutsui JM, Xie F, Cano M, Chomas J, Phillips P, Radio SJ, et al. Detection of retained microbubbles in carotid arteries with real-time low mechanical index imaging in the setting of endothelial dysfunction. *J Am Coll Cardiol.* 2004;44(5):1036-46.
33. ten Kate GL, Renaud GGJ, Akkus Z, van den Oord SCH, ten Cate FJ, Shamdasani V, et al. Far-wall pseudoenhancement during contrast-enhanced ultrasound of the carotid arteries: Clinical description and in vitro reproduction *Ultrasound Med Biol.* 2012;38(4):593-600.
34. Kaufmann BA, Sanders JM, Davis C, Xie A, Aldred P, Sarembock IJ, et al. Molecular imaging of inflammation in atherosclerosis with targeted ultrasound detection of vascular cell adhesion molecule-1. *Circulation.* 2007;116(3):276-84.
35. Smeenge M, Mischi M, Laguna Pes M, de la Rosette J, Wijkstra H. Novel contrast-enhanced ultrasound imaging in prostate cancer. *World J Urol.* 2011;29(5):581-7.



PART II

CONTRAST ENHANCED ULTRASOUND
FOR IMAGING ATHEROSCLEROSIS





Chapter 4

Assessment of subclinical atherosclerosis using contrast-enhanced ultrasound

Stijn C.H. van den Oord, Gerrit L. ten Kate, Zeynettin Akkus,
Guillaume Renaud, Eric J.G. Sijbrands, Folkert J. ten Cate, Aad van
der Lugt, Johan G. Bosch, Nico de Jong, Antonius F.W. van der
Steen and Arend F.L. Schinkel

Eur Heart J Cardiovasc Imaging. 2013; 14(1):56-61

ABSTRACT

Aims The sensitivity of standard carotid ultrasound and colour Doppler for the detection of subclinical atherosclerotic plaques is suboptimal. The aim of this study is to assess whether contrast-enhanced ultrasound (CEUS) added to standard carotid ultrasound improves the detection of subclinical atherosclerosis.

Methods and results Carotid intima–media thickness (CIMT) measurement, standard carotid ultrasound including colour Doppler imaging, and CEUS were performed in 100 asymptomatic patients with one or more risk factors for atherosclerosis. CEUS was performed using intravenous administration of SonoVue™ contrast agent (Bracco S.p.A., Milan, Italy). CIMT, standard ultrasound, colour Doppler, and CEUS were reviewed by two independent observers. Standard ultrasound, colour Doppler, and CEUS were scored for the presence of atherosclerotic plaques. Subclinical atherosclerosis was diagnosed if patients had a CIMT above their age-corrected threshold value or if atherosclerotic plaques were present on standard carotid ultrasound clips or CEUS clips. McNemar's test was performed to compare between groups. Twenty-one patients (21%) had a thickened CIMT value and were considered to have subclinical atherosclerosis. Standard carotid ultrasound including colour Doppler demonstrated atherosclerotic plaques in 77 patients (77%). The addition of CEUS to the standard ultrasound protocol demonstrated atherosclerotic plaques in 88 patients (88%). The incorporation of CEUS into the standard carotid ultrasound protocol resulted in a significantly improved detection of patients with subclinical atherosclerosis ($P < 0.01$).

Conclusion CEUS has an incremental value for the detection of subclinical atherosclerosis in the carotid arteries. Atherosclerotic plaques which were only detected with CEUS and not with standard carotid ultrasound and colour Doppler imaging were predominantly hypoechoic.

INTRODUCTION

Atherosclerosis is the leading cause of morbidity and mortality in western countries.¹ It is by far the most frequent underlying cause of coronary artery disease, carotid artery disease, and peripheral arterial disease. Generally, the development of atherosclerosis starts at young age and progresses asymptotically through adult life. The progression of atherosclerosis may result in atherosclerotic plaques prone to rupture. The rupture of these atherosclerotic plaques may cause acute thrombosis leading to clinical events.² The detection of atherosclerosis before it leads to clinical events may improve risk-reducing strategies.

Carotid ultrasound is a widely available and relatively inexpensive technique to detect subclinical atherosclerosis. Carotid intima-media thickness (CIMT), as measured by B-mode ultrasound, has frequently been used as a surrogate marker for atherosclerosis.^{3,4} CIMT measurement is accurate, reproducible, and significantly related with clinical outcome. Still, there are indications that a systematic examination of the extracranial carotid arteries, including screening for the presence of plaques, may increase the sensitivity of ultrasound for identifying subclinical atherosclerosis. A recent meta-analysis demonstrated that the presence of plaques is a better predictor of clinical events when compared with CIMT measurement.⁵ Nevertheless, the sensitivity of standard carotid ultrasound of the carotid arteries to detect atherosclerotic plaques is suboptimal.⁶

Contrast-enhanced ultrasound (CEUS) provides a better delineation of the carotid arterial lumen than standard carotid ultrasound.^{7,8} However, the incremental value of CEUS for the detection of subclinical atherosclerosis in the carotid arteries has not been tested. The purpose of the present study is to assess whether CEUS added to standard carotid ultrasound improves the detection of subclinical atherosclerosis.

METHODS

Patient population and study protocol

The study protocol was approved by the local Ethics Committee and all study participants provided informed consent prior to the ultrasound examination. Between April 2010 and February 2011, 100 consecutive patients (45 females) from the outpatient clinics of vascular medicine and cardiology were included in this prospective study. All patients had no known atherosclerosis but had an increased cardiovascular risk profile. Inclusion criteria were: one or more clinical risk factors for atherosclerosis and age ≥ 18 years. Risk factors were dyslipidaemia, hypertension, diabetes mellitus, smoking, and a familial history of cardiovascular disease. Exclusion criteria were contraindications for the use of ultrasound contrast agent, such as unstable angina, acute cardiac failure,

acute endocarditis, known right-to-left shunts, and known allergy for microbubble contrast agents. Patient characteristics were registered, and a structured clinical interview and physical examination were performed. All patients underwent CIMT measurement and a standard carotid ultrasound examination in conjunction with CEUS.

Carotid ultrasound acquisition

Standard carotid ultrasound including colour Doppler, and CEUS were performed with a Philips iU-22 ultrasound system (Philips Medical Systems, Bothell, WA, USA), equipped with an L9-3 transducer. Image acquisition was performed by a trained sonography technician using a standard scanning protocol according to the American Society of Echocardiography consensus statement.⁹ In short, both left and right carotid arteries were examined with the patient in a supine position with the head supported at a 45° angle turned to the contralateral side. The left and the right common carotid artery (CCA), carotid bifurcation, internal carotid artery (ICA), external carotid artery (ECA), and vertebral arteries were imaged by B-mode ultrasound, colour Doppler, and pulse-wave Doppler. All anatomical sites were examined from different angles of view. Gain and imaging depth were adjusted per patient to obtain optimal ultrasound images. Each side was extensively evaluated for the presence of carotid plaques (Figure 1A). The degree of stenosis of the CCA, ICA, and ECA was assessed according to the current guidelines on the basis of spectral Doppler velocities.¹⁰

After standard carotid ultrasound, CEUS was performed using intravenous administration of SonoVue™ contrast agent (Bracco S.p.A., Milan, Italy). The contrast mode of the ultrasound system, using amplitude modulation and a mechanical index of 0.06–0.08, was used to optimize the CEUS examination. CEUS clips were recorded with a dual display mode for simultaneous standard B-mode ultrasound and CEUS view (Figure 1B). Before injection of the ultrasound contrast agent, the intravenous access was flushed with a 5.0 mL NaCl 0.9% solution bolus injection. The ultrasound contrast agent was injected in boluses of 0.5 mL. Each contrast agent bolus was followed by a saline flush using 2.0 mL NaCl 0.9% solution. After administration of contrast agent, high-quality contrast images could be obtained for ~1 min. Contrast administration was repeated when required up to a maximum total dose of 10.0 mL. Both carotid arteries were examined using a standard acquisition protocol. Still frames and cineclips were digitally stored for offline analysis.

Carotid ultrasound analysis

Standard ultrasound and CEUS were reviewed offline by two independent observers unaware of the clinical data. For each patient, the same analysis protocol was followed. First, CIMT was measured in the left CCA, followed by screening for the presence of atherosclerotic plaques in the left carotid artery using the standard ultrasound clips.

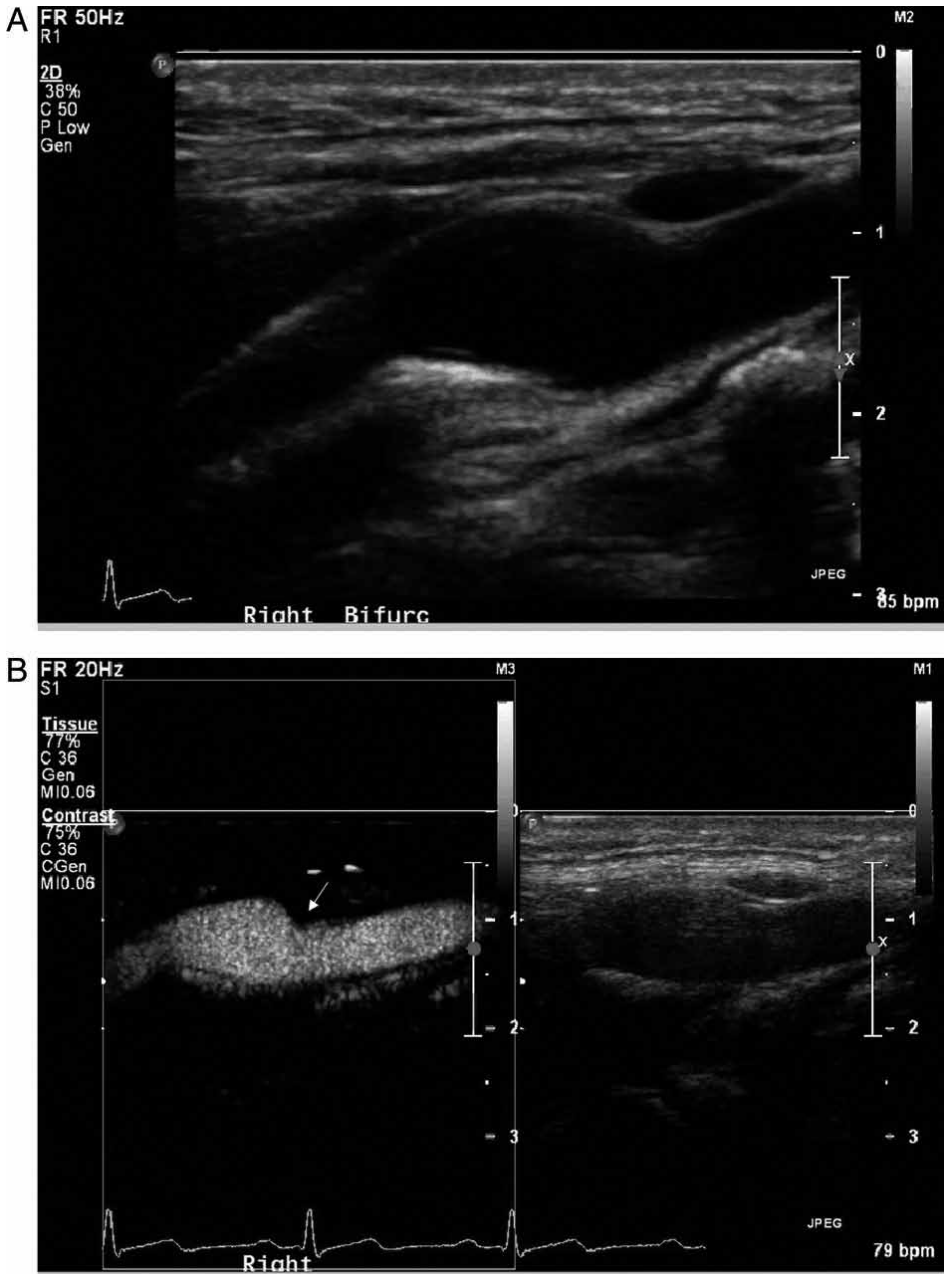


Figure 1. Assessment of subclinical atherosclerosis using standard carotid ultrasound and CEUS. (A) B-mode still frame of the right carotid artery. On the image, the distal CCA, bifurcation, and proximal ICA are visible (from right to left). No atherosclerotic plaques were detected. (B) Corresponding combined B-mode and CEUS still frame. An atherosclerotic plaque is visible on the contrast-enhanced still frame. It is located in the distal CCA and bifurcation (white arrow).

This analysis was repeated for the right carotid artery. Finally, CEUS clips were analysed; first, the left carotid artery was screened for the presence of atherosclerotic plaques. This analysis was repeated for the right carotid artery. In accordance with previously published studies, the CIMT was measured in the far wall of the distal 1 cm of the CCA.¹¹ Semi-automated CIMT measurement was performed using Qlab quantification software (Philips Healthcare, Best, The Netherlands). For each side, the CIMT measurement was performed three times on selected still frames on different R-peaks of the ECG signal. The mean value of three measurements was used in further statistical analysis. The threshold for a high CIMT value was calculated for each patient individually according to the formula reported by Jäger and Staub¹² (threshold value in mm = decade of life/10 + 0.2 mm). Patients were considered to have subclinical atherosclerosis if their mean CIMT was above this threshold value.

Carotid plaque screening was performed using the standard carotid ultrasound images and colour Doppler clips. Atherosclerotic plaque was defined as a focal structure encroaching into the lumen of at least 0.5 mm or 50% of the surrounding CIMT or demonstrates a thickness of >1.5 mm as measured from the media–adventitia interface to the intima–lumen interface.¹³ The presence of plaques was recorded for each side.

Subsequently, carotid plaque screening was performed using the CEUS images. In the CEUS images, the carotid lumen is enhanced by the presence of contrast agent, resulting in enhanced visualization of plaque and luminal morphology. Typically, the lumen appears hyperechoic, plaques and intima–media complex are hypoechoic, and the adventitial layer is hyperechoic. The definition of atherosclerotic plaques was identical to that used for standard ultrasound.¹³ The presence of plaques was recorded for each side.

If a new atherosclerotic plaque was found on CEUS, both standard carotid ultrasound and CEUS clips were reviewed in order to investigate why this plaque had been initially missed on standard carotid ultrasound alone. A systematic analysis of the standard carotid ultrasound clips of the region of the missed plaque was performed using the dual-display mode with simultaneous standard carotid ultrasound and CEUS. First, the image quality of the region of interest was scored based on a three-point scale as good-, moderate-, or poor-quality depending on artefacts or ultrasound shadowing. Secondly, echolucency was determined in the region of the missed plaque using the Gray-Weale score¹⁴ as follows: 1, predominantly echolucent plaque; 2, substantially echolucent lesions with small areas of echogenicity; 3, predominantly echogenic lesions with small areas of echolucency; and 4, uniformly echogenic lesions.

Statistical analyses

Statistical analysis was performed using SPSS PASW software for Windows (Version 17.0.2, SPSS Inc., Chicago, IL, USA). Continuous data were expressed as mean \pm standard deviation, and categorical variables were expressed as counts and percentages and/or

median value. McNemar's test was used to compare between groups. Intra- and inter-observer reproducibility for the assessment of CIMT and atherosclerotic plaque was calculated using Pearson's correlation and κ -statistics. A value of $P < 0.05$ was considered statistically significant.

RESULTS

Patient characteristics

Clinical characteristics of the 100 patients (mean age 56 ± 9 years, 45% females) are summarized in Table 1. A total of 27 patients had one clinical risk factor for atherosclerosis, 34 patients had two clinical risk factors, 33 patients had three clinical risk factors, and 6 patients had four clinical risk factors. The standard carotid ultrasound and CEUS examinations were performed without adverse reactions in all patients.

Table 1. Clinical characteristics of the study population (N = 100)

| Characteristic | Data |
|------------------------------------|--------------|
| Age (years) | 56 ± 9 |
| Female gender | 45 (45%) |
| Height (cm) | 174 ± 10 |
| Weight (kg) | 83 ± 17 |
| BMI (kg/m^2) | 27 ± 5 |
| Cardiovascular risk factors | |
| Diabetes | 22 (22%) |
| Dyslipidaemia | 88 (88%) |
| Familial history of CVD | 51 (51%) |
| Hypertension | 33 (33%) |
| Smoker (current) | 24 (24%) |
| Smoker (former) | 23 (23%) |

BMI, body mass index; CVD, cardiovascular disease. Data are presented as the numbers of patients (percentages) or as mean \pm standard deviation.

Analysis of carotid arteries

A total of 200 carotid arteries were evaluated. The mean CIMT was 0.69 ± 0.16 mm. The standard ultrasound examination, including colour Doppler, revealed atherosclerotic plaques in 129 carotid arteries (65%), and in the remaining 71 carotid arteries (36%), no atherosclerotic plaques were detected. There were no haemodynamically significant carotid stenoses detected. The addition of CEUS to the standard ultrasound protocol demonstrated atherosclerotic plaques in 155 carotid arteries (78%). In 26 carotid arteries

(13%), standard ultrasound demonstrated no atherosclerosis, whereas CEUS demonstrated atherosclerotic plaques (Figures 1 and 2). In another 26 carotid arteries (13%), atherosclerotic plaques were detected on standard carotid ultrasound, and additional atherosclerotic plaques were detected using CEUS. The incorporation of CEUS into the standard carotid ultrasound protocol resulted in a significantly improved detection of subclinical atherosclerotic plaques ($P < 0.001$).

The atherosclerotic plaques which were only detected with CEUS and had been missed using the standard carotid ultrasound examination including colour Doppler were predominantly hypoechoic, with a median Gray-Weale score of 1. A total of 39 plaque regions (70%) had Gray-Weale score 1; 13 plaque regions (23%) had Gray-Weale score 2; 4 plaque regions (7%) had Gray-Weale score 3; and 0 plaque region (0%) had Gray-Weale score 4. The image quality of standard carotid ultrasound in the regions with plaques that were detected using CEUS but missed using standard carotid ultrasound only was good in 32 regions (57%), moderate in 17 regions (30%), and poor in 7 regions (13%).

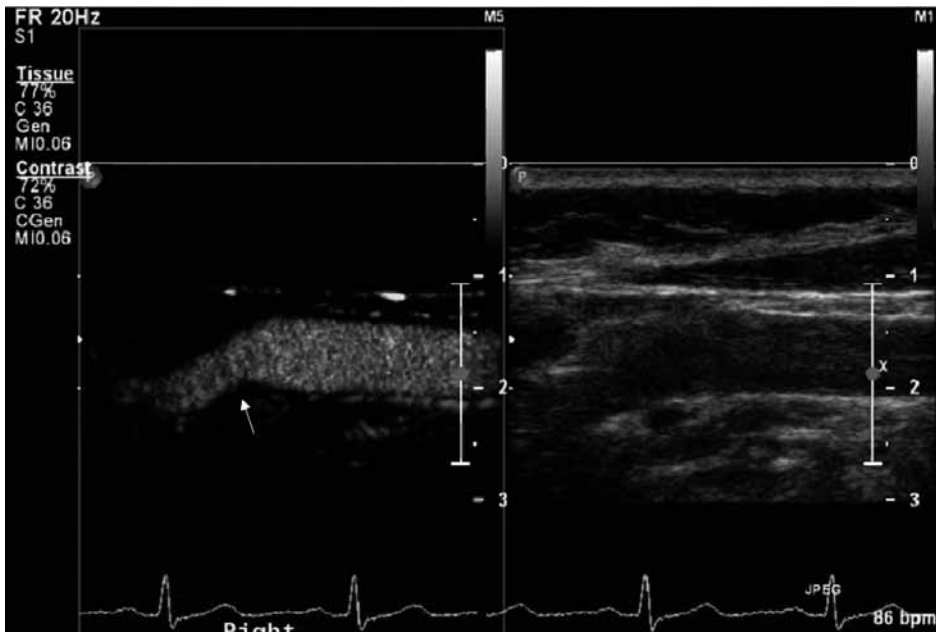


Figure 2. Detection of an atherosclerotic plaque using CEUS. Combined B-mode and CEUS still frame of a right carotid artery. An atherosclerotic plaque is visible on the contrast enhanced still frame. It is located in the bulbous and proximal ECA (white arrow).

Analysis of patients

A total of 21 patients (21%) had a CIMT value above their age-corrected threshold and were considered to have subclinical atherosclerosis. Standard carotid ultrasound demonstrated atherosclerotic plaques in a total of 77 patients (77%). All 21 patients with a CIMT value above their age-corrected threshold had atherosclerotic plaques on standard carotid ultrasound. Using standard carotid ultrasound, no atherosclerotic plaques were detected in the remaining 23 patients (23%). The addition of CEUS to the standard ultrasound protocol demonstrated atherosclerotic plaques in 88 patients (88%). In 11 patients (11%), standard carotid ultrasound demonstrated no atherosclerosis, but CEUS revealed atherosclerotic plaques. In 43 patients (43%), standard carotid ultrasound demonstrated atherosclerotic plaques and additional atherosclerotic plaques were detected using CEUS. The incorporation of CEUS into the standard carotid ultrasound protocol resulted in a significantly improved detection of patients with subclinical atherosclerosis ($P < 0.01$; Figure 3).

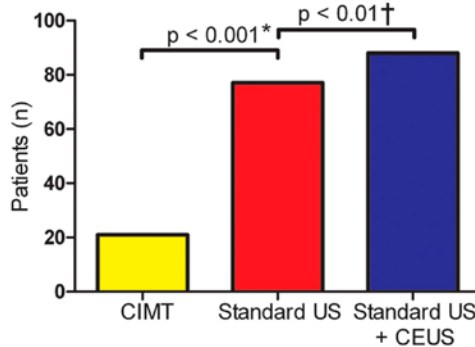


Figure 3. Identification of subclinical atherosclerosis by different imaging strategies. CIMT, carotid intima-media thickness measurement; standard US, standard carotid ultrasound; CEUS, contrast-enhanced ultrasound. *Standard ultrasound identified significantly more patients with subclinical atherosclerosis when compared with CIMT measurement. †When standard carotid ultrasound was combined with CEUS, significantly more patients with subclinical atherosclerosis were detected than with standard carotid ultrasound only.

Reproducibility

Reproducibility of ultrasound-clip analysis was assessed using the complete ultrasound examinations of all 100 patients. The mean difference between inter-observer measurements of the CIMT was 0.02 ± 0.03 mm. The correlation coefficient for inter-observer measurements of the CIMT was good ($r = 0.97$). The κ -statistics for the inter-observer agreement of atherosclerotic plaque detection with standard carotid ultrasound was 0.68. For combined standard carotid ultrasound and CEUS, the κ -statistics for inter-

observer agreement of atherosclerotic plaque detection was 0.65, which suggests a substantial agreement.

DISCUSSION

The main finding of the current study is that CEUS has incremental value for the detection of subclinical atherosclerosis. According to a previously suggested age-specific threshold formula for CIMT,¹² 21% of the patients had subclinical atherosclerosis. Standard carotid ultrasound including colour Doppler images demonstrated atherosclerotic plaques in 77% of the patients. The addition of CEUS to the standard ultrasound protocol demonstrated atherosclerotic plaques in 88% of the study population. In 11% of the patients, atherosclerotic plaques were only detected by CEUS and not with standard ultrasound. These plaques were predominantly hypoechoic. The combination of standard carotid ultrasound and CEUS may thus be the preferred strategy for evaluation of subclinical atherosclerosis.

These results are in line with previous experimental studies. Sirlin et al.⁸ reported that CEUS provides more accurate delineation of the arterial lumen than standard ultrasound. In an *ex vivo* human carotid artery model and an *in vivo* rabbit aorta model, CEUS enabled an improved depiction of wall abnormalities, while this study was performed without contrast-specific imaging settings. Kono et al.⁷ demonstrated that phase-inversion harmonic imaging further increases the sensitivity of ultrasound to contrast agent, leading to an improved visualization of the vascular lumen and tissues. To the best of our knowledge, the current study is the first to demonstrate that CEUS has an additional value for the detection of subclinical atherosclerosis.

The atherosclerotic plaques that were only detected using CEUS and not with the standard carotid ultrasound examination were predominantly hypoechoic. A number of studies have demonstrated that hypoechoic plaques contain a large lipid pool, are related with intraplaque haemorrhage, and an increased incidence of cardiovascular events.¹⁵⁻¹⁷ Large lipid pool and intraplaque haemorrhage are histopathological features of the vulnerable atherosclerotic plaque, which is at risk to rupture and may cause cardiovascular events.² The hypoechoic atherosclerotic plaques detected with CEUS may be of the vulnerable plaque type. A follow-up study is required to investigate whether the newly found hypoechoic atherosclerotic plaques are associated with an increased incidence of cardiovascular events.

The present study demonstrates that CEUS provides an incremental value for the detection of subclinical atherosclerosis, irrespective of the image quality of the standard carotid ultrasound images. The image quality of standard carotid ultrasound in the

regions with plaques that were detected by CEUS but missed using standard ultrasound was good in 57% and impaired (moderate-or-poor image quality) in 43%.

The current findings may have implications for cardiovascular risk assessment. Carotid ultrasound has been extensively used for the non-invasive detection of subclinical atherosclerosis. Large prospective studies have demonstrated that an increased CIMT is associated with clinical events, including myocardial infarction and stroke.¹⁸⁻²⁰ CIMT measurement is an excellent research tool and numerous clinical trials have studied the effect of medical therapy on CIMT instead of hard cardiovascular endpoints. Still, an increased CIMT is associated with but not necessarily synonymous with atherosclerosis. Moreover, individual risk prediction using CIMT is challenging because well-established threshold values for CIMT do not exist. Carotid plaque screening has therefore been suggested as a better surrogate outcome for coronary artery disease.²¹ Systematic examination of the extracranial carotid arteries, including screening for the presence of plaques, may increase the sensitivity of ultrasound for identifying subclinical atherosclerosis and improve cardiovascular risk stratification.^{5, 22, 23} A recent meta-analysis demonstrated that carotid ultrasound screening for the presence of plaques is a better predictor of hard cardiovascular events when compared with CIMT measurement.⁵

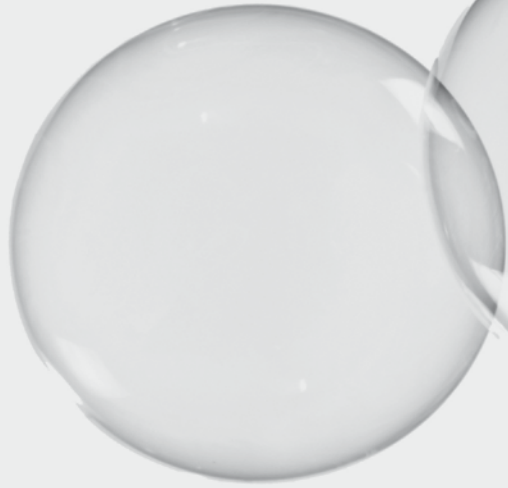
A limitation of this study is that well-established threshold values for CIMT do not exist. The formula used to calculate the threshold for abnormal CIMT only adjusts for age.¹² Previous studies have demonstrated that multiple factors including gender and ethnicity may influence CIMT. Therefore, in this study, CIMT measurement may have over- or underestimated the presence of subclinical atherosclerosis. Furthermore, the predictive value of the newly detected atherosclerotic plaques for cardiovascular risk assessment has not been investigated yet. Follow-up studies are required to determine the additional predictive value of the absence or presence of subclinical atherosclerosis detected with CEUS.

In conclusion, CEUS has an additional value for the detection of subclinical atherosclerosis in the carotid arteries. The atherosclerotic plaques that were detected by CEUS but missed using standard carotid ultrasound including colour Doppler were predominantly hypoechoic. These results suggest that the combination of standard carotid ultrasound and CEUS may thus be the preferred strategy for the evaluation of subclinical atherosclerosis.

REFERENCES

1. Viles-Gonzalez JF, Fuster V, Badimon JJ. Atherothrombosis: A widespread disease with unpredictable and life-threatening consequences. *Eur Heart J.* 2004;25(14):1197-207.
2. Schaar JA, Muller JE, Falk E, Virmani R, Fuster V, Serruys PW, et al. Terminology for high-risk and vulnerable coronary artery plaques. *Eur Heart J.* 2004;25(12):1077-82.
3. O'Leary DH, Bots ML. Imaging of atherosclerosis: Carotid intima-media thickness. *Eur Heart J.* 2010;31(14):1682-9.
4. de Groot E, Jukema JW, Montauban van Swijndregt AD, Zwinderman AH, Ackerstaff RGA, van der Steen AFW, et al. B-mode ultrasound assessment of pravastatin treatment effect on carotid and femoral artery walls and its correlations with coronary arteriographic findings: A report of the regression growth evaluation statin study (REGRESS). *J Am Coll Cardiol.* 1998;31(7):1561-7.
5. Inaba Y, Chen JA, Bergmann SR. Carotid plaque, compared with carotid intima-media thickness, more accurately predicts coronary artery disease events: A meta-analysis. *Atherosclerosis.* 2012;220(1):128-33.
6. Ray A, Tamsma JT, Hovens MMC, op 't Roodt J, Huisman MV. Accuracy of carotid plaque detection and intima-media thickness measurement with ultrasonography in routine clinical practice. *Eur J Intern Med.* 2010;21(1):35-9.
7. Kono Y, Pinnell SP, Sirlin CB, Sparks SR, Georgy B, Wong W, et al. Carotid arteries: Contrast-enhanced US angiography—Preliminary clinical experience. *Radiology.* 2004;230(2):561-8.
8. Sirlin CB, Lee YZ, Girard MS, Peterson TM, Steinbach GC, Baker KG, et al. Contrast-enhanced B-mode US angiography in the assessment of experimental in vivo and in vitro atherosclerotic disease. *Acad Radiol.* 2001;8(2):162-72.
9. Stein JH, Korcarz CE, Hurst RT, Lonn E, Kendall CB, Mohler ER, et al. Use of carotid ultrasound to identify subclinical vascular disease and evaluate cardiovascular disease risk: A consensus statement from the American Society of Echocardiography carotid intima-media thickness task force endorsed by the Society for Vascular Medicine. *J Am Soc Echocardiogr.* 2008;21(2):93-111.
10. Grant EG, Benson CB, Moneta GL, Alexandrov AV, Baker JD, Bluth EI, et al. Carotid artery stenosis: gray-scale and Doppler US diagnosis—Society of Radiologists in Ultrasound Consensus Conference. *Radiology.* 2003;229(2):340-6.
11. Montauban van Swijndregt AD, The SHK, Gussenhoven EJ, Lancee CT, Rijsterborgh H, de Groot E, et al. An in vitro evaluation of the line pattern of the near and far walls of carotid arteries using B-mode ultrasound. *Ultrasound Med Biol.* 1996;22(8):1007-15.
12. Jäger KA, Staub D. Haben Sie die Intima-Media-Dicke gemessen? (Did You Measure the Intima-Media Thickness?). *Ultraschall Med.* 2009;30(05):434-7.
13. Touboul PJ, Hennerici MG, Meairs S, Adams H, Amarenco P, Bornstein N, et al. Mannheim carotid intima-media thickness consensus (2004–2006). An update on behalf of the Advisory Board of the 3rd and 4th Watching the Risk Symposium, 13th and 15th European Stroke Conferences, Mannheim, Germany, 2004, and Brussels, Belgium, 2006. *Cerebrovasc Dis.* 2007;23(1):75-80.
14. Gray-Weale AC, Graham JC, Burnett JR, Byrne K, Lusby RJ. Carotid artery atheroma: comparison of preoperative B-mode ultrasound appearance with carotid endarterectomy specimen pathology. *J Cardiovasc Surg.* 1988;29(6):676-81.
15. Grønholdt ML, Wiebe BM, Laursen H, Nielsen TG, Schroeder TV, Sillesen H. Lipid-rich carotid artery plaques appear echolucent on ultrasound B-mode images and may be associated with intraplaque haemorrhage. *Eur J Vasc Endovasc Surg.* 1997;14(6):439-45.

16. Polak JF, Shemanski L, O'Leary DH, Lefkowitz D, Price TR, Savage PJ, et al. Hypoechoic plaque at US of the carotid artery: an independent risk factor for incident stroke in adults aged 65 years or older. *Cardiovascular Health Study. Radiology*. 1998;208(3):649-54.
17. Tegos TJ, Sabetai MM, Nicolaidis AN, Robless P, Kalodiki E, Elatrozy TS, et al. Correlates of embolic events detected by means of transcranial Doppler in patients with carotid atheroma. *J Vasc Surg*. 2001;33(1):131-8.
18. Chambless LE, Heiss G, Folsom AR, Rosamond W, Szklo M, Sharrett AR, et al. Association of Coronary Heart Disease Incidence with Carotid Arterial Wall Thickness and Major Risk Factors: The Atherosclerosis Risk in Communities (ARIC) Study, 1987–1993. *Am J Epidemiol*. 1997;146(6):483-94.
19. Bots ML, Hoes AW, Koudstaal PJ, Hofman A, Grobbee DE. Common carotid intima-media thickness and risk of stroke and myocardial infarction: the Rotterdam Study. *Circulation*. 1997;96(5):1432-7.
20. O'Leary DH, Polak JF, Kronmal RA, Manolio TA, Burke GL, Wolfson SK, et al. Carotid-artery intima and media thickness as a risk factor for myocardial infarction and stroke in older adults. *N Engl J Med*. 1999;340(1):14-22.
21. Spence JD. Ultrasound measurement of carotid plaque as a surrogate outcome for coronary artery disease. *Am J Cardiol*. 2002;89(4, Supplement 1):10-5.
22. Salonen JT, Salonen R. Ultrasonographically assessed carotid morphology and the risk of coronary heart disease. *Arterioscler Thromb Vasc Biol*. 1991;11(5):1245-9.
23. Novo S, Visconti CL, Amoroso GR, Corrado E, Fazio G, Muratori I, et al. Asymptomatic carotid lesions add to cardiovascular risk prediction. *Eur J Cardiovasc Prev Rehabil*. 2010;17(5):514-8.



Chapter 5

Usefulness of Contrast Enhanced Ultrasound for the Detection of Carotid Plaque Ulceration in Patients with Symptomatic Carotid Atherosclerosis

Gerrit L. ten Kate, Anouk C. van Dijk, Stijn C.H. van den Oord,
Burhan Hussain, Hence J.M. Verhagen, Eric J.G. Sijbrands, Antonius
F.W. van der Steen, Aad van der Lugt, Arend F.L. Schinkel

Am J Cardiol. 2013; 112(2):292-298



ABSTRACT

Previous data have indicated that carotid plaque ulceration is a strong predictor of cerebrovascular events. Standard ultrasound and color Doppler ultrasound (CDUS) scans have poor diagnostic accuracy for the detection of carotid plaque ulceration. The aim of the present prospective study was to assess the value of contrast-enhanced ultrasound (CEUS) scans for the detection of carotid plaque ulceration. The Institutional Ethics Committee approved the study protocol, and all patients provided informed consent. The patients had symptomatic stenosis of the internal carotid artery and underwent carotid computed tomographic angiography as part of their clinical evaluation. All patients underwent a CDUS examination in conjunction with CEUS. Carotid plaque ulceration was defined as the presence of ≥ 1 disruptions in the plaque-lumen border $\geq 1 \times 1$ mm. Carotid computed tomographic angiography was used as reference technique. The study population consisted of 20 patients (mean age 64 ± 9 years, 80% men), and 39 carotid arteries were included in the present analysis. Computed tomographic angiography demonstrated that the plaque surface was smooth in 15 (38%), irregular in 7 (18%) and ulcerated in 17 (44%) carotid arteries. The sensitivity, specificity, accuracy, positive predictive value, and negative predictive value of CDUS for the detection of ulceration was 29%, 73%, 54%, 46%, and 57%, respectively. The sensitivity, specificity, accuracy, positive predictive value, and negative predictive value of CEUS for the detection of ulceration was 88%, 59%, 72%, 63%, and 87%, respectively. CEUS had superior sensitivity and diagnostic accuracy for the assessment of carotid plaque ulceration compared with CDUS. CEUS improved the intrareader and inter-reader variability for the assessment of carotid plaque ulceration compared with CDUS. In conclusion, CEUS could be an additional method for the detection of carotid plaque ulceration. The role of CDUS for the assessment of carotid plaque ulceration seems limited.

INTRODUCTION

Previous studies have demonstrated that carotid plaque ulceration is a strong predictor of cerebrovascular events.^{1,2} Ultrasound is the most frequently used imaging technique for the assessment of carotid atherosclerosis. It is readily available, of low cost, safe, and accurately identifies the presence of flow-limiting stenosis.³⁻⁵ Nevertheless, ultrasound, including color Doppler ultrasound (CDUS), fails to accurately identify carotid plaque ulceration.⁴⁻⁹ Contrast-enhanced ultrasound (CEUS) is an advanced form of ultrasound imaging using a microbubble contrast agent. CEUS provides a better delineation of the carotid lumen than does CDUS.¹⁰⁻¹⁴ The use of CEUS for the detection of carotid plaque ulceration has not yet been studied. The aim of the present prospective study was to assess the value of CEUS for the detection of carotid plaque ulceration in patients with symptomatic carotid atherosclerosis. Carotid computed tomographic angiography (CTA) was used as the reference technique.

METHODS

The Institutional Ethics Committee approved the study protocol. All patients provided informed consent. A total of 20 consecutive patients were included in the present study. All patients had symptomatic stenosis of the internal carotid artery and underwent carotid CTA as part of their clinical evaluation. All patients also underwent a carotid CDUS examination in conjunction with CEUS. The exclusion criteria included contraindications for the use of an ultrasound contrast agent, such as unstable angina, acute cardiac failure, acute endocarditis, known right-to-left shunts, and a known allergy to microbubble contrast agents.

CDUS and CEUS were performed using a Philips iU-22 ultrasound system (Philips Medical Systems, Bothell, Washington), equipped with an L9-3 transducer. CDUS consisted of standard B-mode and color Doppler imaging and was performed using a standard scanning protocol.¹⁵ In brief, both left and right carotid arteries were examined with the patient in the supine position with the head supported at a 45° angle turned to the contralateral side. The common carotid artery, carotid bulb, internal carotid artery, and external carotid artery were evaluated using CDUS and pulsed wave Doppler imaging. All anatomic sites were examined from different angles of view, and each site was scanned in the cross-sectional view and longitudinal view.

After the CDUS examination, CEUS was performed using intravenous administration of SonoVue contrast agent (Bracco SpA, Milan, Italy). The contrast mode of the ultrasound system, using amplitude modulation and a mechanical index of 0.06, was used to optimize the CEUS examination. The ultrasound contrast agent was injected in 0.5 ml

boluses. Each contrast agent bolus was followed by a saline flush using 2.0 ml NaCl 0.9% solution. After administration of the contrast agent, high-quality contrast images could be obtained for approximately 1 minute. The bolus injection of the contrast agent was repeated when necessary. Both carotid arteries were examined using a standard acquisition protocol, and still frames and cine clips were digitally stored for offline analysis.

All studies were analyzed by 2 readers who were unaware of the clinical and CTA data. Discrepancies in their readings were resolved by consensus; if a consensus could not be reached, a third experienced reader was consulted. The CDUS and CEUS studies

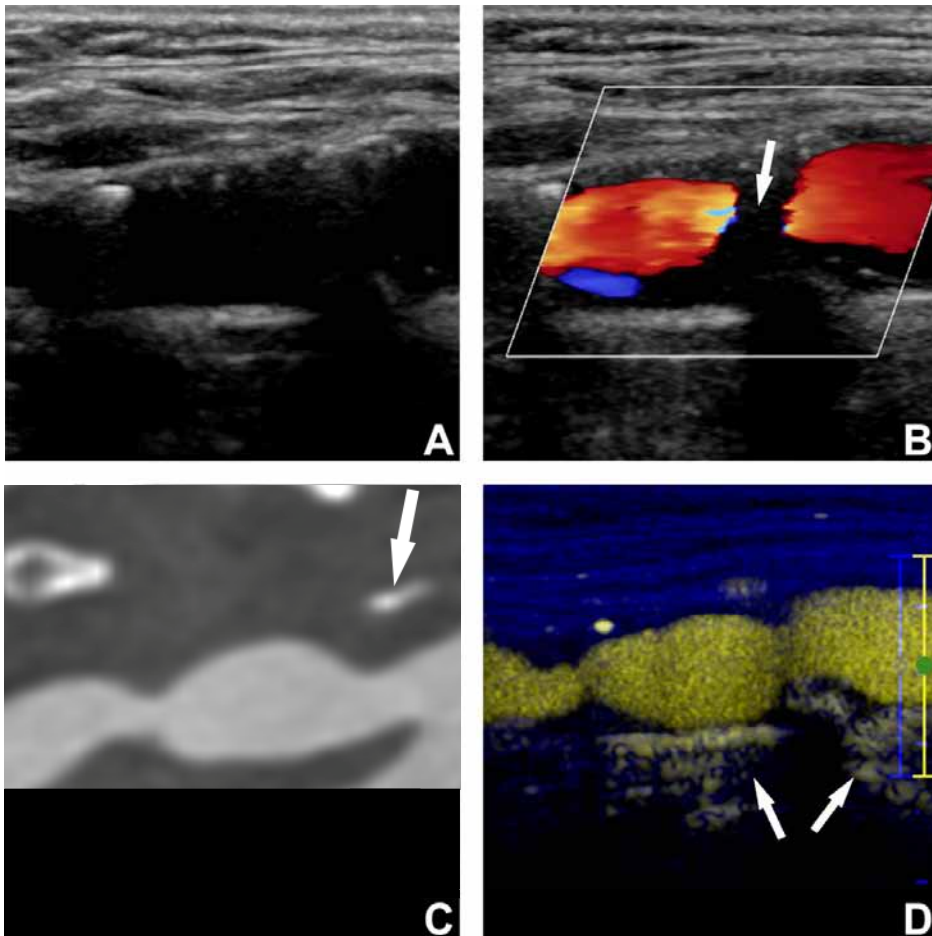


Figure 1. Longitudinal B-mode ultrasound (A), CDUS (B), CTA (C), and CEUS (D) images of carotid plaque classified as irregular using both CEUS and CTA. Calcification of carotid artery (C, arrow) caused acoustic shadow that hindered accurate color Doppler evaluation (B, arrow). A clear evaluation is possible with CEUS (D), providing information similar to that obtained with CTA (C). The enhancement underneath the vessel (D, arrows) is a pseudoenhancement artifact.

were analyzed separately. The image quality of the region of interest was scored using a 3-point scale as good, moderate, or poor image quality. The plaque border was visually scored as smooth, irregular (Figure 1), or ulcerated (Figures 2 and 3).¹⁶ Carotid plaque ulceration was defined as the presence of ≥ 1 disruptions of the plaque-lumen border $\geq 1 \times 1$ mm. The presence of calcification was scored using a semiquantitative grading system: 0, no calcification; 1, limited calcification; 2, moderate calcification; and 3, severe calcification. For each study, the readers indicated whether the presence of calcification hindered the evaluation of the plaque surface morphology.

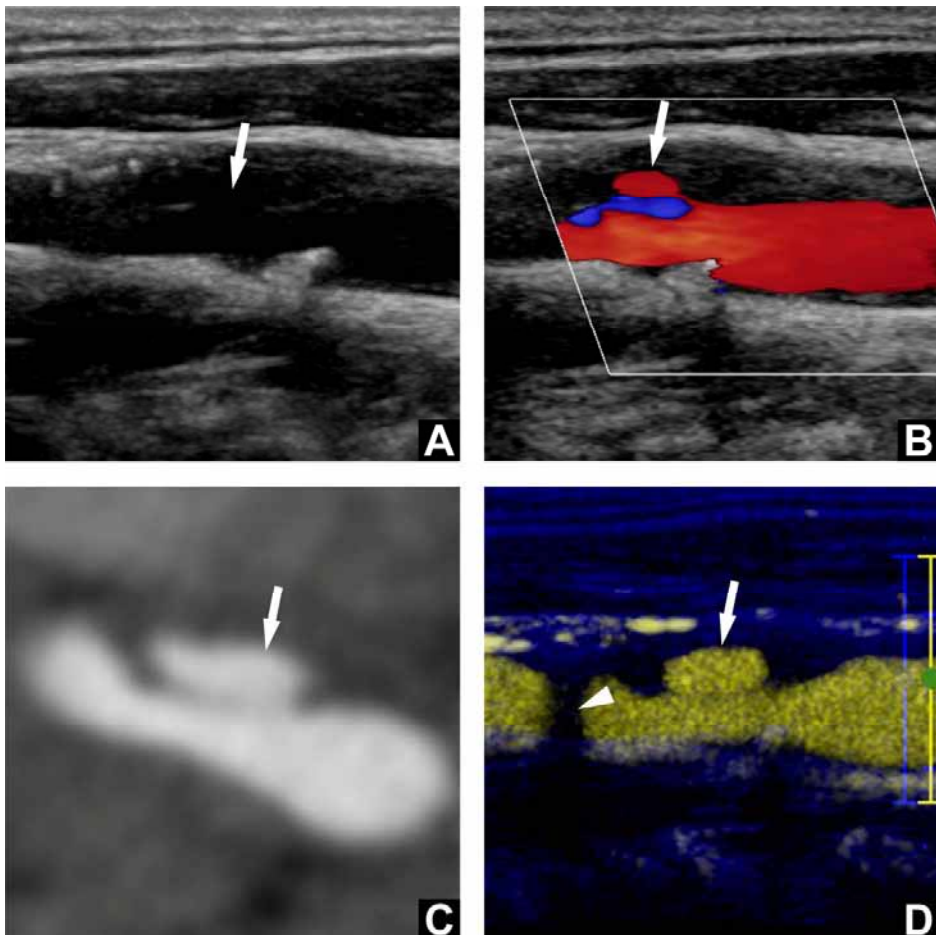


Figure 2. Longitudinal images of carotid plaque classified as ulcerated using CDUS, CEUS, and CTA. Longitudinal B-mode ultrasound (A), CDUS (B), CTA (C), and CEUS (D). A hypoechoic plaque with ulceration is present in carotid bulb (arrows). A small calcification causes shadowing that hindered visualization of a small part of the plaque surface (D, arrowhead).

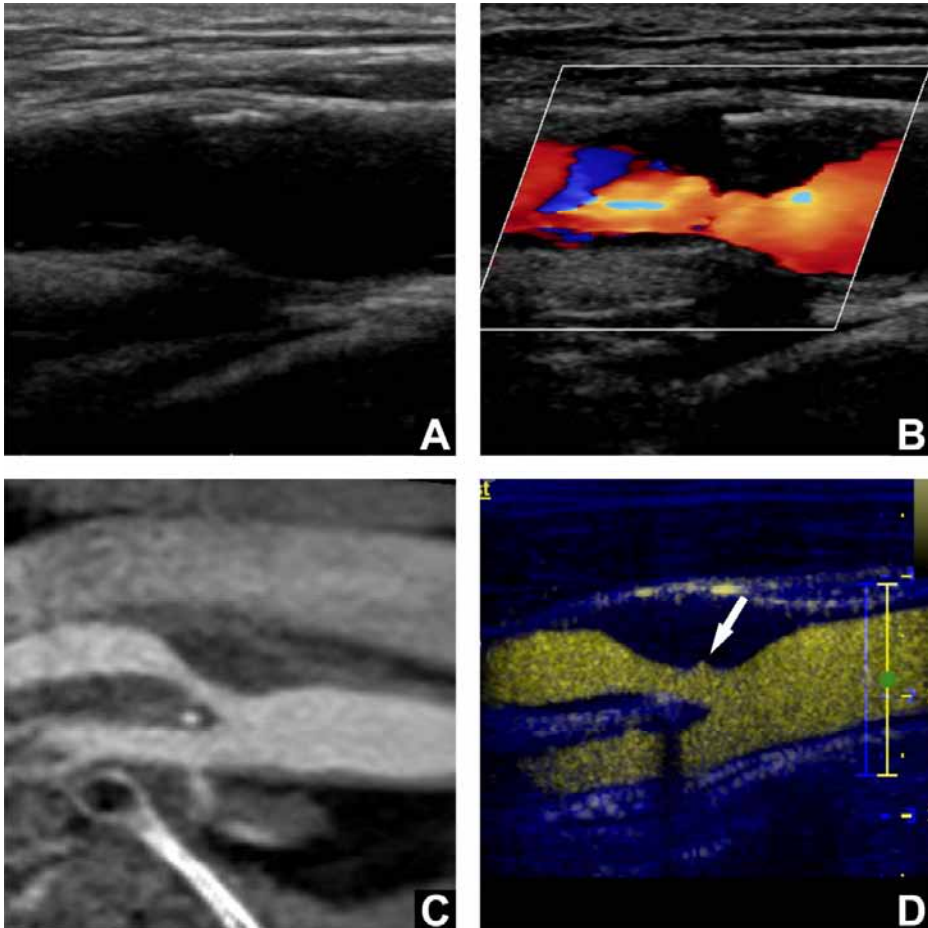


Figure 3. Longitudinal images of carotid plaque classified as ulcerated with CEUS and smooth with CTA. Longitudinal B-mode ultrasound (A), CDUS (B), CTA (C), and CEUS (D). A hypoechoic plaque was present in the near wall of the carotid artery, the full extent of which was not visible on B-mode ultrasound (A). CDUS (B) provided improved visualization of the plaque size but did not identify an ulcer. (D) CEUS demonstrated a small ($\sim 1 \times 2$ mm) ulcer (arrow) not visible using CDUS or CTA (C).

CTA was performed using a 128-slice, multidetector CT system (Definition AS+ or Definition flash [1 patient], Siemens Medical Solutions, Forchheim, Germany) using a contrast-enhanced CTA protocol (120 kVp, 180 mA, collimation $64 \times 2 \times 0.6$ mm, pitch < 1). The scan range extended from the ascending aorta to the intracranial circulation (3 cm above the sella turcica). Of the 20 patients, 19 received 80 ml of contrast agent (320 mg/ml iodixanol, Visipaque, Amersham Health, Little Chalfont, United Kingdom), followed by 45 ml saline bolus chaser, both at an injection rate of 5 ml/s. One patient received 60 ml of contrast agent, followed by a 45 ml saline bolus chaser, both at an injection rate of 4 ml/s. Real-time bolus tracking at the level of the ascending aorta

was used to synchronize the passage of the contrast agent and data acquisition. Image reconstructions were made with a field of view of 120 to 170 mm, matrix size 512 × 512, slice thickness 1.0 mm, increment 0.6 mm, and an intermediate reconstruction algorithm.

All CTA studies were evaluated with the reviewers unaware of the clinical and ultrasound data. A 2-dimensional axial image viewer was used to assess the image quality and degree of stenosis of both carotid arteries. The image quality of the region of interest was scored using a 3-point scale as good, moderate, or poor image quality. The degree of stenosis was calculated using the North American Symptomatic Carotid Endarterectomy Trial (NASCET) criteria perpendicular to the central lumen line.¹⁷ Dedicated 3-dimensional analysis software with multiplanar reformatting was used to evaluate the plaque surface in the oblique, coronal, and sagittal plane. The plaque surface of all carotid arteries was independently evaluated by 2 readers. Discrepancies in their evaluation were solved by consensus; if consensus could not be reached, a third experienced reader was consulted. The CTA and ultrasound studies were analyzed by different readers. The surface of the plaque was scored as smooth, irregular, or ulcerated. Carotid plaque ulceration was defined as the presence of contrast extending beyond the vascular lumen ≥ 1 mm in ≥ 2 planes. The calcium volume was measured from 3 cm proximal to 3 cm distal of the flow divider using semiautomated quantification software. A threshold of 600 Hounsfield units was used to differentiate calcium from contrast.

Statistical analyses were performed using the Statistical Package for Social Sciences for Windows, version 17.0 (SPSS, Chicago, Illinois). Continuous variables are reported as the mean \pm SD or median and interquartile range. Categorical variables are expressed as numbers and percentages. The CDUS and CEUS studies of the right and left carotid artery were analyzed independently, with the corresponding CTA study as the reference technique. The measurements of accuracy (sensitivity, specificity, accuracy, positive predictive value, and negative predictive value) were calculated. Differences in diagnostic accuracy were compared using McNemar's test. The CTA determined calcium volume and ultrasound calcium scores were compared using Spearman's rank correlation. The interreader and intrareader reproducibility was assessed using weighted κ statistics. *p* Values < 0.05 were considered statistically significant.

RESULTS

The clinical characteristics of the study population (mean age 64 ± 9 years, 80% men) are listed in Table 1. All CDUS, CEUS, and CTA studies were performed without adverse reactions. One patient had previously undergone right-sided endarterectomy; this carotid

Table 1. Patient characteristics (n = 20)

| Variable | Value |
|--------------------------------------|----------|
| Men | 16 (80%) |
| Age (years) | 64 ± 9 |
| Body mass index (kg/m ²) | 29 ± 6 |
| Hypertension | 10 (50%) |
| Diabetes mellitus | 5 (25%) |
| Smoker | 9 (45%) |
| Quit smoking | 6 (30%) |
| Dyslipidemia | 7 (35%) |
| Coronary artery bypass grafting | 2 (10%) |
| Myocardial infarction | 1 (5%) |
| Amaurosis fugax | 5 (25%) |
| Transient ischemic attack | 8 (40%) |
| Ischemic stroke | 5 (25%) |
| Retinal infarction | 1 (5%) |
| Pulsatile tinnitus | 1 (5%) |
| Platelet aggregation inhibitor use | 19 (95%) |
| β blocker therapy | 12 (60%) |
| Statin therapy | 19 (95%) |

Data are presented as mean ± SD or n (%)

Dyslipidemia was defined as a total cholesterol ≥6.4 mmol/L (≥247 mg/dL).

Table 2. Computed tomography angiography results (n = 39 carotid arteries)

| Variable | Value |
|-----------------------------------|-----------|
| Mean stenosis (NASCET [%]) | 43 ± 24 |
| <50% NASCET stenosis | 18 (46%) |
| 50-69% NASCET stenosis | 17 (44%) |
| ≥70% NASCET stenosis | 4 (10%) |
| Plaque surface morphology | |
| Ulcerated | 17 (44%) |
| Irregular | 7 (18%) |
| Smooth | 15 (38%) |
| Presence of calcium | 35 (90%) |
| Calcium volume (mm ³) | |
| Median | 35.2 |
| Interquartile range | 7.1-127.4 |

Data are presented as mean ± SD or n (%), unless otherwise noted.

NASCET = North American symptomatic carotid endarterectomy trial.

artery was excluded from the analysis, resulting in 39 carotid arteries for the present analysis.

The image quality of the CDUS studies was good in 31 (79%), moderate in 6 (15%), and poor in 2 (5%) carotid arteries. CEUS resulted in improved image quality, with 37 (95%) studies of good, 2 (5%) of moderate, and 0 of poor quality. None of the ultrasound studies were judged to be uninterpretable. The CTA image quality was good in 37 (95%) and moderate in 2 (5%) arteries. No CTA scan was judged to be uninterpretable.

CTA demonstrated that the plaque surface was smooth in 15 (38%), irregular in 7 (18%), and ulcerated in 17 (44%) carotid arteries (Table 2). The performance characteristics of CDUS for the evaluation of the carotid plaque surface are listed in Table 3. CDUS revealed 5 of 17 ulcerations (29%) identified at CTA, with 6 additional ulcerations detected that could not be confirmed. This resulted in a poor agreement between CDUS and CTA ($\kappa = 0.19$, 95% confidence interval [CI] 0.00 to 0.42).

Table 3. Standard ultrasound including color Doppler (CDUS) evaluation of carotid plaque surface compared with computed tomography angiography (CTA)

| CDUS | CTA | | | Total |
|-----------|---------|-----------|-----------|-------|
| | Smooth | Irregular | Ulcerated | |
| Smooth | 7 (19%) | 1 (3%) | 2 (5%) | 10 |
| Irregular | 6 (15%) | 2 (5%) | 10 (26%) | 18 |
| Ulcerated | 2 (5%) | 4 (10%) | 5 (13%) | 11 |
| Total | 15 | 7 | 17 | 39 |

Data are presented as n (%)

Carotid CEUS detected 15 of 17 ulcerations (88%) identified at CTA and identified 9 additional ulcerations that were not confirmed at CTA (Table 4). The addition of CEUS to the CDUS study provided a substantial improvement in agreement between ultrasound and CTA ($\kappa = 0.42$, 95% CI 0.26 to 0.62). CEUS significantly improved the sensitivity for identifying ulcerations (sensitivity 29% for CDUS vs 88% for CEUS, $p < 0.01$), without

Table 4. Contrast-enhanced ultrasound (CEUS) of carotid plaque surface compared with computed tomography angiography (CTA)

| CEUS | CTA | | | Total |
|-----------|---------|-----------|-----------|-------|
| | Smooth | Irregular | Ulcerated | |
| Smooth | 5 (13%) | 0 | 0 | 5 |
| Irregular | 7 (19%) | 1 (3%) | 2 (5%) | 10 |
| Ulcerated | 3 (8%) | 6 (15%) | 15 (38%) | 24 |
| Total | 15 | 7 | 17 | 39 |

Data are presented as n (%)

significantly decreasing the specificity (specificity 73% for CDUS vs 59% for CEUS, $p = 0.45$). The diagnostic accuracy of CDUS and CEUS for the detection of carotid plaque ulceration is summarized in Table 5.

Table 5. Comparison of color Doppler ultrasound (CDUS) with contrast-enhanced ultrasound (CEUS) for the detection of carotid plaque ulceration

| Variable | Method | |
|------------------------|-----------|-----------|
| | CDUS | CEUS |
| Sensitivity (%) | 29 | 88 |
| Specificity (%) | 73 | 59 |
| Accuracy (%) | 54 | 72 |
| PPV (%) | 46 | 63 |
| NPV (%) | 57 | 87 |

NPV = negative predictive value, PPV = positive predictive value.

CTA demonstrated the presence of calcification in 35 carotid arteries (90%), with a median calcium volume of 35.2 mm³ (interquartile range 7.1 to 127.4). CDUS demonstrated no calcification (grade 0) in 3 (8%), limited (grade 2) in 11 (28%), and severe calcification (grade 3) in 10 (26%) carotid arteries. CEUS demonstrated no calcification (grade 0) in 5 (13%), limited calcification (grade 1) in 11 (28%), moderate calcifications (grade 2) in 19 (49%), and severe calcification (grade 3) in 4 (10%) carotid arteries. Both the CDUS and CEUS semiquantitative calcium grading showed a strong correlation with the CTA determined calcium volume (Spearman's $r = 0.69$, $p < 0.001$, and $r = 0.72$, $p < 0.001$, respectively; Figure 4). In none of the patients, did the observers judge the calcification to obscure the plaque such that an evaluation with ultrasound was not possible. The exclusion of studies with heavy calcification did not change the accuracy of ulceration detection.

The inter-reader and intrareader reproducibility of CDUS for the detection of plaque ulceration was moderate (intrareader variability, $\kappa = 0.38$, 95% CI 0.15 to 0.61; intrareader variability, $\kappa = 0.61$, 95% CI 0.40 to 0.81). CEUS improved the inter-reader and intrareader variability for the assessment of carotid plaque ulceration compared with CDUS (inter-reader variability, $\kappa = 0.65$, 95% CI 0.42 to 0.88; intrareader variability, $\kappa = 0.69$, 95% CI 0.52 to 0.85).

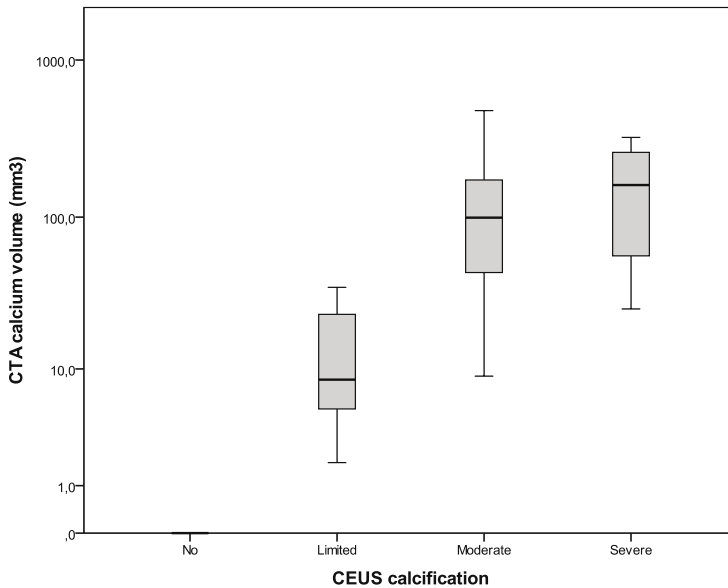


Figure 4. Box plot of semiquantitative calcium grading obtained with CEUS compared with CTA determined calcium volume (logarithmic).

DISCUSSION

The main finding of the present study was that CEUS could be an additional method for the detection of carotid plaque ulceration in patients with symptomatic carotid atherosclerosis. CEUS had a significantly greater sensitivity and diagnostic accuracy for the assessment of carotid plaque ulceration compared with CDUS. CEUS improved the intrareader and inter-reader variability for the assessment of carotid plaque ulceration compared with CDUS. These findings suggest that the role of CDUS for the assessment of carotid plaque ulceration is limited. The results of the present study could have implications for the use of CEUS in the evaluation of patients with carotid plaques.

These results have confirmed the findings from previous studies using CDUS for the detection of carotid plaque ulceration. Previous studies have shown that CDUS has a limited accuracy for the detection of carotid plaque ulceration.⁶⁻¹¹ Saba et al.⁷ studied 103 carotid arteries with CDUS using the histologic examination as the reference method and demonstrated a sensitivity similar to our study (sensitivity 37.5%, specificity 91.5%). The poor sensitivity led the investigators to conclude that CDUS has no place in the evaluation of carotid plaque morphology.⁷ They consequently recommended the use of CTA for this purpose.⁷ The present results are in line with those from previous experimental studies. Sirlin et al.¹⁰ demonstrated that CEUS provides a more accurate delineation of the vascular lumen than CDUS. In that initial study, CEUS was performed

without a contrast-specific image acquisition setting, but CEUS improved the depiction of the luminal and wall abnormalities in an *in vivo* rabbit model of atherosclerosis and in replicas of diseased human carotid arteries. Kono et al.¹¹ showed that phase-inversion harmonic imaging further increased the sensitivity of ultrasound to a contrast agent, leading to improved visualization of the vascular lumen and tissues.

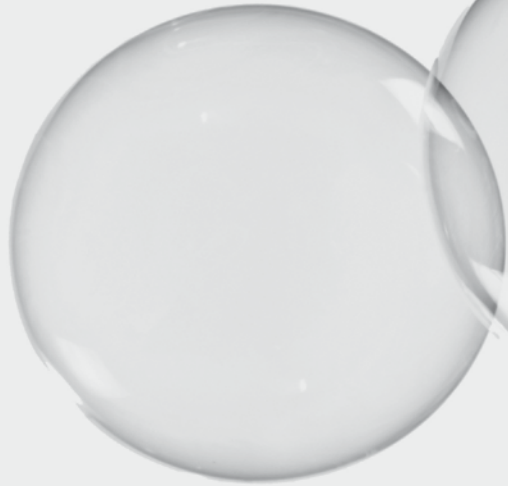
The present study is the first to evaluate the value of CEUS for the detection of carotid plaque ulceration. CEUS was relatively easily incorporated into the standard carotid ultrasound acquisition protocol and significantly improved the accuracy for the assessment of plaque ulceration. However, the agreement between CEUS and CTA in our study was not perfect. This could have been caused by several factors. First, the ultrasound acquisition might have been hindered because of calcified plaques owing to acoustic shadowing. CDUS and CEUS demonstrated severe calcium in 26% and 10% of the carotid arteries, respectively. The semiquantitative calcium scales obtained by ultrasound were in line with the semiautomated quantification of calcium using CTA. None of the ultrasound studies was judged to be uninterpretable, and the exclusion of severely calcified plaques did not change the diagnostic accuracy. However, we could not exclude that ulcerations could have been missed as a result of acoustic shadowing. Second, both CDUS and CEUS were performed using 2-dimensional acquisition, but CTA is a 3-dimensional imaging technique. The 2-dimensional acquisition might have decreased the accuracy of CEUS for the assessment of plaque ulceration. Third, in the present study, carotid CEUS identified 9 additional ulcerations that were not detected using CTA. This fact raises the question of whether CTA is a reliable reference standard for detecting plaque ulcerations. Because of the lower local and temporal resolution of CTA compared with ultrasound imaging, CEUS might even exceed the diagnostic performance for detecting plaque ulcerations compared with CTA. Finally, the present study was limited by the relatively small number of patients ($n = 20$) and carotid lesions ($n = 39$).

The results of our study should be viewed in the context of risk assessment of patients with atherosclerosis of the carotid artery. The presence of ulceration is 1 of the specific risk features of the unstable atherosclerotic plaque.¹⁸ Carotid plaque ulceration can lead to embolism and occlusion, and previous studies have indicated that ulceration is an important risk marker for neurologic symptoms and acute ischemic stroke.^{1,2} These studies have focused on plaque ulceration in patients with symptomatic carotid atherosclerosis. Additional studies are needed to assess the predictive value of carotid plaque ulceration in asymptomatic patients. The detection of plaque ulceration using CEUS could be implemented in clinical practice for the identification of plaques at high risk of causing thromboembolic events. The assessment of these unstable or vulnerable plaques could help to further improve the identification of patients who might benefit from aggressive medical therapy or carotid surgery. The challenge for the future is to develop accurate risk stratification models.

REFERENCES

1. Eliasziw M, Streifler JY, Fox AJ, Hachinski VC, Ferguson GG, Barnett HJ. Significance of plaque ulceration in symptomatic patients with high-grade carotid stenosis. North American Symptomatic Carotid Endarterectomy Trial. *Stroke*. 1994;25(2):304-8.
2. Handa N, Matsumoto M, Maeda H, Hougaku H, Kamada T. Ischemic stroke events and carotid atherosclerosis : Results of the Osaka Follow-up Study for Ultrasonographic Assessment of Carotid Atherosclerosis (the OSACA Study). *Stroke*. 1995;26(10):1781-6.
3. Patel SG, Collie DA, Wardlaw JM, Lewis SC, Wright AR, Gibson RJ, et al. Outcome, observer reliability, and patient preferences if CTA, MRA, or Doppler ultrasound were used, individually or together, instead of digital subtraction angiography before carotid endarterectomy. *J Neurol Neurosurg Psychiatry*. 2002;73(1):21-8.
4. Anzidei M, Napoli A, Zaccagna F, Di Paolo P, Saba L, Cavallo Marincola B, et al. Diagnostic accuracy of colour Doppler ultrasonography, CT angiography and blood-pool-enhanced MR angiography in assessing carotid stenosis: a comparative study with DSA in 170 patients. *Radiol Med*. 2012;117:54-71.
5. Wardlaw JM, Chappell FM, Best JJK, Wartolowska K, Berry E. Non-invasive imaging compared with intra-arterial angiography in the diagnosis of symptomatic carotid stenosis: A meta-analysis. *Lancet*. 2006;367(9521):1503-12.
6. O'Leary DH, Holen J, Ricotta JJ, Roe S, Schenk EA. Carotid bifurcation disease: prediction of ulceration with B-mode US. *Radiology*. 1987;162(2):523-5.
7. Saba L, Caddeo G, Sanfilippo R, Montisci R, Mallarini G. CT and ultrasound in the study of ulcerated carotid plaque compared with surgical results: potentialities and advantages of multidetector row CT angiography. *AJNR Am J Neuroradiol*. 2007;28(6):1061-6.
8. Sitzer M, Müller W, Rademacher J, Siebler M, Hort W, Kniemeyer HW, et al. Color-flow Doppler-assisted duplex imaging fails to detect ulceration in high-grade internal carotid artery stenosis. *J Vasc Surg*. 1996;23(3):461-5.
9. Comerota AJ, Katz ML, White JV, Grosh JD. The preoperative diagnosis of the ulcerated carotid atheroma. *J Vasc Surg*. 1990;11(4):505-10.
10. Sirlin CB, Lee YZ, Girard MS, Peterson TM, Steinbach GC, Baker KG, et al. Contrast-enhanced B-mode US angiography in the assessment of experimental in vivo and in vitro atherosclerotic disease. *Acad Radiol*. 2001;8(2):162-72.
11. Kono Y, Pinnell SP, Sirlin CB, Sparks SR, Georgy B, Wong W, et al. Carotid arteries: Contrast-enhanced US angiography—Preliminary clinical experience. *Radiology*. 2004;230(2):561-8.
12. Feinstein SB, Coll B, Staub D, Adam D, Schinkel AF, ten Cate FJ, et al. Contrast enhanced ultrasound imaging. *J Nucl Cardiol*. 2010;17(1):106-15.
13. Clevert DA, Sommer WH, Helck A, Saam T, Reiser M. Improved carotid atherosclerotic plaques imaging with contrast-enhanced ultrasound (CEUS). *Clin Hemorheol Microcirc*. 2011;48(1):141-8.
14. van den Oord SCH, ten Kate GL, Akkus Z, Renaud G, Sijbrands EJJ, ten Cate FJ, et al. Assessment of subclinical atherosclerosis using contrast-enhanced ultrasound. *Eur Heart J Cardiovasc Imaging*. 2012;14(1):56-61.
15. Stein JH, Korcarz CE, Hurst RT, Lonn E, Kendall CB, Mohler ER, et al. Use of carotid ultrasound to identify subclinical vascular disease and evaluate cardiovascular disease risk: A consensus statement from the american society of echocardiography carotid intima-media thickness task force endorsed by the society for vascular medicine. *J Am Soc Echocardiogr*. 2008;21(2):93-111.

16. Lovett JK, Gallagher PJ, Hands LJ, Walton J, Rothwell PM. Histological correlates of carotid plaque surface morphology on lumen contrast imaging. *Circulation*. 2004;110(15):2190-7.
17. North American Symptomatic Carotid Endarterectomy Trial Collaborators. Beneficial effect of carotid endarterectomy in symptomatic patients with high-grade carotid stenosis. *N Engl J Med*. 1991;325(7):445-53.
18. ten Kate GL, Sijbrands EJ, Staub D, Coll B, ten Cate FJ, Feinstein SB, Schinkel. Noninvasive imaging of the vulnerable atherosclerotic plaque. *Curr Probl Cardiol*. 2010;35:556-91



Chapter 6

Carotid Plaque Burden as a Measure of Subclinical Coronary Artery Disease in Patients with Heterozygous Familial Hypercholesterolemia

Gerrit L. ten Kate, Gert-Jan R. ten Kate, Stijn C.H. van den Oord, Admir Dedic, Anoeshka S Dharampal, Koen Nieman, Pim J. de Feyter, Eric J.G. Sijbrands, Antonius F.W. van der Steen, Arend F.L. Schinkel

Am J Cardiol. 2013; 111(9):1305-1310



ABSTRACT

Patients with familial hypercholesterolemia (FH) are at markedly increased risk of developing premature coronary artery disease. The objective of the present study was to evaluate the role of carotid ultrasonography as a measure of subclinical coronary artery disease in patients with FH. The present prospective study compared the presence of subclinical carotid and coronary artery disease in 67 patients with FH (mean age 55 ± 8 years, 52% men) to that in 30 controls with nonanginal chest pain (mean age 56 ± 9 years, 57% men). The carotid intima-media thickness and carotid plaque burden were assessed using B-mode ultrasonography, according to the Mannheim consensus. Coronary artery disease was assessed using computed tomographic coronary angiography. A lumen reduction $>50\%$ was considered indicative of obstructive coronary artery disease. The patients with FH and the controls had a comparable carotid intima-media thickness (0.64 vs 0.66 mm, $p = 0.490$), prevalence of carotid plaque (93% vs 83%, $p = 0.361$), and median carotid plaque score (3 vs 2, $p = 0.216$). Patients with FH had a significantly greater median coronary calcium score than did the controls (62 vs 5, $p = 0.015$). However, the prevalence of obstructive coronary artery disease was comparable (27% vs 31%, $p = 0.677$). No association was found between the carotid intima-media thickness and coronary artery disease. An association was found between the presence of carotid plaque and coronary artery disease in the patients with FH and the controls. The absence of carotid plaque, observed in 5 patients (7%) with FH, excluded the presence of obstructive coronary artery disease. In conclusion, the patients with FH had a high prevalence of carotid plaque and a significantly greater median coronary calcium score than did the controls. A correlation was found between carotid plaque and coronary artery disease in patients with FH; however, the presence of carotid plaque and carotid plaque burden are not reliable indicators of obstructive coronary artery disease.

INTRODUCTION

Heterozygous familial hypercholesterolemia (FH) is an autosomal dominantly inherited disorder of the lipid metabolism causing severely increased serum levels of low-density lipoprotein (LDL) cholesterol. Patients with FH are at a markedly increased risk of developing premature coronary artery disease.¹⁻³ The introduction of statin therapy has significantly improved the outcome of patients with FH⁴; however, these patients can still present with myocardial infarction at a relatively young age. The traditional risk prediction models fail to fully recognize the risk of future cardiovascular events in patients with FH. Noninvasive imaging studies allow early detection and quantification of subclinical atherosclerosis and might improve risk assessment.^{5,6} The current American College of Cardiology Foundation/American Heart Association guidelines have recommended the use of ultrasonography for measurement of the carotid intima-media thickness (CIMT) and detection of carotid plaque to assess the cardiovascular risk in asymptomatic patients at intermediate risk of cardiovascular events.⁷ Recent data have indicated that the carotid plaque burden correlates more strongly with the coronary artery calcium score than other tests, including the CIMT.⁶ Currently, information on the relation between carotid and coronary artery disease in patients with FH is not available. The objective of the present study was to evaluate the role of carotid ultrasonography as a measure of subclinical coronary artery disease in patients with FH.

METHODS

The local ethical committee approved the study protocol, and all study participants provided informed consent. The present prospective study compared the presence of subclinical carotid and coronary artery disease in 67 patients with FH to that in 30 controls with nonanginal chest pain from the outpatient clinics of vascular medicine and cardiology at a university medical center. The CIMT and carotid plaque burden were assessed using B-mode ultrasonography, and coronary artery disease was assessed using computed tomographic coronary angiography (CTCA). Patients were asked to participate in the present study if they were asymptomatic, had no known cardiovascular disease, and had an increased cardiovascular risk profile. The inclusion criteria were FH or the presence of ≥ 1 other clinical risk factor for atherosclerosis and an inclusion age of 45 to 70 years for women and 40 to 70 years for men. The exclusion criteria for CTCA were renal insufficiency (serum creatinine $>120 \mu\text{mol/L}$), known contrast allergy, and irregular heart rhythm (atrial fibrillation).

FH was diagnosed according to the criteria by van Aalst-Cohen et al.⁸ The criteria can be summarized as the presence of a documented LDL receptor mutation or an LDL

cholesterol level >95th percentile for gender and age combined with the presence of typical tendon xanthomas in the patient or a first-degree relative; an LDL cholesterol level >95th percentile for gender and age in a first-degree relative; or proven coronary artery disease in the patient or a first-degree relative aged <60 years.

The control group consisted of 30 patients referred for CTCA for the evaluation of coronary atherosclerosis. The Diamond classification⁹ was used to select the patients presenting with chest pain complaints atypical for cardiovascular disease. Patients with chest pain or discomfort were eligible for inclusion if they met ≤ 1 of the following typical angina characteristics: substernal chest pain or discomfort provoked by exertion or emotional stress and relieved by rest and/or nitroglycerin.

Carotid ultrasonography, including Doppler, was performed with a Philips iU-22 ultrasound system (Philips Medical Systems, Bothell, WA), equipped with an L9-3 transducer. Image acquisition was performed using a standard scanning protocol according to the American Society of Echocardiography consensus statement.¹⁰ In brief, the left and right carotid arteries were both examined with the patient in a supine position with the head supported at a 45° angle and turned to the contralateral side. The left and right common carotid arteries, carotid bifurcation, internal carotid artery, external carotid artery, and vertebral arteries were imaged using B-mode ultrasonography, color Doppler, and pulse-wave Doppler. All anatomic sites were examined from different angles of view, and each site was scanned in the cross-sectional and longitudinal views. Each side was extensively evaluated for the presence of carotid plaque.

The carotid ultrasound studies were reviewed offline by 2 independent observers who were unaware of the clinical data. Discrepancies in their evaluation were resolved by consensus. In accordance with previously published studies, the CIMT was measured in the far wall of the distal 1 cm of the common carotid artery.¹¹ A semiautomated CIMT measurement was performed using Qlab quantification software (Philips Healthcare, Best, The Netherlands). For each side, the CIMT measurement was performed 3 times on selected still frames on different R peaks of the electrocardiographic signal. The mean value of 3 measurements from the left and right carotid arteries was used in additional statistical analysis. Carotid plaque screening was performed using the standard carotid ultrasound images and color Doppler clips. Atherosclerotic plaque was defined as a focal structure encroaching into the lumen of ≥ 0.5 mm or $\geq 50\%$ of the surrounding CIMT or demonstrating a thickness >1.5 mm, as measured from the media-adventitia interface to the intima-lumen interface.¹² The presence of plaque was recorded for each side. Stenosis severity was assessed using the criteria from the Society of Radiologists in Ultrasound.¹³ In brief, abnormal CIMT or plaque and a peak systolic velocity <125 cm/s were considered indicative of $<50\%$ diameter stenosis; plaque and a peak systolic velocity of 125 to 230 cm/s as 50% to 69% stenosis; and plaque and peak systolic velocity >230 cm/s as $\geq 70\%$ stenosis. No detectable patent lumen and no flow at spectral, power,

and color Doppler were considered indicative of total occlusion. The carotid artery was divided into 4 segments (common carotid, bifurcation, internal carotid, and external carotid). The plaque thickness was measured, and the segments were divided into 4 categories: 0, no plaque; 1, <2.5 mm; 2, 2.5 - 3.5 mm; and 3, >3.5-mm plaque. Summing the score of all segments gave the carotid plaque score.

All computed tomographic scans were performed with a dual-source scanner (Somatom Definition, Siemens Medical Solutions, Forchheim, Germany). For the non-enhanced scan, a prospective electrocardiographically triggered scan protocol was applied. The computed tomographic coronary angiographic scan protocol, contrast protocol, and reconstruction procedure have been described previously.¹⁴ In brief, CTCA was obtained using a retrospective electrocardiographic-gated scan protocol with optimal heart rate-dependent electrocardiographic pulsing to lower the radiation dose. The maximum tube current was 380 mA, and the tube voltage was 120 kV. Just before the scan, all patients received nitroglycerin (0.4 mg/dose) sublingually. An iodinated contrast agent (Ultravist 370 mg/ml, Schering AG, Berlin, Germany), with a scan-time dependent volume (94 ml, range 80 to 100), was administered for enhancement of the coronary arteries. The calcium score data sets were reconstructed with a slice thickness of 3 mm and an increment of 1.5 mm at 70% of the RR interval. The computed tomographic coronary angiographic data sets were reconstructed using a slice thickness of 0.75 mm and an increment of 0.4 mm at an automatically or manually determined optimal phase of the RR interval. The data sets were sent to a dedicated workstation (MMWP, Siemens Medical Solutions, Forchheim, Germany). Two readers, unaware of the carotid ultrasound and clinical data, analyzed the computed tomographic scans. Discrepancies in their evaluations were resolved by consensus. The coronary calcium score (CCS) was calculated semiautomatically using dedicated software and expressed as the Agatston score per patient.¹⁵ Coronary plaque was defined as a separate structure within the vessel wall that could be clearly distinguished from the contrast-enhanced lumen and the surrounding pericardial tissue. For each segment, using the American Heart Association 16-segment model, the absence or presence of a coronary plaque was determined, as was the severity of the lumen narrowing. Obstructive coronary artery disease was defined as the presence of a >50% diameter stenosis. The coronary plaque burden was assessed using a segment involvement score (summing the number of segments containing plaque >20% lumen stenosis) and a coronary artery disease extent score (summing the segments with plaque weighted for the stenosis severity; 0%, 0; 0% to 20%, 1; 20% to 50%, 2; 50% to 70%, 3, >70%, 4).

The statistical analyses were performed using SPSS, version 17.0 (SPSS, Chicago, Illinois). Continuous variables are presented as the mean \pm SD or median and interquartile range. Categorical variables are expressed as numbers and percentages. The percentages were rounded. The Student *t* test was used to compare continuous variables.

The chi-square test was used to compare the categorical variables. The correlation of carotid ultrasound and coronary artery disease was evaluated using Spearman's rank correlation coefficient. Because of the non-normal distribution, the nonparametric Mann-Whitney U test was used to compare the CIMT and carotid plaque score with the CCS, segment involvement score, and coronary artery disease extent score between the 2 groups. Receiver operating characteristic curves and the area under the curve were used to determine the optimal cutoff values of the carotid plaque sum for the prediction of a CCS >100 or the presence of obstructive coronary artery disease. The optimal cutoff value was that that yielded the greatest sum of sensitivity and specificity. p Values <0.05 were considered statistically significant.

RESULTS

The patient characteristics are listed in Table 1. The gender distribution and mean age were comparable between the patients with FH and the controls. As expected, the patients with FH had significantly greater total cholesterol and LDL cholesterol levels

Table 1. Patient characteristics

| Variable | FH (n = 67) | Control (n = 30) | p Value |
|--|----------------------|----------------------|---------|
| Men | 35 (52%) | 17 (57%) | 0.686 |
| Age (years) | 55 ± 7.8 | 56 ± 9.4 | 0.636 |
| Smoker | 31 (46%) | 18 (60%) | 0.211 |
| Hypertension | 16 (24%) | 11 (37%) | 0.194 |
| Diabetes mellitus | 2 (3%) | 2 (7%) | 0.399 |
| Dyslipidemia | 66 (100%) | 6 (20%) | <0.001 |
| Family history of coronary disease | 47 (70%) | 13(43%) | 0.012 |
| Body mass index (kg/m ²) | 26 ± 3.7 | 27 ± 4.0 | 0.152 |
| Total cholesterol (mmol/L; mg/dL) | 5.7 ± 1.5; 220 ± 58 | 5.1 ± 1.1; 197 ± 43 | 0.031 |
| LDL cholesterol (mmol/L; mg/dL) | 3.8 ± 1.4; 147 ± 54 | 3.1 ± 1.1; 120 ± 43 | 0.030 |
| HDL cholesterol (mmol/L; mg/dL) | 1.6 ± 1.4; 62 ± 54 | 1.4 ± 0.4; 54 ± 15 | 0.407 |
| Triglycerides (mmol/L; mg/dL) | 1.3 ± 0.8; 115 ± 71 | 1.5 ± 1.2; 133 ± 106 | 0.368 |
| Greatest total cholesterol (mmol/L; mg/dL) | 10.2 ± 2.4; 394 ± 93 | 5.6 ± 1.2; 217 ± 46 | <0.001 |
| Statin medication | 67 (100%) | 14 (47%) | <0.001 |
| Duration of statin use (yrs) | 11 (7.7) | 2 (3.0) | <0.001 |
| Intensive statin treatment | 42 (63%) | 0 (0%) | <0.001 |
| Tendon xanthomas | 18 (27%) | NA | |
| Arcus cornealis | 19 (28%) | NA | |

Continuous data is expressed as mean ± SD and dichotomous data as n (%).

NA = not applicable

than the controls, although the patients with FH had received more frequent and more intensive statin treatment.

The results of carotid ultrasonography, CCS, and CTCA are summarized in Table 2. No complications occurred during carotid ultrasonography, and all studies were included in the analysis. The patients with FH and the controls had a comparable CIMT, prevalence of carotid plaque, and median carotid plaque score. CTCA failed because of contrast extravasation in 1 control patient; hence, the analyses concerning the coronary plaque burden included 29 controls. The patients with FH had a significantly greater median CCS than that of the controls (62 vs 5, $p = 0.015$). Additionally, the patients with FH were less likely to have a CCS of 0 (21% vs 47%, $p = 0.010$). The prevalence of obstructive coronary artery disease was comparable in the patients with FH and the controls (Table 2). The presence of obstructive 1-, 2-, or 3-vessel coronary artery disease did not differ between the patients with FH and the controls ($p = 0.965$). The coronary plaque burden, as assessed by the median segment involvement score and median coronary artery disease extent score, was comparable in the patients with FH and controls (3, interquartile range 0 to 8, vs 1, interquartile range 0 to 5, $p = 0.192$; and 10, interquartile range 2 to 16, vs 6, interquartile range 0 to 16, $p = 0.099$, respectively). In the 67 patients

Table 2. Non-invasive imaging results

| Variable | FH (n = 67) | Control (n = 30) | p Value |
|--|------------------|------------------|---------|
| Carotid ultrasound | | | |
| Median carotid intima media thickness (mm) | 0.64 (0.59-0.73) | 0.66 (0.60-0.78) | 0.490 |
| Any carotid plaque | 62 (93%) | 25 (83%) | 0.361 |
| Unilateral carotid plaque | 19 (28%) | 10 (33%) | 0.621 |
| Bilateral carotid plaque | 43 (64%) | 15 (50%) | 0.277 |
| Carotid stenosis $\leq 70\%$ | 0 (0%) | 0 (0%) | 1.000 |
| Median carotid plaque score | 3 (1-5) | 2 (1-4) | 0.216 |
| Computed tomography coronary angiography | | | |
| Median coronary calcium score | 62 (1-352) | 5 (0-219) | 0.015 |
| Coronary calcium score 0 | 14 (21%) | 14 (47%) | 0.010 |
| Coronary calcium score 1 – 100 | 23 (34%) | 8 (27%) | 0.455 |
| Coronary calcium score 101 – 400 | 15 (22%) | 6 (20%) | 0.792 |
| Coronary calcium score >400 | 15 (22%) | 2 (7%) | 0.060 |
| Any obstructive coronary disease | 18 (27%) | 8 (30%) | 0.667 |
| Single vessel disease >50% | 11 (17%) | 5 (19%) | 0.921 |
| 2 Vessel disease >50% | 5 (8%) | 3 (12%) | 0.639 |
| 3 Vessel disease >50% | 2 (3%) | 1 (4%) | 0.905 |
| Segment involvement score | 3 (0-6) | 1 (0-4) | 0.099 |
| Coronary artery disease extent score | 10 (2-16) | 6 (0-16) | 0.192 |

Continuous data are expressed as median (interquartile range) and dichotomous data as n (%).

with FH, the CIMT did not correlate with the CCS, segment involvement score, coronary artery disease extent score, or obstructive coronary artery disease ($r = 0.18$, $r = 0.15$, $r = 0.17$, $r = 0.05$, respectively, $p = \text{NS}$ for all). A statistically significant correlation was found between the carotid plaque score and coronary artery disease, as expressed by the CCS, segment involvement score, coronary artery disease extent score, and $>50\%$ coronary stenosis ($r = 0.54$, $r = 0.55$, $r = 0.54$, $r = 0.28$, respectively, $p < 0.05$ for all).

The predictive values of the presence of carotid plaque in the diagnosis of obstructive coronary artery disease and for the prediction of a CCS >100 in the 67 patients with FH are summarized in Table 3. The absence of carotid plaque, observed in 5 patients with FH (7%), excluded the presence of obstructive coronary artery disease. The presence of carotid plaque had a low positive predictive value for the presence of an obstructive coronary plaque. The predictive values of the carotid plaque score in the diagnosis of obstructive coronary artery disease and for the prediction of a CCS >100 in the patients with FH are summarized in Table 4. Receiver operating characteristic curve analysis demonstrated that a carotid plaque sum >1.5 was related to a high likelihood of obstructive coronary artery disease. This carotid plaque sum value of >1.5 had the greatest sensitivity and specificity (94% and 35%, respectively) for diagnosing obstructive coronary artery disease. The receiver operating characteristic curve analysis also showed that a carotid plaque sum >4.5 had the greatest sensitivity and specificity to predict a CCS >100 .

Table 3. Predictive value of carotid plaque for the presence of coronary stenosis $>50\%$ or a coronary calcium score >100 in patients with FH ($n = 67$).

| Carotid plaque | Coronary stenosis $>50\%$ * | | Coronary calcium score [†] | |
|----------------|-----------------------------|----------|-------------------------------------|------------|
| | Yes | No | >100 | ≤ 100 |
| Yes | 18 (27%) | 44 (66%) | 29 (43%) | 33 (49%) |
| No | 0 (0%) | 5 (7%) | 1 (1%) | 4 (6%) |

NPV = negative predictive value; PPV = positive predictive value.

* Sensitivity 100%, specificity 10%, PPV 29%, NPV 100%.

† Sensitivity 97%, specificity 11%, PPV 47%, NPV 80%.

Table 4. Predictive value of carotid plaque score for the presence of a coronary stenosis $>50\%$ or a coronary calcium score >100 in patients with FH ($n = 67$).

| Carotid plaque score | Coronary stenosis $>50\%$ * | | Carotid plaque score | Coronary calcium score [†] | |
|----------------------|-----------------------------|----------|----------------------|-------------------------------------|------------|
| | Yes | No | | >100 | ≤ 100 |
| >1.5 | 17 (25%) | 32 (48%) | >4.5 | 16 (24%) | 7 (10%) |
| ≤ 1.5 | 1 (1%) | 17 (25%) | ≤ 4.5 | 14 (21%) | 30 (45%) |

NPV = negative predictive value; PPV = positive predictive value.

* Sensitivity 95%, specificity 35%, PPV 35%, NPV 94%.

† Sensitivity 53%, specificity 81%, PPV 70%, NPV 68%

DISCUSSION

The results of the present study have demonstrated that patients with FH have a high prevalence of subclinical carotid and coronary artery disease, even after long-term intensive treatment with statin therapy. The carotid plaque burden, assessed using carotid ultrasonography, was associated with the presence of obstructive coronary artery disease. This association was observed in both patients with FH and a control group of patients with nonanginal chest pain. The patients with FH had a significantly greater median CCS than did the controls. However, in both patient groups, the presence of carotid plaque and carotid plaque burden on the carotid ultrasound scans were not reliable indicators of obstructive coronary artery disease.

Previous studies have demonstrated that patients with FH have an increased CIMT and a high prevalence of carotid plaque.^{16,17} Long-term statin therapy might normalize CIMT in patients with FH^{17,18} and retard the progression of carotid plaque growth.^{19,20} In the present study, the patients with FH had received statin therapy for a mean period of 11 ± 7.8 years; nevertheless, the prevalence of carotid plaque was very high (93%). This prevalence was significantly greater than that previously reported,²¹ despite the relatively young age of our patients (mean age 55 ± 8 years). The greater prevalence of carotid plaque might have been caused by several factors. Previous reports studying the effect of statin therapy on carotid plaque had a limited follow-up duration after the initiation of therapy. In contrast, the present population was studied an average of 11 ± 7.8 years after the initiation of therapy. During this period, the natural progression of carotid and coronary artery disease could have occurred, despite the use of statin therapy. The present study was performed in a referral center for patients with FH, and these patients might have had an increased cardiovascular risk profile. Finally, in the present study, an extensive carotid ultrasound study was performed, and each carotid artery was carefully evaluated for the presence of plaque. The high prevalence of carotid plaque and coronary artery disease in the present study draw attention to the high risk of cardiovascular events for these patients. These findings also demonstrate the need for novel (additional) therapies for patients with FH targeted at the prevention or stabilization of atherosclerotic plaques and decreasing the risk of cardiovascular events.

A meta-analysis of population-based studies demonstrated a statistically significant, but clinically not important, relation between CIMT and coronary artery disease.²² For individual patients, the assessment of carotid plaque is probably a better predictor of the cardiovascular outcome. The relation between carotid plaque burden and coronary artery disease is substantially stronger.⁶ Currently, information on the association between carotid and coronary artery disease in patients with FH is limited. Patients with FH have increased serum LDL cholesterol levels, even during long-term statin therapy, leading to premature carotid and coronary artery disease. These patients are at increased

risk of cardiovascular events at a relatively young age.¹⁻⁴ Asymptomatic patients with FH might benefit from noninvasive imaging techniques to identify those with subclinical disease and to initiate additional preventive measures and therapy at an early stage. The carotid arteries are easily accessible for noninvasive evaluation; therefore, the objective of the present study was to evaluate the role of carotid ultrasonography as a measure of subclinical coronary artery disease in patients with FH. An accurate predictor of coronary artery disease could be helpful in the selection of patients for CTCA or invasive coronary angiography. This could be particularly relevant in young patients and those with an increased risk of contrast medium-induced renal failure. The present study has demonstrated a correlation between carotid plaque and coronary artery disease in patients with FH; however, the presence of carotid plaque and carotid plaque burden were not reliable indicators of obstructive coronary artery disease. Therefore, the clinical applicability of carotid ultrasonography as a selection tool for CTCA was limited in this population.

The present study had several limitations. First, the number of patients and controls was relatively small. Second, carotid ultrasonography provides a 2-dimensional view of the vessel lumen, making this technique operator dependent. Third, the accuracy of CTCA for the detection of small coronary plaques, in particular, in the distal coronary arteries, is limited. Fourth, the degree of coronary stenosis using CTCA can be difficult to assess near heavily calcified plaques. Finally, additional studies are needed to test whether the use of carotid ultrasonography improves the selection of patients for CTCA or invasive coronary angiography and whether the use of carotid ultrasonography results in better patient outcomes.

REFERENCES

1. Marks D, Thorogood M, Neil HAW, Humphries SE. A review on the diagnosis, natural history, and treatment of familial hypercholesterolaemia. *Atherosclerosis*. 2003;168(1):1-14.
2. Austin MA, Hutter CM, Zimmern RL, Humphries SE. Familial hypercholesterolemia and coronary heart disease: A HuGE association review. *Am J Epidemiol*. 2004;160(5):421-9.
3. Scientific Steering Committee on behalf of the Simon Broome Register Group. Risk of fatal coronary heart disease in familial hypercholesterolaemia. *BMJ*. 1991;303(6807):893-6.
4. Elis A, Zhou R, Stein EA. Effect of Lipid-Lowering Treatment on Natural History of Heterozygous Familial Hypercholesterolemia in Past Three Decades. *Am J Cardiol*. 2011;108(2):223-6.
5. Nguyen-Thanh HT, Benzaquen BS. Screening for Subclinical Coronary Artery Disease Measuring Carotid Intima Media Thickness. *Am J Cardiol*. 2009;104(10):1383-8.
6. Sillesen H, Muntendam P, Adourian A, Entrekin R, Garcia M, Falk E, et al. Carotid Plaque Burden as a Measure of Subclinical Atherosclerosis: Comparison With Other Tests for Subclinical Arterial Disease in the High Risk Plaque Biolmage Study. *JACC Cardiovascular Imaging*. 2012;5(7):681-9.
7. Greenland P, Alpert JS, Beller GA, Benjamin EJ, Budoff MJ, Fayad ZA, et al. ACCF/AHA Guideline for assessment of cardiovascular risk in asymptomatic adults: A report of the American College of Cardiology Foundation/American Heart Association task force on practice guidelines. *J Am Coll Cardiol*. 2010;56(25):e50-103.
8. van Aalst-Cohen ES, Jansen ACM, Tanck MWT, Defesche JC, Trip MD, Lansberg PJ, et al. Diagnosing familial hypercholesterolaemia: the relevance of genetic testing. *Eur Heart J*. 2006;27(18):2240-6.
9. Diamond GA. A clinically relevant classification of chest discomfort. *J Am Coll Cardiol*. 1983;1:574-5.
10. Stein JH, Korcarz CE, Hurst RT, Lonn E, Kendall CB, Mohler ER, et al. Use of carotid ultrasound to identify subclinical vascular disease and evaluate cardiovascular disease risk: A consensus statement from the american society of echocardiography carotid intima-media thickness task force endorsed by the society for vascular medicine. *J Am Soc Echocardiogr*. 2008;21(2):93-111.
11. Montauban van Swijndregt AD, The SHK, Gussenhoven EJ, Lancee CT, Rijsterborgh H, de Groot E, et al. An in vitro evaluation of the line pattern of the near and far walls of carotid arteries using B-mode ultrasound. *Ultrasound Med Biol*. 1996;22(8):1007-15.
12. Touboul PJ, Hennerici MG, Meairs S, Adams H, Amarenco P, Bornstein N, et al. Mannheim carotid intima-media thickness consensus (2004–2006). An update on behalf of the Advisory Board of the 3rd and 4th Watching the Risk Symposium, 13th and 15th European Stroke Conferences, Mannheim, Germany, 2004, and Brussels, Belgium, 2006. *Cerebrovasc Dis*. 2007;23(1):75-80.
13. Grant EG, Benson CB, Moneta GL, Alexandrov AV, Baker JD, Bluth EI, et al. Carotid artery stenosis: gray-scale and Doppler US diagnosis—Society of Radiologists in Ultrasound Consensus Conference. *Radiology*. 2003;229(2):340-6.
14. Neefjes LA, ten Kate GJR, Rossi A, Galema-Boers AJ, Langendonk JG, Weustink AC, et al. CT coronary plaque burden in asymptomatic patients with familial hypercholesterolaemia. *Heart*. 2011;97(14):1151-7.
15. Agatston AS, Janowitz WR, Hildner FJ, Zusmer NR, Viamonte M, Detrano R. Quantification of coronary artery calcium using ultrafast computed tomography. *J Am Coll Cardiol*. 1990;15(4):827-32.
16. Wendelhag I, Wiklund O, Wikstrand J. Atherosclerotic changes in the femoral and carotid arteries in familial hypercholesterolemia. Ultrasonographic assessment of intima-media thickness and plaque occurrence. *Arterioscler Thromb Vasc Biol*. 1993;13(10):1404-11.

17. Nolting PRW, de Groot E, Zwinderman AH, Buirma RJA, Trip MD, Kastelein JJP. Regression of carotid and femoral artery intima-media thickness in familial hypercholesterolemia: Treatment with simvastatin. *Arch Intern Med.* 2003;163(15):1837-41.
18. Sivapalaratnam S, van Loendersloot LL, Hutten BA, Kastelein JJP, Trip MD, de Groot E. Long-term LDL-c lowering in heterozygous familial hypercholesterolemia normalizes carotid intima-media thickness. *Atherosclerosis.* 2010;212(2):571-4.
19. Ainsworth CD, Blake CC, Tamayo A, Beletsky V, Fenster A, Spence JD. 3D Ultrasound measurement of change in carotid plaque volume: A tool for rapid evaluation of new therapies. *Stroke.* 2005;36(9):1904-9.
20. Corti R, Fuster V, Fayad ZA, Worthley SG, Helft G, Smith D, et al. Lipid lowering by simvastatin induces regression of human atherosclerotic lesions: Two years' follow-up by high-resolution noninvasive magnetic resonance imaging. *Circulation.* 2002;106(23):2884-7.
21. Tonstad S, Joakimsen O, Stensland-Bugge E, Ose L, Bønaa K, Leren T. Carotid intima-media thickness and plaque in patients with familial hypercholesterolaemia mutations and control subjects. *Eur J Clin Invest.* 1998;28(12):971-9.
22. Den Ruijter HM, Peters SE, Anderson TJ, Britton AR, Dekker JM, Eijkemans MJ, et al. Common carotid intima-media thickness measurements in cardiovascular risk prediction: A meta-analysis. *JAMA.* 2012;308(8):796-803.



PART III

TECHNICAL INNOVATIONS
IN PLAQUE IMAGING





Chapter 7

Far-Wall Pseudoenhancement During Contrast-Enhanced Ultrasound of the Carotid Arteries: Clinical Description and in Vitro Reproduction

Gerrit L. ten Kate, Guillaume G.J. Renaud, Zeynettin Akkus, Stijn C.H. van den Oord, Folkert J. ten Cate, Vijay Shamdasani, Rob R Entrekin, Eric J.G. Sijbrands, Nico de Jong, Johan G. Bosch, Arend F.L. Schinkel, Antonius F.W. van der Steen

Ultrasound Med Biol. 2012; 38(4):593-600



ABSTRACT

The present study describes the presence of pseudoenhancement during contrast-enhanced ultrasound (CEUS) imaging of human carotid arteries and the reproduction of this pseudoenhancement *in vitro*. 70 Patients underwent bilateral CEUS examination of the carotid arteries using a Philips iU22 ultrasound system equipped with a L9-3 ultrasound probe and SonoVue microbubble contrast. During CEUS of the carotid arteries we identified enhancement in close proximity to the far wall, parallel to the main lumen. The location of this enhancement does not correlate to the anatomical location of a parallel vessel. To corroborate the hypothesis that this is a pseudoenhancement artifact the enhancement was recreated in a tissue-mimicking material phantom, using the same ultrasound system, settings and contrast agent as the patient study. The phantom study showed that pseudoenhancement may be present during vascular CEUS and that the degree of pseudoenhancement is influenced by the size and concentration of the microbubbles. During vascular CEUS identification of the artifact is important to prevent misinterpretation of enhancement in and near the far wall.

INTRODUCTION

Contrast-enhanced ultrasound (CEUS) is increasingly used to noninvasively evaluate macrovasculature and microvasculature. CEUS has recently gained interest as a technique for improving the accuracy of vascular ultrasound examinations. Ultrasound contrast agents are used to enhance the echo signal of blood, thus improving the vessel-wall delineation and the evaluation of atherosclerotic plaques, ulcerations and stenosis.¹ CEUS has also been shown to improve intima-media thickness measurements and can be used to identify intraplaque vasa vasorum, which are associated with plaque vulnerability.²⁻⁴

During CEUS investigations of the carotid arteries we observed enhancement parallel to the lumen in close proximity to the arterial wall opposite the ultrasound probe, i.e. the far wall. The location of this enhancement does not correspond with the anatomical location of a parallel vessel. Although there have been previous reports of pseudoenhancement in regions without vasculature due to the nonlinear propagation of the ultrasound beam through contrast agent⁵⁻⁷, there have been no reports of pseudoenhancement during vascular CEUS. The present study describes enhancement in the proximity of the far wall during clinical CEUS studies of human carotid arteries. To support the hypothesis that this is a pseudoenhancement artifact we reproduce the enhancement *in vitro*.

MATERIAL AND METHODS

Patient study

The patient study was approved by the Medical Ethics Committee at the Erasmus University Medical Center. All patients provided written informed consent. From April until October 2010, 70 adult patients with ≥ 1 cardiovascular risk factor (hypercholesterolemia, diabetes, hypertension, smoking and/or family history of cardiovascular disease) were recruited from the local outpatient clinic. Patients with unstable clinical symptoms or known allergies to ultrasound contrast agents were excluded.

All patients underwent bilateral standard ultrasound and CEUS examination of the carotid arteries. During the examination they were placed in a supine position with their head turned to the contralateral side from the vessel under investigation. After completion of the standard ultrasound protocol, CEUS was performed. The contrast agent (SonoVue; Bracco SpA., Milan, Italy) was injected through a catheter in the antecubital vein. A bolus of 0.5 - 1.0 ml was injected followed by a 2 ml saline flush. Contrast injections were repeated throughout the examination, with a maximum total dose of 10 ml. Cine loop acquisition was started when an increase in contrast enhancement was observed.

All patient studies were reviewed by three investigators (GtK, SvdO and AS) blinded to the patient's medical history. Pseudoenhancement was defined by three characteristics. First it was always present near the far wall and parallel to the main lumen. Secondly, its appearance was synchronized with the inflow of contrast in the lumen. Finally it presented as a speckle pattern which remained stationary throughout the cine loop, only increasing and decreasing in intensity with the intensity of lumen enhancement.

Phantom study

A phantom vessel was constructed from an agar-based tissue-mimicking material, previously described by Teirlinck et al.⁸ Scattering particles (silicon carbide and aluminum oxide powder) were added to provide an ultrasound attenuation of 0.5 dB/cm/MHz in the frequency range 4-6 MHz. The phantom vessels consisted of two vertical cylindrical cavities (13mm and 15mm in diameter) in a cube (10x10 cm) of tissue-mimicking material. The vessels were located 1.5 cm from the lateral surface. During the examination one vessel was filled with degassed water and used as a reference, while the other was filled with the microbubble contrast agent diluted in degassed water. A magnetic stirrer was used to prevent the bubbles from rising to the surface and to obtain a homogeneous mixture of microbubbles in the vessel.

Three dilutions (1:400, 1:2,000 and 1:10,000) of the contrast agent (SonoVue; Bracco SpA., Milan, Italy) were prepared in degassed water. A 1:2,000 dilution corresponds approximately to the dilution of the contrast agent in the vascular system during an *in-vivo* examination.⁹ Additionally, the dilutions were filtered through a mechanical filter, creating a solution containing microbubbles with a diameter <3 μm , as described by Emmer et al.¹⁰ Microbubbles <3 μm represent around 15% of the total volume occupied by a native bubble population of SonoVue.¹¹ The phantom vessels were imaged with degassed water only and the different dilutions of unfiltered (native) and filtered contrast agent.

Image acquisition

Both the patient and phantom study were performed using the same Philips iU22 ultrasound system (Philips Healthcare, Best, the Netherlands) equipped with a linear-array L9-3 MHz probe. CEUS examinations were performed using a tissue-suppressing contrast mode with a 3-pulse amplitude-modulation sequence at a low mechanical index (MI) of 0.06. Using the side-by-side contrast functionality, images of the contrast and the fundamental B-mode were obtained simultaneously. Longitudinal and transversal images of all patient and phantom vessels were obtained and stored as cine loops according to the digital imaging and communications in medicine (DICOM) standard for later analysis. In the patient study, to destroy the contrast agent present and to evaluate the inflow of new contrast as it refilled the carotid lumen and surrounding microvasculature, a high MI (0.75) flash of 3 frames was given during cine-loop acquisition. During the

phantom study radio frequency data was collected and band-pass filtered to evaluate the pseudoenhancement at the fundamental (3.5 MHz) and second-harmonic (7 MHz) frequency.

RESULTS

Patient study

General patient characteristics are listed in Table 1. The contrast images showed a clear enhancement of the carotid lumen. Enhancement in proximity to the far wall of the artery was present in all patients. Figures 1 and 2 show examples of enhancement in proximity to the far wall, which was present in all patients. The longitudinal images showed an enhancement parallel to the main lumen. The transverse images showed a more or less triangular pattern of enhancement. The far wall enhancement coincides with high echogenicity on the B-mode images, more echogenic areas showed stronger enhanced far wall regions in the contrast mode than echolucent areas (Figure 1). When insonifying the vessels from a different angle the enhancement remained present at the far wall, indicating the enhancement is not associated with an anatomical structure. The intensity of enhancement at the far wall is synchronized with the intensity of contrast enhancement in the lumen (Figure 3). Peak enhancement in the lumen and the far wall are reached at the same time after contrast injection.

Table 1. Patient characteristics. Continuous data are expressed as mean \pm standard deviation, categorical variables are expressed by absolute and relative frequencies.

| Characteristic | N=70 |
|-------------------------------|------------|
| Age, years | 54 \pm 8 |
| Male gender | 38 (54%) |
| BMI | 27 \pm 4 |
| Dyslipidemia | 67 (96%) |
| Familial Hypercholesterolemia | 56 (80%) |
| Diabetes mellitus | 5 (7%) |
| Hypertension | 15 (21%) |
| Smoking | 13 (19%) |
| Former smoking | 23 (33%) |

Phantom study

After injection of the native contrast agent in the phantom vessel hardly any enhancement was observed in the far wall (Figure 4). This was independent of the dilution of the

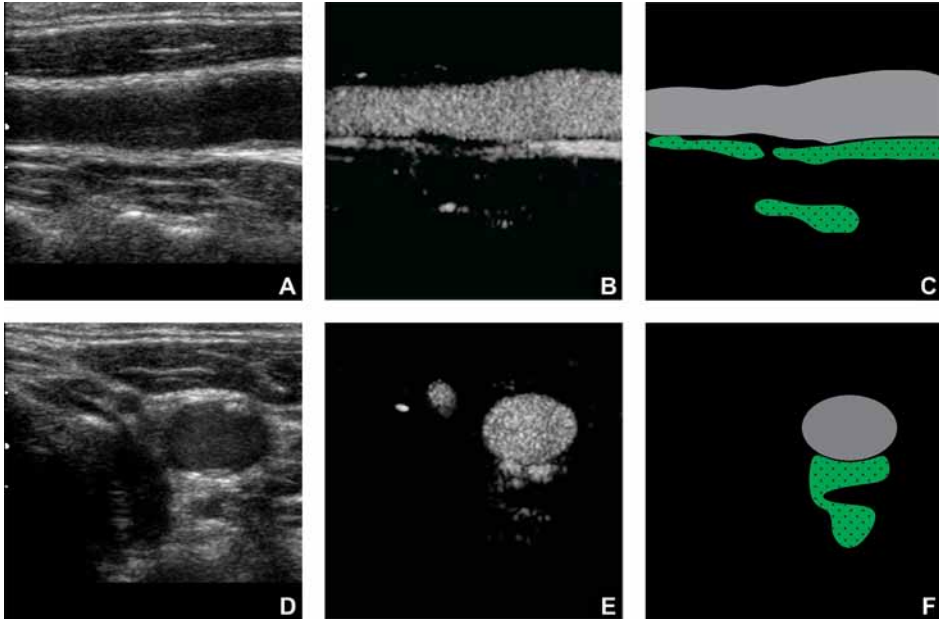


Figure 1. Carotid artery B-mode (Panel A and D) and contrast enhanced (Panel B and E) ultrasound images in a representative patient. The schematic representations (Panel C and F) show the location of the pseudoenhancement in green. Additionally it can be observed that the intensity of the pseudoenhancement correlates with echogenic locations on the B-mode images.

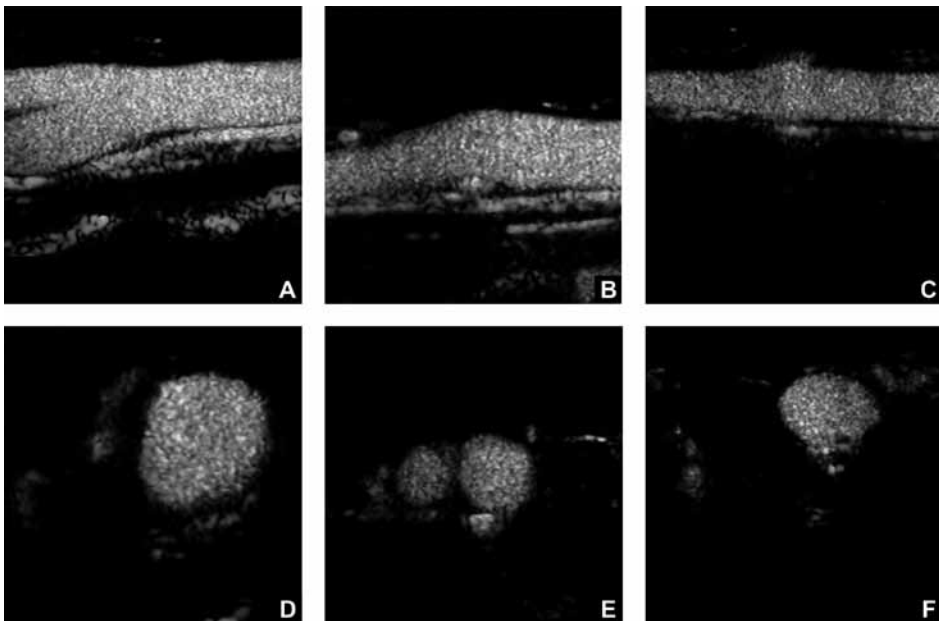


Figure 2. Longitudinal (Panel A-C) and transverse (Panel D-F) contrast enhanced ultrasound images of 3 patients. In all patients pseudoenhancement can be observed parallel to the main lumen.

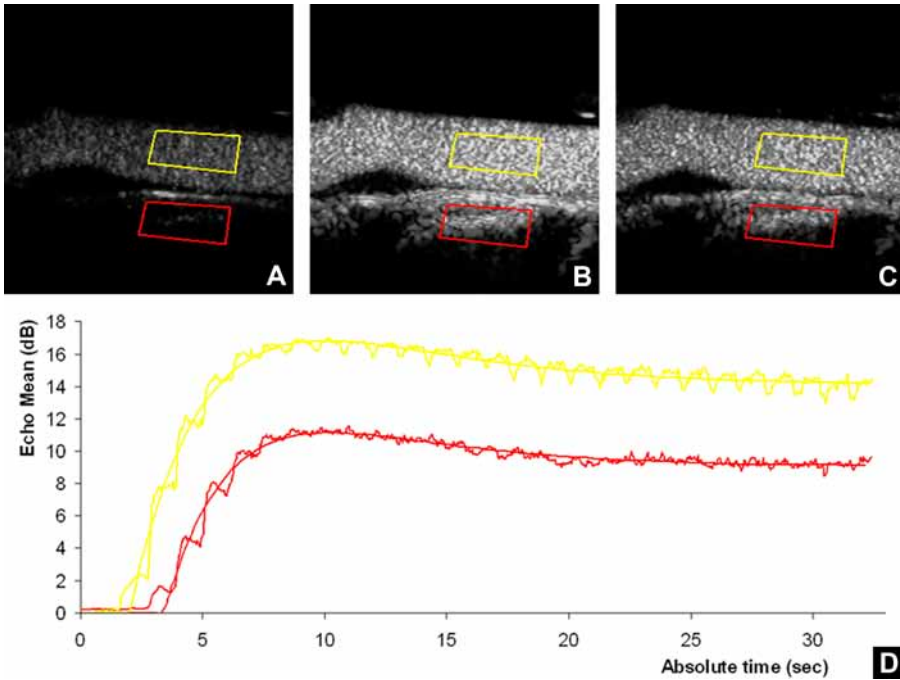


Figure 3. Three longitudinal images (Panel A-C) in the same patient acquired at 4, 9 and 22 seconds after contrast injection and the time intensity curves (Panel D) for a region of interest in the lumen (Yellow) and far wall (Red). The region of interest in the far wall has been placed away from the lumen to prevent direct interaction with the lumen enhancement. A clear association can be observed between the intensity of enhancement in the lumen and the artifact.

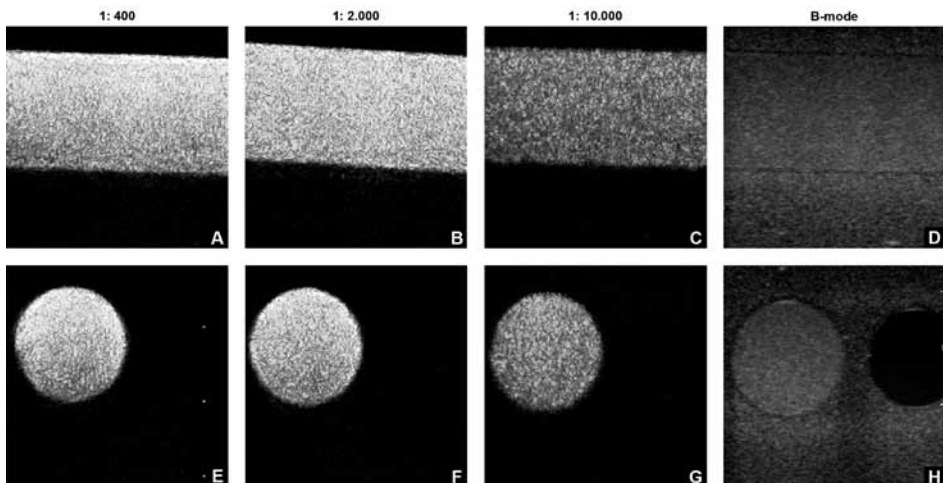


Figure 4. Longitudinal (Panel A-D) and transverse (Panel E-H) images of the phantom, imaged with native contrast agent in different dilutions and a corresponding B-mode image. On the transverse images, the right vessel is filled with degassed water only. A very limited amount of pseudoenhancement can be observed in the 1:2,000 dilution. The other dilutions show hardly any pseudoenhancement.

contrast agent. After injection of the filtered contrast agent, enhancement in the far wall was observed in both the longitudinal and transverse images (Figure 5). The longitudinal images showed an enhancement parallel to the vessel and the transverse images showed enhancement in a triangular pattern. The intensity of the enhancement was dependent on the concentration of the filtered microbubbles with the highest concentration producing the highest enhancement. Band-pass filtering of the radio frequency data revealed that pseudoenhancement was present at both the fundamental and the second harmonic frequency (Figure 6).

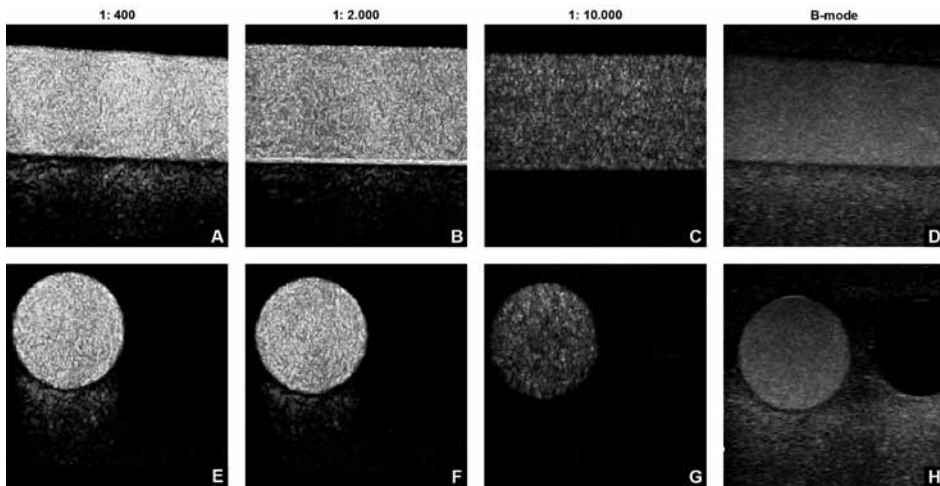


Figure 5. Longitudinal (Panel A-D) and transverse (Panel E-H) images of the phantom, imaged with filtered ($<3\ \mu\text{m}$ microbubbles) contrast agent in different dilutions and a corresponding B-mode image. On the transverse images the right vessel is filled with degassed water only. Clear pseudoenhancement can be observed in both the 1:400 and 1:2,000 dilutions. The strongest pseudoenhancement is present in the 1:400 dilution. The 1:10,000 dilution shows hardly any pseudoenhancement.

DISCUSSION

Patient study

The main finding of this study is that enhancement is present parallel to the far wall of the carotid artery in all patients. There are a number of reasons why we found this to be a pseudoenhancement artifact. First of all, a parallel vessel is unlikely, because the location of the enhancement is not in agreement with the anatomical localization of such a vessel. Moreover, anatomical variation would result in vessels that are not all exactly parallel to the carotid arteries in all patients. Secondly, insonification from a different angle would move a vessel out of view, while the enhancement stays in view during our examinations. Finally, it is unlikely that the enhancement is due to contrast

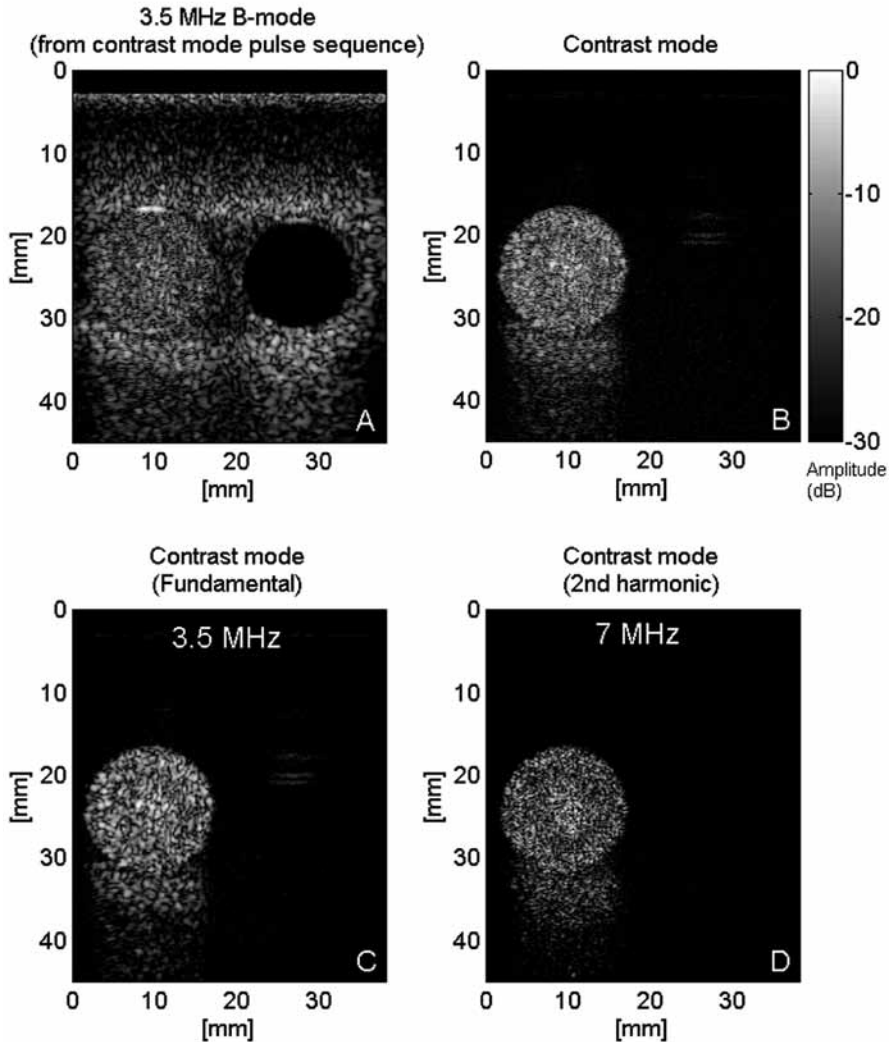


Figure 6. Transverse images of the phantom vessels. The left vessel is filled with the filtered contrast agent (1:2,000) and the right vessel is filled with water. Images were created from radio frequency data retrieved from the iU22 system in the contrast mode. Panel A shows the B-mode image created from the backscattered signals of one of the three transmitted pulses in the contrast mode. Panel B. shows the contrast mode image obtained when the single-amplitude backscattered signals are summed and subtracted from the double-amplitude pulse backscattered signals. Panel C and D show contrast mode images after band-pass frequency filtering around the fundamental frequency (3.5 MHz) and the second harmonic frequency (7 MHz) respectively.

agent present in the microvascular network in the adventitia (vasa vasorum), since the enhancement is limited to the far side of the vessel and the appearance is synchronized with the lumen contrast enhancement. If this was enhancement of the vasa vasorum it would wrap around the vessel in accordance with the anatomical distribution of vasa vasorum¹², and its appearance would later than the lumen enhancement due to the low flow velocities in the vasa vasorum and they origin which is predominantly from side branches, not the main lumen.¹³

Phantom study

The phantom study shows that it is possible to create pseudoenhancement at the far wall of the vessel (Figure 5). The presence of microbubbles outside the lumen of our phantom is impossible. The formation of this pseudoenhancement is dependent on the concentration and size of the microbubbles. Using native contrast agent the pseudoenhancement is hardly visible for any of the three concentrations investigated. Using filtered contrast agent ($< 3 \mu\text{m}$ microbubbles), enhancement parallel to the far wall of the phantom vessel is observed, with a similar shape as observed during the *in-vivo* study. The degree of enhancement is dependent on the concentration of the contrast agent, with high concentrations causing stronger enhancement.

Origins of the artifact

Microbubbles are nonlinear scatterers. Ideally a contrast image would only show the presence of these nonlinear scatterers (i.e. contrast agent), while linear scatterers (i.e. tissue) would be suppressed. However, during the propagation of an ultrasound wave through the human body nonlinear components build up in the wave. The magnitude of this nonlinearity (NL) is dependent on the medium (tissue, blood, microbubbles (the NL of the medium is expressed as the parameter B/A)), the travelled distance (e.g. for a plane wave in a weakly nonlinear situation the NL is 2 times higher at 4 cm than at 2 cm) and the acoustic pressure (quadratic related; 2 times higher pressure results in 4 times higher NL).

Normally during carotid imaging at low acoustic pressures ($MI < 0.15$) the NL created is very low. However, when contrast agent is present in the carotid artery the NL produced during propagation has been shown to be significant, even with the very low acoustic pressures used in this study ($MI 0.06$). This is due to an enormous increase in the B/A value when the vessel contains contrast agent. Wu and Tong¹⁴ reported B/A values to be more than 100 times higher than in soft tissues and blood.

Most common contrast detection methods (amplitude modulation, pulse inversion and combination of these¹⁵) extract the second harmonic component from the received signal. These received signals contain information on both the nonlinear scattering from microbubbles and the nonlinear propagation of ultrasound scattered by linear scatter-

ers. It is clear that if the nonlinear propagation is low, the presence of microbubbles will be shown by the presence of a second harmonic component in the signal. On the other hand if the propagation is highly nonlinear there will be a second harmonic component present even if the nonlinear scattering from microbubbles is zero. This can be interpreted wrongly as the presence of microbubbles.

A second nonlinear property of the contrast agent is the amplitude-dependent attenuation.^{10, 16-18} Microbubbles show thresholding, they only vibrate when they are insonified with an acoustic pressure above a threshold that varies, dependent on the bubble size and ultrasound frequency, between 20 and 150 kPa. This results in an acoustic amplitude-dependent attenuation.¹⁰ Consequently, when performing amplitude modulation the ratio between the transmitted pulses of single and double amplitude is altered during propagation through a vessel containing contrast agent. The linear scatterers behind the vessel will respond with signals of the same amplitude ratio and therefore can be misclassified as contrast agent.

Figure 6 illustrates the effect of nonlinear propagation and amplitude-dependent attenuation when ultrasound propagates through a suspension of contrast agent. It shows images of a phantom with 2 vessels. One vessel filled with contrast, the other one with water. Panel A show the B-mode image and Panel B the contrast image as acquired with amplitude modulation, in which the vessel with contrast shows a clear enhancement. Behind the vessel filled with contrast pseudoenhancement is present. The pseudoenhancement at the fundamental frequency (Panel C) is caused by both the NL propagation and amplitude-dependent attenuation. The NL propagation will also cause pseudoenhancement at the second harmonic frequency as can be seen in panel D.

The effect of nonlinear propagation and amplitude-dependent attenuation on the ultrasound wave propagating through contrast agent is dependent on the size distribution of the microbubbles in the contrast agent. Due to filtration the average resonance frequency (1.5 - 2 MHz for native SonoVue^{5, 6}) of the contrast agent will increase and come closer to the frequency used in our study (3.5 MHz). This results in a slight increase in B/A and amplitude-dependent attenuation, while the attenuation through the contrast agent decreases dramatically as shown in Figure 7.¹⁰ Therefore a significant signal can be retrieved from the far wall when using filtered microbubbles, while this signal is barely present when using a native population of microbubbles. Table 2 summarizes the relative importance of the mechanisms involved in the formation of the pseudoenhancement in contrast images.

In summary, the transmitted ultrasound waves are distorted by nonlinear propagation, which will cause significant pseudoenhancement when they are backscattered by tissue located at the far wall of a vessel. In our study this effect is stronger for a size distribution containing predominately small bubbles since the resonance frequency

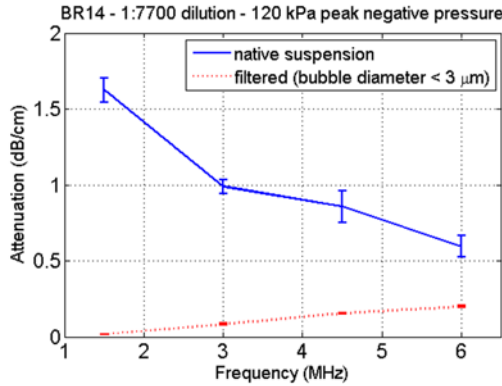


Figure 7. The influence of mechanical filtering of the size of microbubbles on the ultrasound attenuation for a suspension of BR14 (Bracco Research SA, Geneva, Switzerland), a lipid-coated microbubble contrast agent similar to SonoVue. Figure courtesy of Marcia Emmer based on previously published results.¹⁰

Table 2. Relative importance of acoustic properties in different media for the formation of pseudoenhancement at low mechanical index (MI 0.06).

| Substance | Soft tissue | Water | Native SonoVue | Filtered SonoVue |
|--|-------------|-------|----------------|------------------|
| Attenuation | ++ | 0 | +++ | + |
| Nonlinearity | + | + | +++ | ++++ |
| Nonlinearity accumulated at the far wall | NA | + | +++ | ++++ |
| Nonlinearity received by the probe i.e. intensity of the artifact | NA | 0 | + | +++ |

approaches the transmitted frequency, resulting in an increased B/A and amplitude-dependent attenuation are while the overall attenuation is decreased.

The clear presence of pseudoenhancement *in vivo* suggests that the filtration of microbubble contrast agent through lung capillaries and/or environmental, chemical and physical conditions in blood suppresses large bubbles. This has been speculated about previously.¹⁹ However, the *in vivo* size distribution of microbubble contrast agents and the effect of environmental conditions are difficult to investigate and have not been reported in literature.

Finally it is worth noting that pseudoenhancement does not only occur during CEUS of the carotid arteries, but at any locations behind a vessel or a blood pool where contrast agent is present. Reduction of the artifact by lowering the concentration of contrast agent will results in a concomitant reduction of the lumen enhancement. Similarly, changing the display settings or the MI will result in a decreased lumen enhancement, and thus image quality. Other contrast detection techniques currently in clinical use such as pulse inversion imaging¹⁵ are also affected by the pseudoenhancement, since nonlinear propagation through contrast agent similarly distorts the transmitted pulses.

New imaging strategies using a different pulsing scheme or specific imaging post-processing must be developed to overcome this artifact.

CONCLUSION

Pseudoenhancement at the far wall occurs in contrast-enhanced ultrasound examinations of the carotid arteries. The phantom studies showed that the degree of pseudoenhancement is influenced by the size and concentration of the microbubbles. The scattering properties of the tissue behind the vessel (echogenicity) also play a possible role. During vascular CEUS identification of the artifact is important to prevent misinterpretation of enhancement in and near the far wall of a vessel.

REFERENCES

1. Kono Y, Pinnell SP, Sirlin CB, Sparks SR, Georgy B, Wong W, et al. Carotid arteries: Contrast-enhanced US angiography—Preliminary clinical experience. *Radiology*. 2004;230(2):561-8.
2. Macioch JE, Katsamakis CD, Robin J, Liebson PR, Meyer PM, Geohas C, et al. Effect of contrast enhancement on measurement of carotid artery intimal medial thickness. *Vasc Med*. 2004;9(1):7-12.
3. Feinstein SB. Contrast ultrasound imaging of the carotid artery vasa vasorum and atherosclerotic plaque neovascularization. *J Am Coll Cardiol*. 2006;48(2):236-43.
4. Staub D, Schinkel AFL, Coll B, Coli S, van der Steen AFW, Reed JD, et al. Contrast-enhanced ultrasound imaging of the vasa vasorum: From early atherosclerosis to the identification of unstable plaques. *JACC Cardiovasc Imaging*. 2010;3(7):761-71.
5. Tang MX, Eckersley R. Nonlinear propagation of ultrasound through microbubble contrast agents and implications for imaging. *IEEE Trans Ultrason Ferroelectr Freq Control*. 2006;53(12):2406-15.
6. Tang MX, Kamiyama N, Eckersley RJ. Effects of nonlinear propagation in ultrasound contrast agent imaging. *Ultrasound Med Biol*. 2010;36(3):459-66.
7. Yu H, Jang H, Kim T, Khalili K, Williams R, Lueck G, et al. Pseudoenhancement within the local ablation zone of hepatic tumors due to a nonlinear artifact on contrast-enhanced ultrasound. *AJR Am J Roentgenol*. 2010;194:653-9.
8. Teirlinck CJPM, Bezemer RA, Kollmann C, Lubbers J, Hoskins PR, Fish P, et al. Development of an example flow test object and comparison of five of these test objects, constructed in various laboratories. *Ultrasonics*. 1998;36(1-5):653-60.
9. Schneider M. Characteristics of SonoVue™. *Echocardiography*. 1999;16(s1):743-6.
10. Emmer M, Vos HJ, Goertz DE, van Wamel A, Versluis M, de Jong N. Pressure-dependent attenuation and scattering of phospholipid-coated microbubbles at low acoustic pressures. *Ultrasound Med Biol*. 2009;35(1):102-11.
11. Gorce JM, Arditi M, Schneider M. Influence of bubble size distribution on the echogenicity of ultrasound contrast agents: A study of SonoVue™. *Invest Radiol*. 2000;35:661-71.
12. Mulligan-Kehoe MJ. The vasa vasorum in diseased and nondiseased arteries. *Am J Physiol Heart Circ Physiol*. 2010;298(2):H295-305.
13. Ritman EL, Lerman A. The dynamic vasa vasorum. *Cardiovasc Res*. 2007;75(4):649-58.
14. Wu J, Tong J. Measurements of the nonlinearity parameter B/A of contrast agents. *Ultrasound Med Biol*. 1998;24(1):153-9.
15. Powers J, Averkiou M, Bruce M. Principles of cerebral ultrasound contrast imaging. *Cerebrovasc Dis*. 2009;27(Suppl. 2):14-24.
16. Chen Q, Zagzebski J, Wilson T, Stiles T. Pressure-dependent attenuation in ultrasound contrast agents. *Ultrasound Med Biol*. 2002;28(8):1041-51.
17. Tang MX, Eckersley RJ, Noble JA. Pressure-dependent attenuation with microbubbles at low mechanical index. *Ultrasound Med Biol*. 2005;31(3):377-84.
18. Tang MX, Eckersley RJ. Frequency and pressure dependent attenuation and scattering by microbubbles. *Ultrasound Med Biol*. 2007;33(1):164-8.
19. Bouakaz A, de Jong N, Cachard C, Jouini K. On the effect of lung filtering and cardiac pressure on the standard properties of ultrasound contrast agent. *Ultrasonics*. 1998;36:703-8.



Chapter 8

Counter-Propagating Wave Interaction for Contrast-Enhanced Ultrasound Imaging

G. Renaud, J.G. Bosch, G.L. ten Kate, V. Shamdassani, R. Entrekin, N.
de Jong, A.F.W. van der Steen

Phys Med Biol. 2012; 57(21):L9-18.

ABSTRACT

Most techniques for contrast-enhanced ultrasound imaging require linear propagation to detect nonlinear scattering of contrast agent microbubbles. Waveform distortion due to nonlinear propagation impairs their ability to distinguish microbubbles from tissue. As a result, tissue can be misclassified as microbubbles, and contrast agent concentration can be overestimated; therefore, these artifacts can significantly impair the quality of medical diagnoses. Contrary to biological tissue, lipid-coated gas microbubbles used as a contrast agent allow the interaction of two acoustic waves propagating in opposite directions (counter-propagation). Based on that principle, we describe a strategy to detect microbubbles that is free from nonlinear propagation artifacts. *In vitro* images were acquired with an ultrasound scanner in a phantom of tissue-mimicking material with a cavity containing a contrast agent. Unlike the default mode of the scanner using amplitude modulation to detect microbubbles, the pulse sequence exploiting counter-propagating wave interaction creates no pseudoenhancement behind the cavity in the contrast image.

INTRODUCTION

Injection of lipid-coated gas microbubbles in the blood flow as an ultrasound contrast agent (UCA) is well established for the diagnosis of cancers or cardiovascular diseases like atherosclerosis.¹ Aiming at detecting contrast agent microbubbles, the contrast mode of an ultrasound scanner consists in transmitting usually a sequence of one to three ultrasound signals with a time interval of roughly 0.1 ms. The backscattered echoes in response to the transmitted ultrasound waves are processed to retrieve a specific acoustic signature of contrast microbubbles. An image displaying the location of the contrast agent can then be constructed. Repeating the procedure multiple times per second allows one to visualize the flow of the contrast agent through the cardiovascular system. However, most pulse sequences implemented in present ultrasound scanners produce artifacts due to nonlinear propagation through any region containing a UCA.²⁻⁴ Indeed, these pulsing schemes require linear wave propagation in order to reveal nonlinear scattering produced by contrast microbubbles. Even at low acoustic pressures (less than 200 kPa peak negative pressure), the propagation through any vessel or blood pool containing the UCA distorts the transmitted waveforms due to the high acoustic non-linearity (wave-amplitude-dependent speed of sound and wave-amplitude-dependent attenuation^{5,6}) of the UCA. As a consequence, tissue can be misclassified as a contrast agent and the concentration of the contrast agent can be overestimated.⁶ These artifacts obviously impair the quality of the medical diagnoses.²⁻⁴ Figure 1 illustrates the problem of the artifact *in vivo* when imaging the carotid artery.

An efficient technique to detect contrast agent microbubbles and to distinguish them from tissue should preferably use a phenomenon that is fully specific to microbubbles.

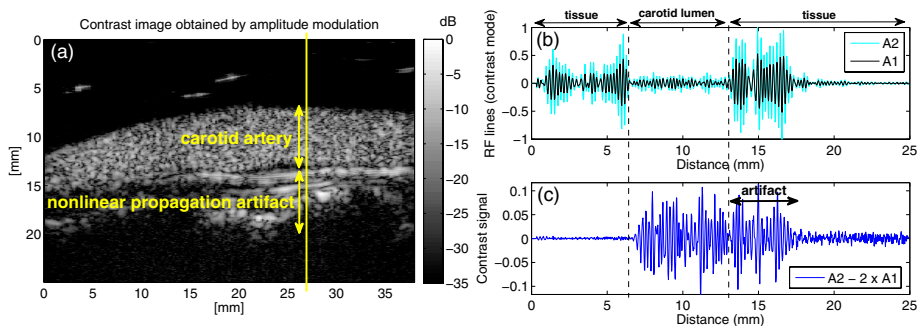


Figure 1. *In vivo* appearance of the artifact due to nonlinear propagation in the UCA. The carotid artery is imaged with an iU22 Philips system and a L9-3 probe using a low mechanical index of 0.06. The UCA is SonoVue (Bracco SpA., Milan, Italy). (a) Contrast image obtained by amplitude modulation (AM). (b) Radio-frequency (RF) lines of single (A1) and double (A2) amplitude recorded at the position marked by the yellow line in (a). (c) Contrast signal obtained by AM at the position marked in (a).

Methods such as amplitude modulation (AM) (also named power modulation)⁷, pulse inversion⁸, combinations of these⁹, radial modulation or surf imaging¹⁰ do not fulfil this requirement. Indeed, tissue can produce the same effects although with a weaker magnitude (single-wave distortion generating higher harmonic frequencies, nonlinear interaction of two co-propagating waves). Subharmonic and ultraharmonic imaging¹¹ and several techniques exploiting the mechanical resonance of the UCA¹²⁻¹⁴ use phenomena fully specific to UCA microbubbles. However, methods like chirp reversal¹² are also impaired by nonlinear propagation artifacts,¹⁵ and they require the transmit frequency to be close to the resonance frequency of the microbubbles. Thus, for a given UCA, only a certain frequency range can be used for the transmit frequency.

In order to overcome these limitations, we developed a detection method based on counter-propagation (CP) wave interaction that is free from nonlinear propagation artifacts.

PRINCIPLE OF COUNTER-PROPAGATION ULTRASTOUND IMAGING

Counter-propagating wave interaction

The interaction of two acoustic waves (typically two sine waves having equal or different frequencies and having equal or different durations) propagating in opposite directions (i.e. CP) is not efficient in biological tissues if the propagation distance is larger than the spatial support of the longest wave,¹⁶ which is the case in medical ultrasound imaging. For acoustic pressures lower than 1 MPa as employed in ultrasound imaging, interaction does not occur because tissues exhibit quadratic elastic nonlinearity, i.e. a linear dependence of the elastic modulus on pressure. In such a medium, and assuming that the amplitude of the first wave is much higher than that of the second one, the first wave appears to modulate the propagation velocity of the second wave. Namely, the propagation velocity of the second wave is successively increased and decreased by the same amount. Therefore no effect is observed after the two waves have passed over each other. However granular and cracked materials like rocks allow the counter-propagating interaction of elastic waves.¹⁶ CP interaction is produced by intergrain contacts or cracks that can be seen as soft nonlinear elastic inclusions embedded in a rigid matrix. Contrast agent microbubbles in a liquid can also behave as such. Therefore we hypothesized that CP can be employed to distinguish the UCA from tissue.

Implementation for contrast-enhanced ultrasound imaging

A simple implementation of CP for contrast ultrasound imaging may use a pulse sequence with two transmission phases. The sequence consists in transmitting first a wave having a center frequency located in the low-frequency (LF) part of the transducer

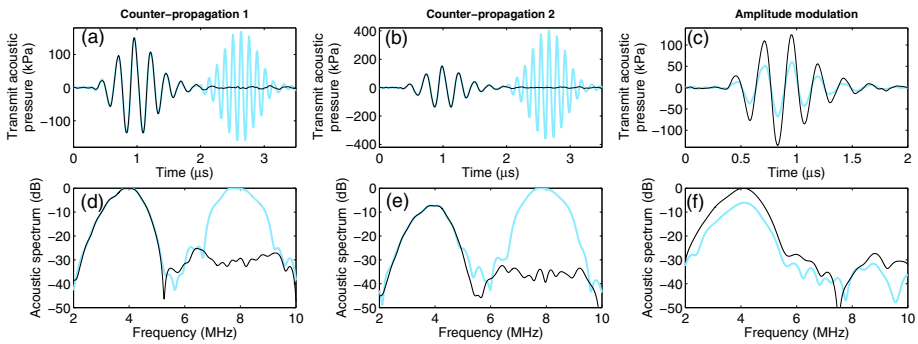


Figure 2. Ultrasound waveforms transmitted by the iU22 Philips scanner for counter-propagation (CP) and AM measured in water by a needle hydrophone at 2 cm from the probe. (a)-(c) Waveforms in the time domain. (d)-(f) Waveforms in the frequency domain. Two versions of the CP pulse sequence, CP 1 (a) and (d) and CP 2 (b) and (e), with a different amplitude for the HF wave were implemented. The thin black line and thick blue line indicate the two waveforms transmitted successively for each method.

frequency bandwidth. Secondly, the same wave is transmitted, immediately followed, with no overlap in time, by a wave of which the center frequency is located in the high-frequency (HF) part of the transducer frequency bandwidth. Figure 2 shows an exemplary pulse sequence to implement CP contrast imaging in an ultrasound scanner with a probe working in the frequency range of 3–9 MHz. Section 3 presents *in vitro* results obtained when LF and HF waves have equal acoustic pressures (Figures 2(a) and 2(d)) and when the amplitude of the HF wave is twice that of the LF wave (Figures 2(b) and 2(e)). These two versions of the CP pulse sequence will be compared to AM (Figures 2(c) and 2(f)). After scattering or reflection of the LF wave in the medium, the resulting back-propagating wave crosses the HF wave, since they propagate in opposite directions. The presence of contrast agent microbubbles at the location where the two waves cross each other allows the HF wave to interact during its forward propagation with waves backscattered or reflected in response to the LF wave. Emitting the LF wave without transmitting the HF wave provides a reference. Thus comparison of the echoes received in the two situations (with and without transmission of the HF wave) allows us to retrieve the effect of CP and therefore to localize the UCA.

In practice, the frequency contents of the LF wave and the HF wave must not overlap significantly (Figures 2(d) and 2(e)) so that the signals received in response to the LF wave can be isolated by means of frequency filtering to suppress echoes at the frequency of the HF wave. Note that the wave transmitted twice is preferably the LF wave. In such a case, the second harmonic component of the HF wave generated by nonlinear propagation does not appear in the frequency bandwidth of the probe. The contrary (transmitting first the HF wave and then transmitting the HF wave followed by the LF wave) may degrade the efficiency of the method since the second harmonic component

of the LF wave would appear at a frequency close to that of the HF wave. The second harmonic component is also produced by tissue, so a residual signal would be obtained even in the absence of the UCA.

Physical mechanisms producing counter-propagating wave interaction in an ultrasound contrast agent

We expect CP interaction to be caused by several physical mechanisms in the UCA. First of all, the CP interaction of the LF and HF waves can produce enhanced subharmonic emission in response to the HF wave. The subharmonic emission of the UCA¹¹ produced by the HF wave creates a signal of frequency (4 MHz) that lies in the frequency range of the LF wave. The signals arising from the backscattering of the LF wave, although of weak amplitude, can stimulate the subharmonic emission of the UCA.¹⁷ Biological tissues (due to heterogeneity of acoustical properties) or a suspension of UCA microbubbles can typically reflect 1% of the transmitted pressure wave. Indeed, the reflection coefficient is given by $(Z_2 - Z_1)/(Z_1 + Z_2)$, where Z_1 and Z_2 are the acoustic impedances of two types of tissues that the wave traverses, and the acoustic impedance of tissues varies by a few per cents.¹⁸ The backscattering coefficient of tissues and a typical dilution of -1 the UCA ranges from 10^{-3} to 10^{-2} $\text{cm}^{-1}\text{sr}^{-1}$ for frequencies from 3 to 9 MHz,^{18, 19} meaning that at least 1% of the transmitted pressure can be scattered at 1 mm away from the scatterer. Numerical simulations solving the Rayleigh–Plesset equation taking into account the additional damping and the additional stiffness created by the lipid coating of a UCA microbubble as well as a possible buckling of the shell²⁰ show that

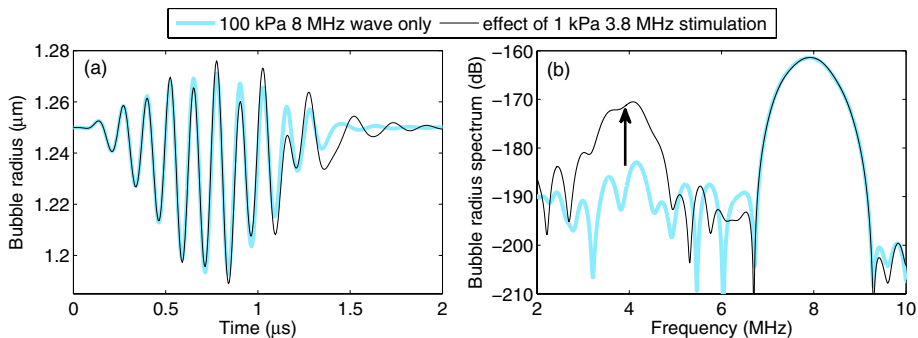


Figure 3. Simulated response of a $2.5 \mu\text{m}$ diameter lipid-coated microbubble to a $1.5 \mu\text{s}$ 8 MHz sine burst tapered with a Hann function of peak acoustic amplitude 100 kPa, with and without the action of a weak $1.5 \mu\text{s}$ 3.8 MHz sine burst of peak acoustic amplitude 1 kPa. (a) Radial response as a function of time. (b) Radial response as a function of frequency. The arrow shows the effect of the 3.8 MHz stimulation on the subharmonic response around 4 MHz. The subharmonic response enhanced by the 3.8 MHz signal is shown after the subtraction of the response of the bubble to the 3.8 MHz signal only. The resonance frequency of a $2.5 \mu\text{m}$ diameter microbubble is close to 4 MHz.

such a small signal can enhance the subharmonic signal (Figure 3). Following the notations in Marmottant et al.²⁰, the stiffness of the lipid coating is $X = 0.5 \text{ N m}^{-1}$ and its surface dilatational viscosity is $K_s = 4 \times 10^{-9} \text{ kg s}^{-1}$. A low equilibrium surface tension is chosen ($\sigma_0 = 0.001 \text{ N m}^{-1}$) based on previous studies on lipid-coated microbubbles.^{21, 22} The microbubble has a diameter of $2.5 \mu\text{m}$, the average size of the UCA microbubbles used for the *in vitro* validation (section 3). The response of the microbubble to three excitations was calculated: response to the small amplitude 3.8 MHz wave only, to the 8 MHz wave only and to the two waves. Numerical simulations were run for an 8 MHz wave with a peak amplitude of 100, 200 and 300 kPa, and a 3.8 MHz stimulation having a peak amplitude ranging from 0.5 to 10 kPa. An enhancement of the signal around the subharmonic frequency (4 MHz) of 6–16 dB is observed, the enhancement increasing monotonously as the amplitude of the 3.8 MHz stimulation increases. Figure 3 depicts the result obtained for a 100 kPa 8 MHz excitation and a 1 kPa 3.8 MHz stimulation. It is seen that without the stimulation created by the 3.8 MHz wave, no clear peak appears at the subharmonic frequency (4 MHz); the signal is -20 dB below the response at the fundamental frequency (8 MHz). When the microbubble is simultaneously excited by the two waves, and after subtraction of the response to the 3.8 MHz wave only from the response to the two waves, a subharmonic signal is clearly visible with an amplitude -10 dB below the response at 8 MHz. This 10 dB enhancement of the subharmonic signal is produced by the low amplitude 3.8 MHz stimulation. The stimulated subharmonic signal around 4 MHz is extracted by the signal processing employed for CP imaging and therefore it contributes to the detection of the UCA.

An additional contribution can arise from the perturbed back-propagation of the LF wave induced by the HF wave. Theoretical work showed that amplitude-dependent dissipation and hysteretic nonlinear elasticity can produce significant interaction between two counter-propagating elastic waves.^{16, 23} Interestingly, amplitude-dependent attenuation^{5, 24, 25} and hysteretic nonlinear elasticity²⁶ were measured in a suspension of UCA microbubbles at low acoustic pressures. Experiments by Moreschi et al.²⁶ also showed that the pressure dependence of the speed of sound (i.e. nonlinear elasticity) in a suspension of the UCA can be higher during compression than during expansion, because of buckling of the lipid shell of microbubbles during compression. Such a compression–expansion asymmetry in the nonlinear elastic behavior of the UCA can also produce CP interaction. Therefore, we hypothesize that these effects are additional mechanisms contributing to the efficiency of UCA detection.

IN VITRO DEMONSTRATION IMPLEMENTATION IN AN ULTRASOUND SCANNER AND COMPARISON WITH A STANDARD METHOD OF CONTRAST AGENT DETECTION

CP imaging was implemented in an iU22 Philips scanner (Philips Healthcare, Bothell, WA, USA) and compared to AM that is the default method for UCA detection in this system. The ultrasound system and a L9-3 linear probe (6 MHz center frequency) were employed to acquire images in a phantom made up of a tissue-mimicking material²⁷ containing a 11 mm diameter cylindrical cavity filled with a 1:1000 dilution of SonoVue contrast agent (Bracco SpA., Milan, Italy). CP was performed with a 1.5 μ s 3.8 MHz wave and a 1.5 μ s 8 MHz wave (Figure 2). AM was performed by transmitting a 1.3 μ s 3.8MHz wave at full and half-amplitude in order to retrieve the nonlinear scattering from UCA microbubbles from the fundamental frequency (3.8 MHz) to the second harmonic frequency (7.6 MHz). For CP and AM, the 3.8 MHz wave transmitted by the probe has a peak negative pressure of 140 kPa, corresponding to a mechanical index of 0.07 (Figures 2(a)-2(c)). Such a low peak negative pressure is commonly used for carotid imaging in order to minimize the destruction of the UCA.^{3,4} CP was tested with two versions, CP1 and CP2, of the pulse sequence having an 8 MHz wave with different amplitudes, namely transmit peak negative pressures of 160 and 360 kPa, corresponding to mechanical indexes of 0.06 and 0.12 (Figures 2(a)-2(b)). The AM image is obtained by the summation of the single-amplitude backscattered signals and subtraction from the double-amplitude backscattered signals. The CP image is obtained by the subtraction of reference backscattered signals (no HF wave transmitted) from backscattered signals when the HF wave is transmitted. Then a low-pass frequency filter (cutoff frequency is 6.2 MHz) is applied to suppress the echoes arising from the linear backscattering of the HF wave. For AM and CP, a 160 μ s time interval is chosen between the transmission of each signal of the pulse sequence. The B-mode image (conventional ultrasound imaging) is performed by transmitting a 0.4 μ s pulse at 6 MHz. Figure 4 shows B-mode, AM and CP images obtained in the tissue-mimicking phantom. The pseudo-enhancement due to nonlinear propagation in the UCA is clearly visible behind the vessel in the transverse and longitudinal images obtained with AM (Figures 4(c)-4(d)). With the two versions of CP, no significant enhancement is observed behind the vessel (Figures 4(e)-4(h)).

In order to compare the performances of AM and the two versions of CP, the maximum amplitude of the signal was calculated in three regions labeled 'C' for contrast, 'T' for tissue and 'A' for tissue located where the artifact appears (Figure 4(a)). Then the contrast-to-tissue ratio (CTR, ratio between maximum signal amplitudes in regions C and T) and the artifact-to-contrast ratio (ACR, ratio between maximum signal amplitudes in regions A and C) were computed (Table 1). The ACR quantifies the importance of the nonlinear propagation artifact. Although AM provides a better CTR (21 dB) than

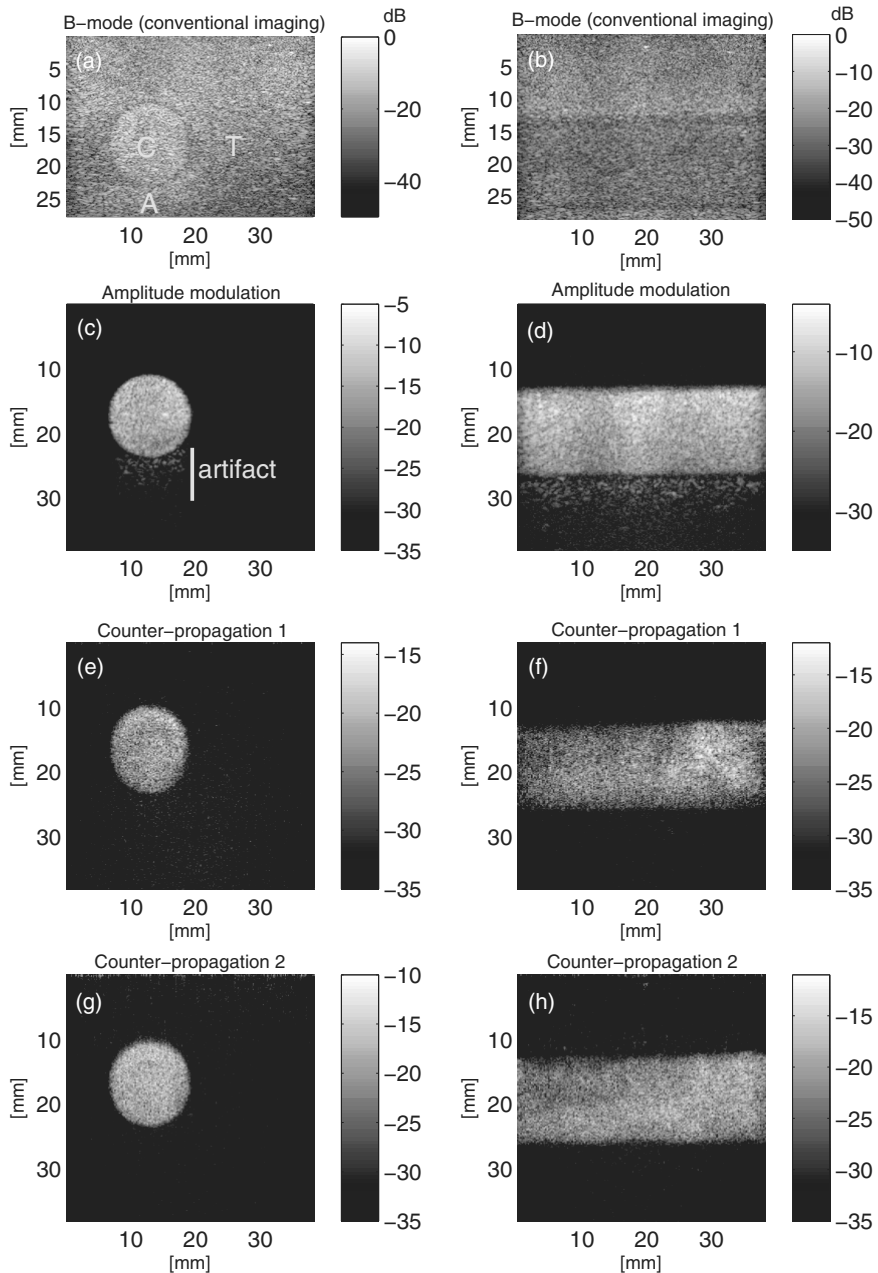


Figure 4. Transverse and longitudinal images acquired by an iU22 Philips scanner in a tissue-mimicking phantom with an L9-3 probe. The cavity is filled with a 1:1000 dilution of SonoVue contrast agent. (a)-(b) Conventional B-mode images at 6 MHz. Labels C, T and A show the areas used to calculate the CTR and ACR. (c)-(d) AM images. (e)-(f) CP images obtained with version 1 of the pulse sequence (Figure 2(a)). (g)-(h) CP images obtained with version 2 of the pulse sequence (Figure 2(b)).

Table 1. Contrast-to-tissue ratio (CTR) and artifact-to-contrast ratio (ACR) measured for the B-mode, counter-propagation (CP) and amplitude modulation (AM).

| | CTR (dB) | ACR (dB) |
|---------------|----------|----------|
| B-mode | 5 | -5 |
| AM | 21 | -11 |
| CP1 | 13.5 | -13 |
| CP2 | 17.5 | -17 |

CP (13.5 dB and 17.5 dB for CP1 and CP2, respectively), AM is dramatically affected by the nonlinear propagation artifact (ACR = -11 dB). An important pseudo-enhancement appears behind the cavity where no contrast agent is present (Figures 4(c)-4(d)). As expected, CP is free from artifacts due to nonlinear propagation (Figures 4(e)-4(h)), and the ACR is improved by 6 dB with CP2 compared to AM. Note that the amplitude of the signals retrieved by CP is smaller than that with AM, but CP images are free from artifacts due to nonlinear propagation. Increasing the amplitude of the HF wave increases the amplitude of the contrast signal obtained with CP; indeed, CP2 provides a higher CTR (17.5 dB) than CP1 (13.5 dB). The echogenicity of the tissue-mimicking material used in this study is weaker than that of the tissue; that is why the artifact appears to be weaker *in vitro* (Figures 4(c)-4(d)) than *in vivo* (Figure 1). During imaging of the carotid artery, the amplitude of the artifact can even exceed that of actual contrast signals produced by AM (Figure 1). Therefore we expect CP to further reduce the ACR compared to AM *in vivo*.

Figure 5 shows spectra of signals acquired with the pulse sequence CP2, in the cavity containing contrast agent ('C' in Figure 4(a)) and in a region of tissue-mimicking material ('T' in Figure 4(a)). After the subtraction of the backscattered signals measured with and without the transmission of the 8 MHz wave, it is seen that the UCA creates a signal in

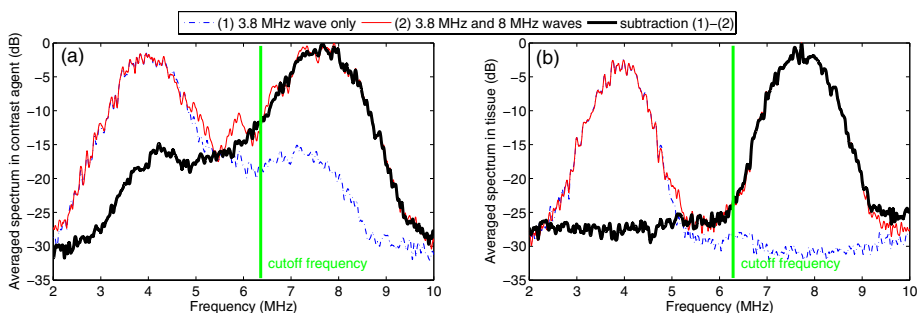


Figure 5. Measured spectra of signals received with the second version of the counter-propagation pulse sequence (Figure 2(b)). (a) From the cavity containing contrast agent ('C' in Figures 4(a)) and (b) from a region of tissue-mimicking material ('T' in Figure 4(a)). The spectrum of the signal resulting from the subtraction of signals acquired with and without the transmission of the 8 MHz wave is also shown. The vertical line shows the cutoff frequency (6.2 MHz) of the low-pass Filter applied to construct the CP image.

a frequency range from 3 to 6.2 MHz. This justifies why we chose a cut-off frequency of 6.2 MHz to construct the CP image. Note that the second harmonic component created by the UCA around 7.5 MHz is clearly observed when the 8 MHz wave is not transmitted (Figure 5(a)).

The axial resolution of an ultrasound image is determined by the duration of the transmitted waveforms, so we expect the axial resolution of AM to be slightly better than CP, although this was not investigated in the present study. However, the lateral resolution is expected to be similar for AM and CP. A waveform duration of 1.5 μ s was first tested for CP (Figures 2(a)–2(b)) to ensure an efficient filtering of the signals arising from the linear scattering of the HF wave.

CONCLUSION

We described a strategy to detect UCA microbubbles for contrast-enhanced ultrasound imaging. The method is based on counter-propagation (CP) interaction between a low-frequency wave and a high-frequency wave. This technique is free from artifacts due to nonlinear propagation that affects most of the methods currently implemented in ultrasound scanners. The method was tested in a tissue-mimicking phantom and compared to the technique called AM that is employed in several clinical ultrasound systems. The *in vitro* experiments proved that the pulse sequence based on CP is free from nonlinear propagation artifacts, whereas AM is severely affected by these artifacts. The use of artifact-free contrast detection strategies can potentially improve the accuracy of contrast-enhanced ultrasound imaging, in particular the assessment of neovascularization within atherosclerotic plaques in the carotid artery²⁸, the coronary artery or aorta²⁹ and the assessment of tissue blood perfusion for the diagnosis of tumor malignancy² or the evaluation of myocardial tissue damage subsequent to a myocardial infarction.³⁰

REFERENCES

1. Liu J-B, Wansaicheong G, Merton DA, Forsberg F, Goldberg BB. Contrast-enhanced ultrasound imaging: State of the art. *J Med Ultrasound*. 2005;13(3):109-26.
2. Yu H, Jang H, Kim T, Khalili K, Williams R, Lueck G, et al. Pseudoenhancement within the local ablation zone of hepatic tumors due to a nonlinear artifact on contrast-enhanced ultrasound. *AJR Am J Roentgenol*. 2010;194:653-9.
3. ten Kate GL, Renaud GGJ, Akkus Z, van den Oord SCH, ten Cate FJ, Shamdasani V, et al. Far-wall pseudoenhancement during contrast-enhanced ultrasound of the carotid arteries: Clinical description and in vitro reproduction *Ultrasound Med Biol*. 2012;38(4):593-600.
4. Thapar A, Shalhoub J, Averkiou M, Mannaris C, Davies AH, Leen ELS. Dose-dependent artifact in the far wall of the carotid artery at dynamic contrast-enhanced US. *Radiology*. 2012;262(2):672-9.
5. Emmer M, Vos HJ, Goertz DE, van Wamel A, Versluis M, de Jong N. Pressure-dependent attenuation and scattering of phospholipid-coated microbubbles at low acoustic pressures. *Ultrasound Med Biol*. 2009;35(1):102-11.
6. Tang MX, Kamiyama N, Eckersley RJ. Effects of nonlinear propagation in ultrasound contrast agent imaging. *Ultrasound Med Biol*. 2010;36(3):459-66.
7. Brock-Fisher G, Poland M, Rafter P. Means for increasing sensitivity in non-linear ultrasound imaging systems 1996. US Patent Specification 5577505.
8. Simpson DH, Chin CT, Burns PN. Pulse inversion Doppler: a new method for detecting nonlinear echoes from microbubble contrast agents. *IEEE Trans Ultrason Ferroelectr Freq Control*. 1999;46(2):372-82.
9. Haider B, Chiao R. Micro-ultrasound for preclinical imaging. *Proc IEEE Int Ultrason Symp*. 1999;vol 2:1527-31.
10. Masoy SE, Standal O, Nasholm P, Johansen TF, Angelsen B, Hansen R. SURF imaging: In vivo demonstration of an ultrasound contrast agent detection technique. *IEEE Trans Ultrason Ferroelectr Freq Control*. 2008;55(5):1112-21.
11. Chomas J, Dayton P, May D, Ferrara K. Nondestructive subharmonic imaging. *IEEE Trans Ultrason Ferroelectr Freq Control*. 2002;49(7):883-92.
12. Novell A, Der Meer S, Versluis M, Jong N, Bouakaz A. Contrast agent response to chirp reversal: simulations, optical observations, and acoustical verification. *IEEE Trans Ultrason Ferroelectr Freq Control*. 2009;56(6):1199-206.
13. Borsboom JMG, Bouakaz A, De Jong N. Pulse subtraction time delay imaging method for ultrasound contrast agent detection. *IEEE Trans Ultrason Ferroelectr Freq Control*. 2009;56(6):1151-8.
14. Hansen R, Angelsen BAJ. Contrast imaging by non-overlapping dual frequency band transmit pulse complexes. *IEEE Trans Ultrason Ferroelectr Freq Control*. 2011;58(2):290-7.
15. Renaud G, Bosch J, de Jong N, van der Steen A. In vitro comparative study of the performance of pulse sequences for ultrasound contrast imaging of the carotid artery *Proc IEEE Int Ultrason Symp*. 2011:628-31.
16. Gusev V, Bailliet H, Lotton P, Bruneau M. Interaction of counterpropagating acoustic waves in media with nonlinear dissipation and in hysteretic media. *Wave Motion*. 1999;29(3):211-21.
17. Daeichin V, Faez T, Renaud G, Bosch JG, Steen AFWvd, Jong Nd. Effect of self-demodulation on the subharmonic response of contrast agent microbubbles. *Phys Med Biol*. 2012;57(12):3675.
18. Duck F. *Physical properties of tissue—A comprehensive reference book* London: Academic; 1990.
19. Gorce JM, Arditi M, Schneider M. Influence of bubble size distribution on the echogenicity of ultrasound contrast agents: A study of SonoVue™. *Invest Radiol*. 2000;35:661-71.

20. Marmottant P, van der Meer S, Emmer M, Versluis M, de Jong N, Hilgenfeldt S, et al. A model for large amplitude oscillations of coated bubbles accounting for buckling and rupture. *J Acoust Soc Am*. 2005;118(6):3499-505.
21. Sijl J, Dollet B, Overvelde M, Garbin V, Rozendal T, de Jong N, et al. Subharmonic behavior of phospholipid-coated ultrasound contrast agent microbubbles. *J Acoust Soc Am*. 2010;128(5):3239-52.
22. Faez T, Emmer M, Docter M, Sijl J, Versluis M, de Jong N. Characterizing the subharmonic response of phospholipid-coated microbubbles for carotid imaging. *Ultrasound Med Biol*. 2011;37(6):958-70.
23. Gusev V. Revised theory for the interaction of the counter-propagating acoustic waves in materials with hysteresis of nonlinearity. *Wave Motion*. 2005;42(2):97-108.
24. Chen Q, Zagzebski J, Wilson T, Stiles T. Pressure-dependent attenuation in ultrasound contrast agents. *Ultrasound Med Biol*. 2002;28(8):1041-51.
25. Tang MX, Eckersley RJ. Frequency and pressure dependent attenuation and scattering by microbubbles. *Ultrasound Med Biol*. 2007;33(1):164-8.
26. Moreschi H, Novell A, Call'e S, Defontaine M, Bouakaz A. Characterization of nonlinear viscoelastic properties of ultrasound contrast agents. *Proc IEEE Int Ultrason Symp*. 2009:251-4.
27. Teirlinck CJPM, Bezemer RA, Kollmann C, Lubbers J, Hoskins PR, Fish P, et al. Development of an example flow test object and comparison of five of these test objects, constructed in various laboratories. *Ultrasonics*. 1998;36(1-5):653-60.
28. Staub D, Schinkel AFL, Coll B, Coli S, van der Steen AFW, Reed JD, et al. Contrast-enhanced ultrasound imaging of the vasa vasorum: From early atherosclerosis to the identification of unstable plaques. *JACC Cardiovasc Imaging*. 2010;3(7):761-71.
29. Goertz DE, Frijlink ME, Tempel D, van Damme LCA, Krams R, Schaar JA, et al. Contrast harmonic intravascular ultrasound: a feasibility study for vasa vasorum imaging. *Invest Radiol*. 2006;41(8):631-8.
30. Dijkmans PA, Senior R, Becher H, Porter TR, Wei K, Visser CA, et al. Myocardial contrast echocardiography evolving as a clinically feasible technique for accurate, rapid, and safe assessment of myocardial perfusion: The evidence so far. *J Am Coll Cardiol*. 2006;48(11):2168-77.



Chapter 9

Quantitative Analysis of Ultrasound Contrast Flow Behaviour in Carotid Plaque Neovasculature

Assaf Hoogi, Zeynetin Akkus, Stijn C. H. van den Oord, Gerrit L.
ten Kate, Arend F. L. Schinkel, Johan G. Bosch, Nico de Jong, Dan
Adam, Antonius F. W. van der Steen

Ultrasound Med Biol. 2012; 38(12):2072-2083.



ABSTRACT

Intraplaque neovascularization is considered as an important indication for plaque vulnerability. We propose a semiautomatic algorithm for quantification of neovasculature, thus, enabling assessment of plaque vulnerability. The algorithm detects and tracks contrast spots using multidimensional dynamic programming. Classification of contrast tracks into blood vessels and artifacts was performed. The results were compared with manual tracking, visual classification and maximal intensity projection. In 28 plaques, 97% of the contrast spots were detected. In 89% of the objects, the automatic tracking determined the contrast motion with an average distance of less than 0.5 mm from the manual marking. Furthermore, 75% were correctly classified into artifacts and vessels. The automated neovascularization grading agreed within 1 grade with visual analysis in 91% of the cases, which was comparable to the interobserver variability of visual grading. These results show that the method can successfully quantify features that are linked to vulnerability of the carotid plaque.

INTRODUCTION

Atherosclerosis, a systemic disease of the arterial wall, may be considered at some stages as a form of cardiovascular inflammatory disease.^{1,2} The important contribution of carotid atherosclerosis to the pathogenesis of cerebral events has been recognized.³ Atherosclerosis-related stroke or myocardial infarction has been linked to the presence of neovascularization and inflammation in the atheromatous plaque, which are considered reliable markers of vulnerability of the plaque and predictors of its rupture.⁴ Moreover, the study of Barger et al.⁵ indicated that in most cases, atherosclerotic plaques and the neovascularization process come together. The role of the neovascularization in the plaque vulnerability is as follows. The first stage in the formation of atherosclerotic plaques is vessel wall thickening as a result of endothelial damage. Vessel wall thickening is caused by infiltration of low-density lipoproteins (LDL) into the intima complex of the vessel wall. Consequently, monocytes are triggered to migrate through the vessel wall and differentiate to macrophages. The macrophages take up the modified LDL and form the so-called macrophage foam cells. This leads to a more complex inflammatory response in the affected vessel wall.⁶ As this process progresses, more advanced atherosclerotic plaques are formed. During the formation of these plaques, the vessel wall thickness will exceed the oxygen diffusion threshold. This will lead to a release of a number of angiogenic growth factors such as hypoxia inducible transcription factor (HIF). These factors will trigger the physiologic vasa vasorum to proliferate into the atherosclerotic plaque.⁷⁻⁹ The immature neovessels may promote the formation and destabilization of this atherosclerotic plaque and these vessels are associated with future cardiovascular events.¹⁰

Hence, the indication for carotid endarterectomy, which is commonly based on the degree of diameter stenosis may be insufficient, whereas risk evaluation based on the plaque composition would be valuable in the treatment decision process.^{11,12} Therefore, developing a noninvasive imaging method based on quantification of plaque vascularization to assess plaque vulnerability is highly desirable. In addition, monitoring neovascularization response to drug treatment, as an expression of the inflammation process, may be obtained.¹³⁻¹⁵ In our study, the plaque is monitored by two-dimensional (2-D) ultrasound (US) imaging, which is a noninvasive, reliable, accessible and inexpensive image acquisition modality.¹⁶ The spatial resolution of carotid ultrasound imaging is approximately 0.1 mm, which is better than with magnetic resonance (MR), computed tomography (CT) or X-ray angiography imaging of the carotids.¹³ This resolution refers to a 4 cm depth and a fundamental frequency of at least 7 MHz.¹⁷ Moreover, contrast-enhanced ultrasound imaging (CEUS) allows detection of contrast microbubbles in very small vessels with high sensitivity. Since CEUS can detect single microbubbles due to their strong reflectivity, blood flow within vessels of sizes less than 50 μm can

be detected.^{18, 19} Several researches used the advantage of CEUS imaging in detecting neovascularization.^{13, 20, 21}

Several semi-quantitative visual approaches to quantify contrast enhancement of intraplaque neovascularization on contrast-enhanced ultrasound images have been reported²²⁻²⁴ usually by using a discrete limited grading system. Those authors categorized the echogenicity as low if no bubbles were detected and as high if extensive contrast enhancement was depicted²⁵ used a semi-quantitative grading system based on visual interpretation alone, from the absence of neovascularization (grade 0) to high echogenicity (grade 3) caused by a high amount of contrast agent enhancement.

Several studies used maximum intensity projection (MIP) to reconstruct an arterial tree.^{20, 26, 27} Maximum intensity projection (MIP) is a 2-D projection image obtained from a time sequence of 2-D data by searching for every pixel the highest intensity value over time. In unenhanced ultrasound imaging, MIP can be used to evaluate the general morphology of relevant objects, such as the carotid plaques. However, in contrast-enhanced ultrasound (CEUS), it has additional contribution in detection of the vessel trajectories. A major drawback of MIP is its high sensitivity to noise and to the quality of the applied motion compensation, thus, a MIP analysis can produce an over-estimated arterial tree. Therefore, using MIP enforces a preliminary high quality filtering.²⁸ Another drawback of MIP is its absence of any temporal information on the examined objects. Therefore, it encounters difficulties in differentiation between artifacts and blood vessels and produces overestimated results of the neovascularization inside the plaque. To our knowledge, there are no other studies published in the literature quantifying the intraplaque neovascularization by demonstrating the 2-D behavior of a contrast spot over time. We use the importance of the temporal behavior as described in the following pages.

In the present study, a semiautomatic algorithm is developed. A multidimensional dynamic programming (MDP) method is implemented to reconstruct the neovascularization tree in a CEUS image of the carotid plaque. The main advantage of this method is its ability to take discrete contrast blobs and generate continuous routes, demonstrating the temporal behavior of bubble flow. It was tested on a large set of clinical cases and required minimal intervention of the operator. In comparison to common methods such as forward tracking, the algorithm is robust to noise and allows differentiation between blood vessels and artifacts. Therefore, it provides much more accurate results than other methods, which do not have any temporal information, such as the MIP described above.

MATERIALS AND METHODS

Patient population and imaging acquisition

Seventy six patients without established atherosclerotic disease were recruited if they had at least one clinical risk factor for the development of atherosclerosis (i.e., hypercholesterolemia, diabetes, smoking, hypertension, positive family history). The study was approved by the institutional review board (Dutch NTR2239) and a written informed consent was obtained from each participant. Standard carotid ultrasound and CEUS were performed with a Philips iU-22 ultrasound system (Philips Medical Systems, Bothell, WA, USA), equipped with an L9-3 probe. Image acquisition was performed by a trained sonography technician using a standard scanning protocol according to the American Society of Echocardiography consensus statement.¹⁷ The left and the right common carotid artery (CCA), carotid bifurcation, internal carotid artery (ICA), external carotid artery (ECA) and vertebral arteries were imaged by B-mode ultrasound, color Doppler and pulse-wave Doppler. Each side was extensively evaluated for the presence of carotid plaques. The degree of stenosis of the CCA, ICA and ECA was assessed according to current guidelines on the basis of spectral Doppler velocities. After standard carotid ultrasound, CEUS was performed using intravenous administration of SonoVue contrast agent (Bracco S.p.A., Milan, Italy). The ultrasound system settings were optimized for CEUS, using a dual display mode for simultaneous standard B-mode ultrasound and CEUS. The mechanical index for CEUS was lowered to 0.06–0.08 and the frame rate was adjusted to 20 Hz. Before injection of the ultrasound contrast agent the intravenous access was flushed with a 5.0 mL saline (NaCl 0.9%) solution bolus injection. The ultrasound contrast agent was injected in boluses of 0.5 mL. Each contrast agent bolus was followed by a 2.0 mL saline flush. After administration of contrast agent, high-quality contrast images could be obtained for approximately 1 min. Contrast administration was repeated when required up to a maximum total dose of 10.0 mL. Still frames and cine clips were digitally stored for offline analysis. Loops were acquired of longitudinal cross-sections that best visualized the plaque. Since we dealt with 2-D planes, they were recorded from different angles, to fully characterize the atherosclerotic plaques. Cine loops were recorded, starting from the time the contrast agent was seen in the carotid lumen (after the flash) until most of it had disappeared. From the total set of acquisitions, cine loops were selected for analysis based on plaque size, plaque location and presence of artifacts. Plaques of thickness below 1.5 mm, or obscured by heavy shadowing or saturation in the plaque were excluded from analysis. Plaques smaller than 1.5 mm are hard to analyze reliably. The effect of out-of-plane motion caused by every heartbeat is more obvious in these small plaques than in the bigger plaques. Small plaques can completely disappear out of plane, making motion compensation and bubble tracking impossible.

Plaques in the distal wall and proximal plaques below significant contrast in the jugular vein were excluded because of the significant contrast-induced artifacts reported for such locations.²⁹ Therefore, we only analyzed plaques that were located at the proximal wall of the artery (CCA, ICA or ECA) near the bifurcation of the carotid.

From the remaining sequences, a subset was drawn randomly. In total, cine loops of 28 different plaques (of 27 different patients) were selected for analysis. The characteristic length of the analyzed sets was 118 ± 49 frames (about 6 s). The high prevalence of atherosclerotic plaques in this asymptomatic population with an increased risk is similar to that found in other studies.³⁰

Data analysis

The cine loops that were acquired during each clinical examination were transferred as DICOM files to a computer workstation for off-line post processing and were analyzed by an algorithm especially developed for this purpose, using Matlab software (The Mathworks Inc., Natick, MA, USA). Figure 1 presents the various steps of the algorithm.

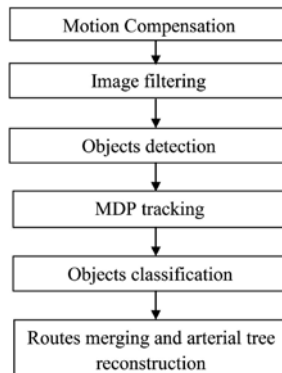


Figure 1. The main steps of the developed algorithm for quantification of the neovascularization inside the plaque.

Motion compensation

The first step of the algorithm is motion compensation that is performed by applying a forward-tracking block matching (BM) method as described in.³¹ The local motion pattern of the plaque region is extracted from the B-mode image with BM and applied to the corresponding region in the contrast image. First, the user selects the point to be tracked in the first image of a given sequence. A fixed template of 49×49 pixels around this point is derived from the first image of the sequence. Then, the plaque displacement is assessed through the sequence by tracking the template's speckle pattern with BM through consecutive frames. The template's center position is scanned over all positions within a defined search field in each image to find the position where they best match.

This determines the shift in location of the template from the first ultrasound image and all subsequent images in the sequence, as shown in Figure 2. The search field extends 10 pixels in each direction from the best position found in the previous frame. This is big enough to handle the maximum motion from frame to frame, which is in the order of a few pixels. The similarity of the template to the image, at each point in the search field, is assessed by normalized cross correlation (NCC). This similarity measure is commonly used since NCC is insensitive to local variations. The local plaque motion pattern is obtained by following the highest correlation values through the image sequence. The contrast images are aligned to the first contrast image based on detected plaque displacement in X and Y direction for motion correction.

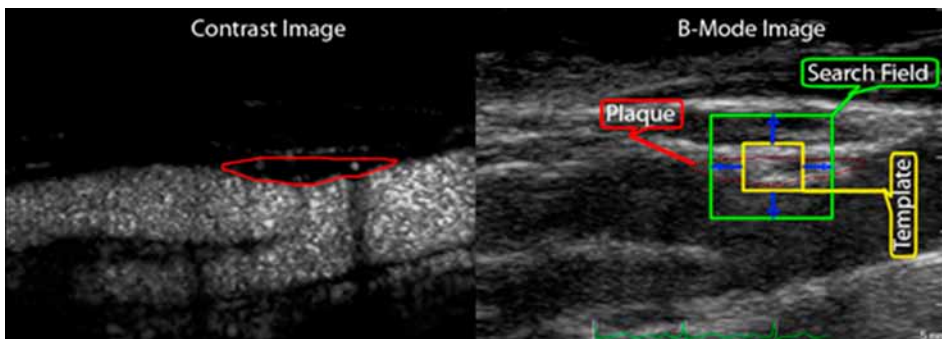


Figure 2. Block matching method. The plaque region is manually outlined in the contrast image (left) and shown in the B-mode image (right). A representative tissue point within the plaque is indicated manually in the B-mode. A template around this point is extracted and compared with all positions within the search field in consecutive B-mode frames. The obtained motion pattern for the plaque region is applied to the contrast images.

Noise reduction

Noise reduction is performed by using a 2-D Gaussian filter of 5×5 pixels with $\sigma = 1$. The width of the window is carefully chosen in order to prevent smoothing and blurring of the contrast accumulations, thus, it should be smaller than the characteristic size of a contrast accumulation. Those accumulations have characteristic size bigger than 7×7 pixels. In addition to the Gaussian filter that is applied over all frames, an adaptive threshold is calculated as an additional way to eliminate noise. This threshold is calculated in a region-of-interest (ROI), which is manually chosen by the user. The ROI should be close enough to the borders of the plaque without taking into account the lumen or the arterial wall, thus, preventing artifacts. The threshold is independently calculated in the first frame for each patient by using the 10th percentile of the gray values in this ROI. All values below the threshold are set to zero and the rest are left intact. The 10th

percentile is a safe choice for the threshold since we assume that most of the plaque area is background (non-contrast).

This low threshold will minimize false negative cases, at the cost of more false positives (that can be eliminated in a later stage).

After applying the noise reduction, the US sequence is divided into overlapping groups of 10 frames each. Time duration of 10 frames is supposed to be sufficient to see continuous presence of an object (as opposed to noise) and to detect a reasonable

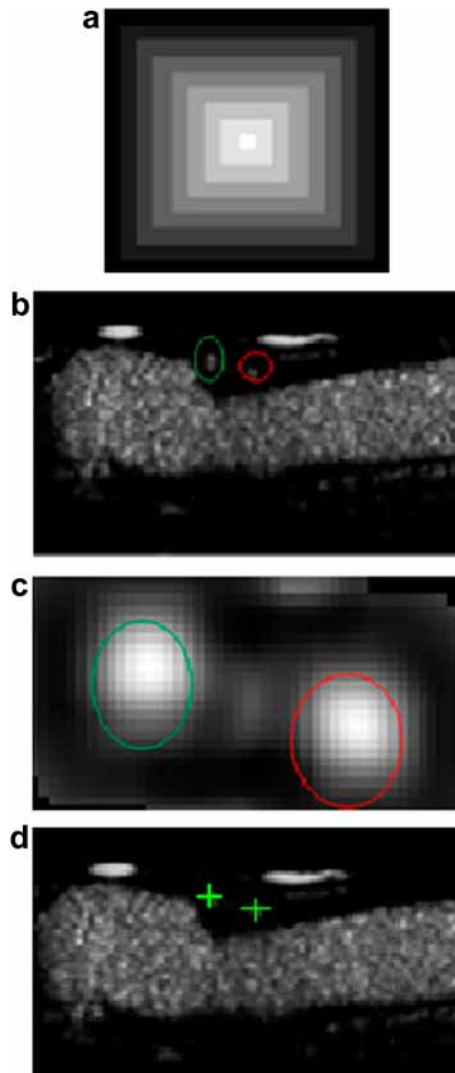


Figure 3. Objects detection by an artificial template. (a) An artificial bubble with a 9-pixel "radius." (b) Original image with two intra-plaque objects and their corresponding locations in the correlation matrix. (c) The correlation matrix. (d) The final detection.

amount of motion of the object (as opposed to artifacts). In the first frame of the group, candidate objects are detected motion of which is followed over the group. An eight-frame overlap (80%) between subsequent groups is chosen to minimize false negative cases. The following object detection is implemented only on the first frame of each group.

Contrast spot detection

An artificial “bubble” template is used for the detection of contrast-like objects. It exploits the geometrical characteristic and the gray levels distribution of a typical contrast spot. An artificial template is constructed resembling a typical pattern of real bubbles (Figure 3a). The template takes into account parameters as reasonable “radius” and varying gray levels. Maximal intensity is determined at the center point and constant linear decrease of gray levels is applied in correspondence with the distance from that point.

The artificial template is correlated with different areas in the chosen ROI using normalized cross correlation. A correlation coefficient matrix is calculated (Figure 3c) and the maximal correlation is located. Then, the correlation values in a 5×5 neighborhood around this location are set to zero. The detection of the maximal correlation, as well as the deletion of its close neighborhood, are performed iteratively till the maximal correlation value is below 0.6, which we take as the threshold for a contrast spot to be considered as a bubble (Figure 3d). Several radii of 3, 5, 7 and 9 pixels are examined for the artificial bubble template. The sets of found points are united to obtain a complete detection of the objects.

After detecting the contrast spots in the first frame of each group, tracking is performed by dynamic programming between the first frame of each group and its last frame.

Bubble tracking by dynamic programming

Dynamic programming (DP) is an optimal approach for solving variational problems by finding locally optimal solutions consecutively. The idea is to track the 2-D displacement of a bubble in the plaque over time. This corresponds to finding a connective path in the time direction through a three-dimensional (3-D) (X, Y, T) matrix with minimal total cost by multidimensional DP (Figure 4).³² After the tracking process has detected the “optimal path” over 10 frames, the gray values of the object along the path are evaluated. By removing all path points where the gray level is below a predefined threshold (the detailed 10th percentile threshold) one can decide when a bubble is gone.

The resulting optimal path is determined by the following parameters described below: costs (correlation values) and path smoothness (allowed step size and side step penalty).

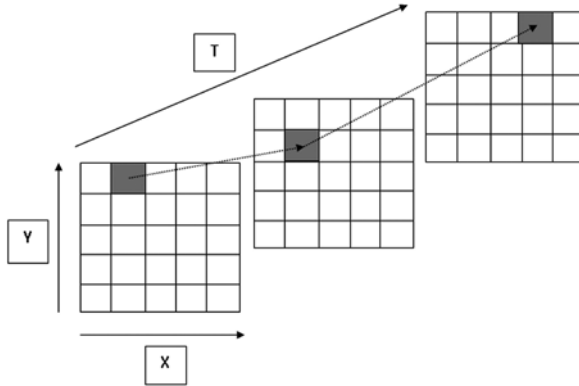


Figure 4. Example of 2-D dynamic programming. Each slice represents the cost function at a certain frame. The optimal path is shown with arrows.

Correlation values

For each object a template of 13×13 pixels around its center is taken from the first frame of each group. Similar to the motion compensation process, each template is correlated for the other 9 frames in the group within a search area of 41×41 pixels around the location of the detected object in the first frame. The size of the search area is large enough to accommodate a maximal displacement of 20 pixels over 10 frames. Before the correlation process takes place, both templates are apodized similar to³² with a 2-D Gaussian weighting characterized by $\sigma = 3$. This weighting is applied to reduce the relative contribution of the background to the NCC. NCC is optimal when it is close to its maximal value of 1. To use NCC properly in the MDP minimization process, we use for the basic cost function: $(1-NCC)^{1/3}$ (Equation 1, part A).

Equation 1:
$$F(x,y) = \underbrace{(1-NCC)^{1/3}}_A \cdot \underbrace{\{(1+1/f_x)^{|\Delta x|} \cdot (1+1/f_y)^{|\Delta y|}\}}_B$$

Step size

The connectivity of the graph should fit the maximum distance that a bubble accumulation can pass in two sequential frames. The allowed step size is taken as 3 pixels, corresponding to 6 mm/s, large enough to handle the possible motion of bubbles in small vessels. Furthermore, temporal smoothness of the motion is controlled by the side step penalty which is presented in (Equation 1, part B)³² where Δ_x and Δ_y are the distances that a specific pixel can go through in sequential frames. These distances can be in the allowed range of $[-3, 3]$, in x and y direction, respectively. f_x and f_y are the weights corresponding to those distances. Their value was chosen to be 10 to penalize fast movements.

Relative to forward tracking, our method has several advantages for evaluating the contrast spots motion. First, it exploits the MDP advantages: relatively insensitive to

noise and small disturbances, efficient and producing a time continuous motion.³³ When the correlation is good the dynamic programming will give the same results as forward tracking of the best correlation. However, in the case of transient loss of correlation or excessive noise, MDP provides an overall optimal continuous path for tracking and thereby is less subject to tracking loss. Another benefit from the MDP search is the 2-D path derived from it. In this way, our technique is capable of evaluating the spatial displacement of the intraplaque objects in both the horizontal and the vertical direction. Third, it takes the advantages of block matching using normalized cross correlation (NCC): robust against linear changes, fast and proven.³²

Contrast spot classification and routes merging

After detecting the objects' routes by using the MDP, the following steps are applied. First, a classification of the objects into two categories is performed: actual blood vessels and artifacts. The classification is necessary to remove artifacts from further processing and exclude them from plaque vulnerability estimates. The classification is based on a minimum expected displacement for moving bubbles as opposed to stationary artifacts. We apply a threshold of 8 pixels (~0.8 mm) for the XY displacement (Equation 2) of an object over a group of 10 frames. Below this threshold, the object is classified as artifact. This threshold corresponds to a bubble velocity of 2 mm/s, which is low for blood flow even in capillaries.

Equation 2: $XY \text{ displacement} = \sqrt{\{(X_{\max} - X_{\min})^2 + (Y_{\max} - Y_{\min})^2\}}$

Second, a merging of reconstructed routes which are supposed to be of the same vessel is performed. Merging means that different routes which probably represent the temporal behavior of the same object should be handled as following: the shorter one is deleted while the longer route remains to represent both of them. For the merging process, two parameters should be measured. The first one is the mean distance between two examined routes. Three-pixel distance (~0.3 mm) threshold was predefined because of experimental trials, taking into account the characteristic size of a bubble (bigger than 7×7 pixels). The second is the overlapping percentage between two routes. Above 60% pixels overlapping is needed for one route deletion (60% of the short route is located in a distance smaller than 3 pixels from the longer one).

Algorithm validation

Manual marking of contrast routes, maximal intensity projection (MIP) and visual grading were performed and compared to the algorithm results for its validation. To evaluate the accuracy of the tracking, two independent observers manually marked the location of each object over time. An object was visually detected based on its area and gray

level. For every plaque with contrast spots inside, the observers manually tracked each object (artifact or vessel) from the frame it appeared till it disappeared. Plaques without any contrast spots inside were visually classified as neovascularization grading 0, and had no manual contrast tracking. For each object, the mean distance between routes that were manually marked by the two observers was measured, as well as standard deviation (SD) values. An average route between those two routes was calculated. The total XY displacement along this route and its total length were calculated. This average route was compared to the algorithm results. Mean and SD values of the distances between the automatically reconstructed route and the average manual route were calculated. Mean distance smaller than 5 pixels (0.525 mm) was considered as a high accuracy of the algorithm analysis, since characteristic size of a contrast spot is above 0.8 mm. Interobserver variation was around 0.2 mm.

The equivalent XY displacement and total length of the automatically reconstructed route was also measured.

The XY displacement results were also compared with the maximal intensity projection (MIP) results to show the advantage of our method over commonly used methods such as the MIP.

The MIP was implemented on the plaque area after motion compensation and after applying the same 10th percentile threshold which is used in the “noise reduction” section of the presented algorithm. The MIP image was examined and analyzed only if discrete routes could be seen inside. If not, the MIP image of the specific plaque was ignored. For plaques of which the MIP image could be analyzed, a skeleton was implemented to extract the blood vessels centerlines. Thresholding followed by a thinning procedure is a common method, which is presented in several papers.^{14, 34, 35} The XY displacement of each reconstructed centerline route was calculated and compared with the results obtained by our method. The detection of blood vessels can be inaccurate because of lack of temporal information and stringent requirements of optimal noise reduction and motion compensation while using MIP.²⁸ As a result, the neovascularization grading will be inaccurate. The visual classification of objects into actual blood vessels and artifacts was based on their visually assessed motion pattern and gray value appearance over time.

The decision process of the automated neovascularization grading is performed analogous to the physician’s decision using the number of detected blood vessels: 0 for no vessels, 1 for 1 vessel, 2 for 2 vessels and 3 for 3 or more vessels.

RESULTS

One hundred and four objects were visually detected in 28 movies. One hundred and one objects were automatically detected and only three objects were missed. The automated detection additionally found four false positive objects.

Figure 5 presents the detection of an object inside a plaque and its entire reconstructed route over time, obtained by the MDP method. In Figure 6, a comparison between the automatic and the manual reconstructed routes of the same object is presented. They show a very similar motion pattern with a small bias of 1–2 pixels.

Ninety objects were accurately tracked, following the constraint that was presented in the methods section. In the other 11 objects, tracking was lost over time because of noisy images or very blurry objects inside the plaque.

The 104 objects were classified visually into 40 actual blood vessels and 64 artifacts. The mean and SD values of the XY displacements of objects visually classified as blood vessels and artifacts were $1.14 \text{ mm} \pm 0.36 \text{ mm}$ and $0.53 \text{ mm} \pm 0.31 \text{ mm}$, respectively.

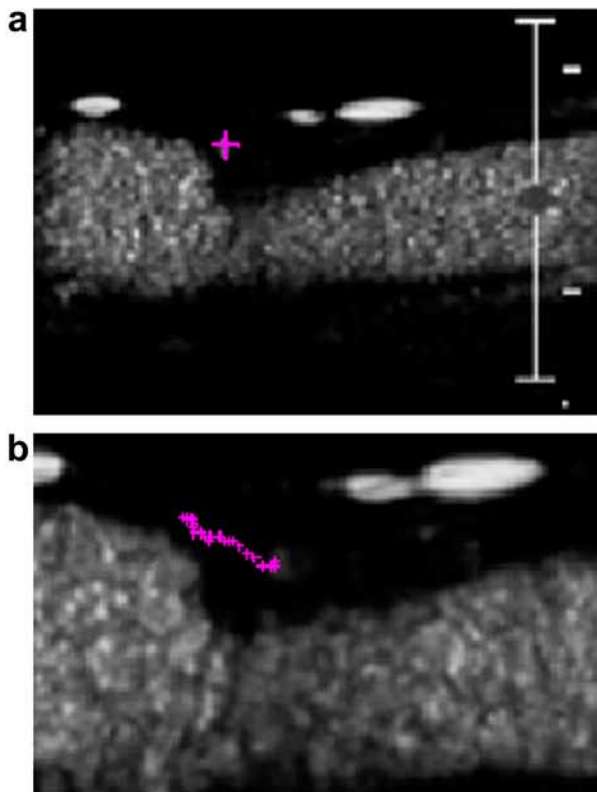


Figure 5. Detecting and tracking an intra-plaque object. (a) The intra-plaque detected object. (b) Its reconstructed route over time.

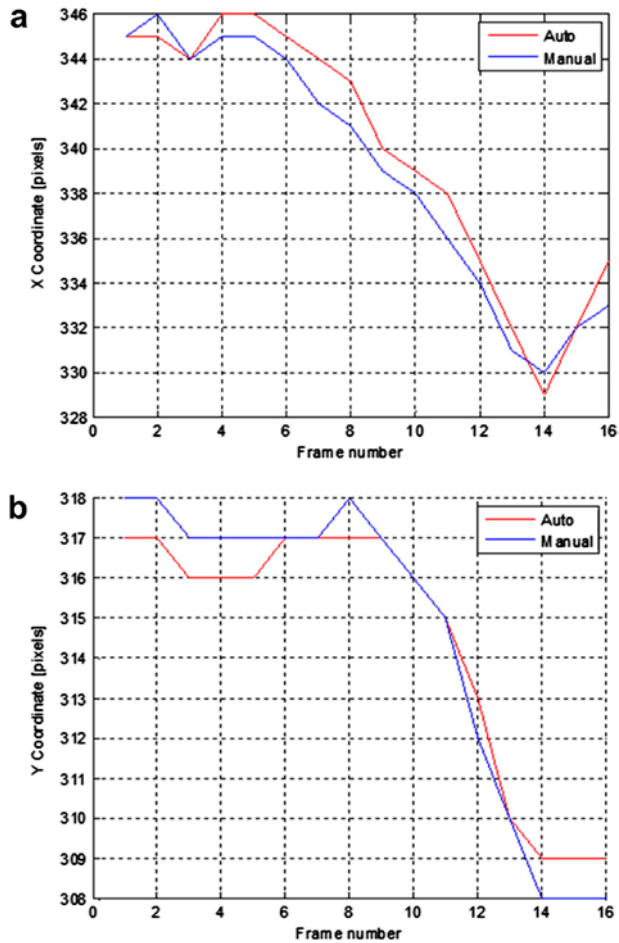


Figure 6. Comparison between a reconstructed route using the presented method and the manual result. (a) X position over time. (b) Y position over time.

Table 1. Classification of 90 objects into blood vessels and artifacts according to visual analysis and automated analysis

| Visual | Blood vessels | Artifacts |
|------------------|---------------|-----------|
| Algorithm | | |
| Blood vessels | 35 | 12 |
| Artifacts | 2 | 41 |

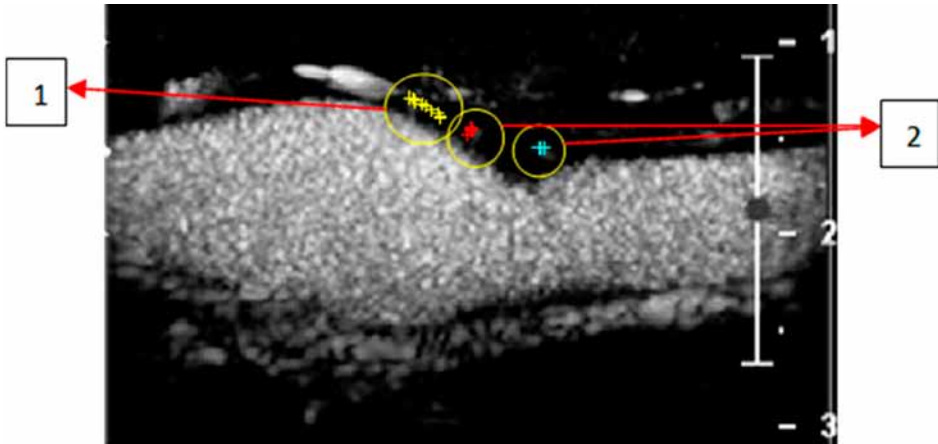


Figure 7. Classification of three detected objects inside a carotid plaque. (1) Blood vessels. (2) Artifacts.

The difference between those populations was significant ($p < 0.001$). Therefore, a 0.8 mm threshold to differentiate between those populations was chosen. Applying this threshold, one can see in Table 1 that 76 of the 90 well tracked contrast spots were correctly classified in comparison to the visual classification.

Figure 7 presents an example of three identified spots in a carotid plaque and their classification.

Figure 8 presents the merging process over two examples of plaques. Figure 8a and 8b present the all detected blood vessels over the whole cine and before the merging process. Figure 8c and 8d show the final neovascularization tree after the routes were merged. In Figure 8a and 8c, two separate routes of different contrast spots were reconstructed. In Figure 8b and 8d, two routes which split from a common “trunk” of the arterial tree are shown (the flow is from the right side of the image to the left side).

Table 2 compares the automatic and the manual results. It presents the average and the SD results that were calculated over 31 classified vessels from the 28 plaques (the vessels that are mentioned in Table 1).

Comparison to the maximal intensity projection (MIP) method was performed. In 22 plaques, discrete routes could be seen, and thus, could be analyzed. In another six plaques the MIP image did not include any clear routes inside but large undefined areas, thus, have not been analyzed. Figure 9 presents a typical example of blood vessels routes that were detected by manual marking (green), the automatic (red) and the MIP algorithms. The presented image is already the MIP image inside the plaque and its skeleton is yellow colored. The cyan marking represents the ROI that was chosen in the first frame of the US cine. It is clearly seen that the MIP generates an inaccurate reconstructed tree, while the manual and the automated reconstructions are similar to each other. This inaccuracy is expressed by the purple and the orange circled areas. Figure 9

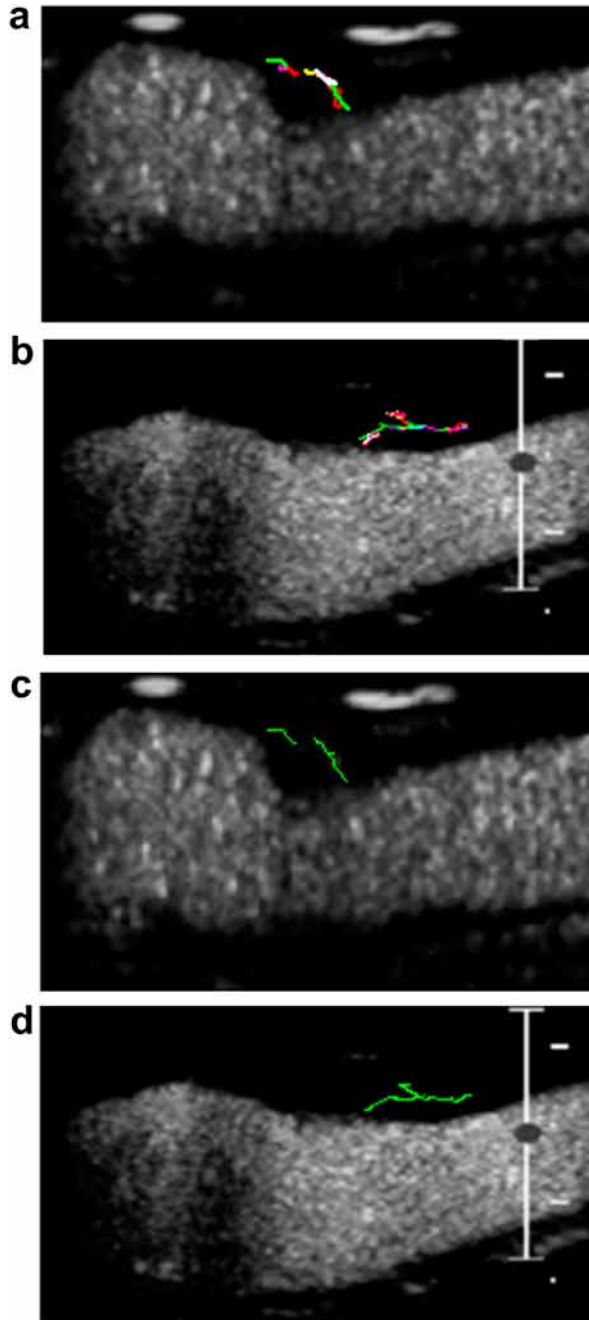


Figure 8. Routes merging. Two different cases of reconstructed arterial tree before and after routes merging: (a) routes which belong to two different vessels before the merging process (over the whole cine); (b) split of two routes from a common “trunk” before the merging process. (c) The plaque which presents in 8 (a), after the merging process. (d) The arterial tree which presents in 8 (b), after the merging process.

Table 2. Comparison of the automatically reconstructed blood vessels routes and the manually reconstructed routes by measuring XY displacement and length of blood vessels. The comparison includes 31 vessel paths from 28 different plaques

| | |
|---|-----------------------|
| Interobserver variability of manual tracking | 0.21 mm \pm 0.14 mm |
| Distance between the average manual route and the automated reconstructions | 0.23 mm \pm 0.15 mm |
| XY displacement of the manually reconstructed blood vessels | 1.19 mm \pm 0.54 mm |
| XY Displacement of the automatically reconstructed blood vessels | 1.14 mm \pm 0.36 mm |
| Mean length of the blood vessels routes—manually reconstructed | 1.93 mm \pm 0.66 mm |
| Mean length of the blood vessels routes—automatically reconstructed | 1.84 mm \pm 0.69 mm |

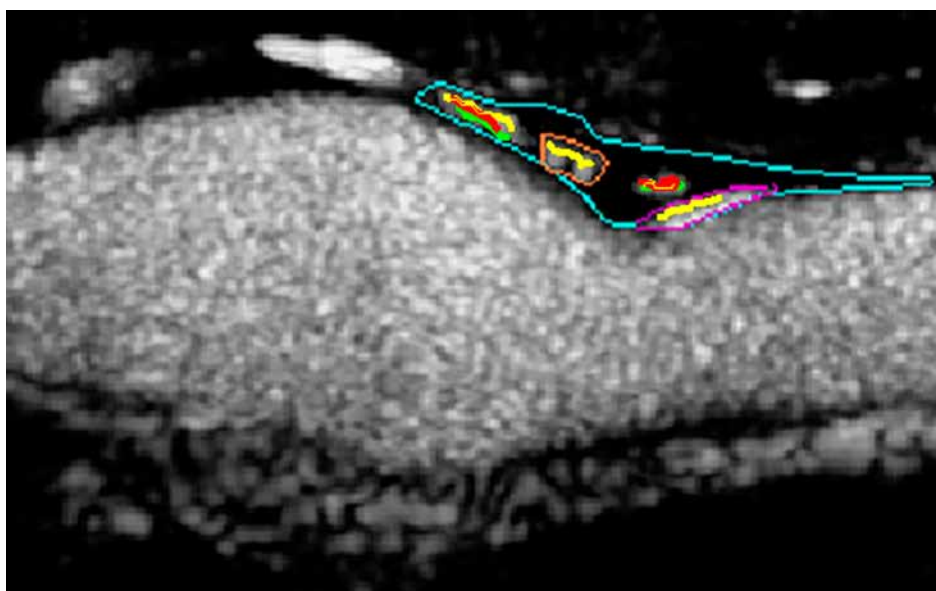


Figure 9. Overestimation neovascularization grading using the MIP. Comparison between the manual marking (green), our method (red) and the MIP (yellow colored skeleton). The ROI is cyan marked. False detection (non-vessels detection) by the MIP is purple and orange colored.

shows an overestimated grading due to intraplaque artifacts (orange) and nonoptimal preliminary noise reduction and motion compensation (purple colored).

The characteristic XY displacement of the defined blood vessels was 2.73 mm \pm 1.24 mm, which is in average 130% bigger than the manual and the automated measured XY displacement for the same vessels.

The last step of the presented method is to determine the neovascularization grading inside the plaques. As one can see in Table 3, the two physicians had consensus on 68% of the cases (19 out of 28 plaques, dark gray), their scores differed 1 grade in 25% (7 cases, mid gray) and 2 grades in 7% (2 cases, light gray). In Table 4, comparison of the automated scoring against the physicians' visual scoring can be seen. Scores of both physicians were

Table 3. Comparison of intraplaque neovascularization visual scores of physician 1 against physician 2. Consensus (dark gray), 1 grade off (mid gray), 2 grades off (light gray). Twenty-eight plaques were examined.

| | | Physician 2 (Visual Scoring) | | | |
|---------------------------------|---------|------------------------------|---------|--------|---------|
| | | Grade 0 | Grade 1 | Grade2 | Grade 3 |
| Physician 1 (Visual scoring) | Grade 0 | 3 | 0 | 2 | 0 |
| | Grade 1 | 0 | 6 | 2 | 0 |
| | Grade 2 | 0 | 4 | 10 | 0 |
| | Grade 3 | 0 | 0 | 1 | 0 |

Table 4. Comparison of intraplaque neovascularization algorithm scoring against visual scores of physicians 1 and 2. Consensus (dark gray), 1 grade off (mid gray), 2 grades off (light gray). Twenty-eight plaques were examined (56 visual scorings for two physicians).

| | | Visual Scoring (Physician 1 & 2) | | | |
|-----------|---------|----------------------------------|---------|--------|---------|
| | | Grade 0 | Grade 1 | Grade2 | Grade 3 |
| Algorithm | Grade 0 | 6 | 2 | 0 | 0 |
| | Grade 1 | 0 | 9 | 1 | 0 |
| | Grade 2 | 2 | 6 | 21 | 1 |
| | Grade 3 | 0 | 3 | 5 | 0 |

treated as independent scores, so there were 56 pairs of scores in total. The automated score was identical to the physicians' visual scoring in 64% of the cases (36 out of 56 cases, dark gray), one grade difference in 27% (15 cases, mid gray), and two grades difference in 9% (five cases, light gray). Obviously, the differences between the automated and the visual scores are very comparable to the differences between two independent observers.

DISCUSSION

In our research, we developed a semiautomatic technique for detecting and tracking the contrast spots motion using MDP combined with block matching, and morphologic artificial templates. Based on that analysis, the reconstruction of the neovascularization arterial tree inside the plaque was performed. Our method deals with a chain of four independent steps: detection of the intraplaque objects, tracking those objects, classification into artifacts and actual blood vessels and overall grading of the neovascularization inside each plaque. Each step can be independently improved, so in this article we report each step's success. We applied this method on clinical recorded data from 27 patients. There was quite some variability in the data. Movies differ by various criteria as movie quality and the extent of change in the shape of the contrast spots over the time. This led us to examine various combinations of the following parameters: the

threshold for noise removal, the allowed step size and its penalty for tracking process. Those parameters were chosen experimentally (see details in the Methods section). The 10th percentile threshold for noise removal and the 0.6 threshold for template correlation were chosen because it allows the detection of almost all (97%) relevant objects at the cost of 3.8% of false positive cases. The maximum allowed step size was selected based on the fastest motion seen in the movies—not larger than 3 pixels over two sequential frames. A side step penalty is applied to penalize large movements. MDP provides an overall optimal continuous path for tracking, less subject to transient loss of correlation and more robust to noise than forward tracking. The side step penalty was carefully selected: if it is too high, it can cause an over-smoothed path and if it is too small, it might not help to improve tracking results.

Detecting the contrast spots inside the plaque using artificial templates exploits the geometrical characteristic and the gray level distribution of the contrast spots. All visually identifiable contrast spots (104 different contrast spots) in 28 plaques were manually marked. Of those, 101 (97%) were also automatically detected. Tracking the intraplaque contrast spots based on manual annotation is a cumbersome and tedious procedure with poor repeatability. To overcome this limitation, we propose a semiautomatic method based on MDP that requires minimal user interaction. In 90 of those 101 detected objects, the automatic tracking determined the contrast motion correctly (89%). We validated the algorithm by using manual and visual interpretations of those cases. The reconstruction of the blood vessels routes was validated by comparing it with a manual tracking of the contrast spots. As shown in the example of Figure 8, in most of the cases, the automatically reconstructed route is smoother than the manual due to the detailed advantages of the MDP method.

The mean and the SD values of the distance between the automatically and the manually reconstructed routes are close to the equivalent values that were calculated between the routes manually marked by the two observers. Therefore, one can conclude that the algorithm results are accurate, within the range that human observers cover. The automatic tracking is a bit smoother than the manual tracking, as is expected because of its smoothness constraint. Moreover, the automated results are objective, since no human interaction is involved. The observers manually selected the brightest location inside the contrast spot, while the algorithm sometimes detected another location inside the object as its representative. A characteristic size of a contrast spot is above 7 pixels and a mean distance threshold of 5 pixels (0.525 mm) was chosen. Therefore, if the mean distance between the manual marking and the automated one was smaller than this threshold, it can be considered as a tracking after different locations inside the same object.

The minor difference between the XY displacement results of manual and automatically found tracks can occur due to the stop term of the algorithm and the manual track-

ing. The algorithm stops tracking when a contrast spot has gray level below 10. However, the manual tracking stops when the observer can no longer distinguish the contrast spot.

Seventy-six of the 90 well tracked contrast spots were correctly classified in comparison to the visual classification (84%). When considering the whole population (104 identified objects), 73% was eventually correctly classified. Twelve objects, which were visually classified as artifacts, were automatically classified as blood vessels due to their large displacements over the time. These displacements were caused because of noisy images or inaccurate motion compensation.

The validation of the automated neovascularisation grading was performed by comparing it with the physicians' grading. The physicians were blind to each other and analyzed all clips related to plaque of each patient. The two physicians had consensus on 68% of the cases. Variability can be caused by taking into account the adventitial vasa vasorum. It can be considered as relevant neovascularization by one observer, while the other one will ignore that. In addition, an artifact may be considered by an observer as a blood vessel due to a significant XY displacement that the second observer will ignore.

Therefore, it is clear that even with well-defined criteria, the visual scores can differ considerably between independent observers. This stresses the need for an objective, automated analysis. The automated score was identical to the physicians' visual scoring in 64% of the cases, one grade difference in 27%, and two grades difference in 9%. Therefore, the automated neovascularisation grading agreed within one grade with visual analysis in 91% of the cases. Obviously, the differences between the automated and the visual scores are very comparable to the differences between two independent observers.

We also compared the results to the maximum intensity projection (MIP) analysis. The XY displacement of the blood vessels reconstructed by the MIP was 130% bigger than the manual analysis of the same parameter. This deviation of the MIP analysis is caused by suboptimal predefined filtering and motion compensation, resulting in overestimated routes. Moreover, because of the absence of temporal behavior of the examined objects, static artifacts are also included in the reconstructed arterial tree. Those MIP inaccuracies can affect the analysis of the blood vessel characteristics and the neovascularization grading.

The proposed algorithm was developed on 2-D echocardiography images. Currently, no high-frame rate 3-D contrast images of carotid arteries are available. Such images would be ideal for analyzing the complete neovasculature in 3-D over the whole plaque, rather than in a single slice. The same analysis method may be applied in 3-D with straightforward extensions.

A limitation of the current study is the fact that there was no strict separation of test and training data. Several of the parameters of the algorithm were determined empiri-

cally from a few sequences in the test set. This article concentrates on the description of the methods and proof of its principles; the reported results are a preliminary estimate of the capabilities of the method. Considerable improvements can still be expected by more elaborate choice of parameters, but given the large variability of the gold standard (visual classification) we consider this very promising. In future work, the algorithm will be evaluated on a larger, independent set of data to establish its overall clinical performance in a blinded way.

CONCLUSIONS

We developed a number of tools for preliminary quantification of neovascularization in carotid plaques. This includes a technique for detection of contrast spots in the plaque, tracking of such spots over time by MDP, classifying them into artifacts and vessels and reconstructing the arterial tree. This study showed that the technique is feasible and valuable in evaluating accurate intraplaque neovascularization grading. The method provides efficient analysis with minimal user interaction and agrees well with manual and visual validations.

REFERENCES

1. Amini AA, Weymouth TE, Jain RC. Using dynamic programming for solving variational problems in vision. *IEEE Trans Pattern Anal Mach Intell.* 1990;12:855-67.
2. Ogata T, Yasaka M, Yamagishi M, Seguchi O, Nagatsuka K, Minematsu K. Atherosclerosis found on carotid ultrasonography is associated with atherosclerosis on coronary intravascular ultrasonography. *J Ultrasound Med.* 2005;24(4):469-74.
3. Gomez CR. Carotid plaque morphology and risk for stroke. *Stroke.* 1990;21(1):148-51.
4. Huang PT, Huang FG, Zou CP, Sun HY, Tian XQ, Yang Y, et al. Contrast-enhanced sonographic characteristics of neovascularization in carotid atherosclerotic plaques. *J Clin Ultrasound.* 2008;36(6):346-51.
5. Barger AC, Beeuwkes R, Lainey LL, Silverman KJ. Hypothesis: vasa vasorum and neovascularization of human coronary arteries. A possible role in the pathophysiology of atherosclerosis. *N Engl J Med.* 1984;310(3):175-7.
6. Libby P, Ridker P, Hansson GK. Progress and challenges in translating the biology of atherosclerosis. *Nature.* 2011;473(7347):317-25.
7. Falk E. Pathogenesis of Atherosclerosis. *J Am Coll Cardiol.* 2006;47(8, Suppl):C7-C12.
8. Sluimer JC, Daemen MJ. Novel concepts in atherogenesis: Angiogenesis and hypoxia in atherosclerosis. *J Pathol.* 2009;218(1):7-29.
9. Sluimer JC, Gasc JM, van Wanroij JL, Kisters N, Groeneweg M, Sollewijn Gelpke MD, et al. Hypoxia, hypoxia-inducible transcription factor, and macrophages in human atherosclerotic plaques are correlated with intraplaque angiogenesis. *J Am Coll Cardiol.* 2008;51(13):1258-65.
10. Hellings WE, Peeters W, Moll FL, Piers SRD, van Setten J, van der Spek PJ, et al. Composition of carotid atherosclerotic plaque is associated with cardiovascular outcome. A prognostic study. *Circulation.* 2010;121(17):1941-50.
11. Nandalur KR, Baskurt E, Hagspiel KD, Phillips CD, Kramer CM. Calcified carotid atherosclerotic plaque is associated less with ischemic symptoms than is noncalcified plaque on MDCT. *AJR Am J Roentgenol.* 2005;184(1):295-8.
12. Barnett HJM, Meldrum H, Eliasziw M. The appropriate use of carotid endarterectomy. *CMAJ.* 2002;166(9):1169-79.
13. Lin E, Alessio A. What are the basic concepts of temporal, contrast, and spatial resolution in cardiac CT? *J Cardiovasc Comput Tomogr.* 2009;3(6):403-8.
14. Parker DL, Wu J, van Bree RE. Three-dimensional vascular reconstruction from projections: a theoretical review. *Engineering in Medicine and Biology Society, 1988 Proceedings of the Annual International Conference of the IEEE.* 1988;1:399-400.
15. Rissanen TT, Korpisalo P, Karvinen H, Liimatainen T, Laidinen S, Gröhn OH, et al. High-resolution ultrasound perfusion imaging of therapeutic angiogenesis. *J Am Coll Cardiol Img.* 2008;1(1):83-91.
16. Molinari F, Liboni W, Pavanelli E, Giustetto P, Badalamenti S, Suri JS. Accurate and automatic carotid plaque characterization in contrast enhanced 2-D ultrasound images. *EMBS 2007 Proceedings of the 29th Annual International Conference of the IEEE.* 2007:335-8.
17. Stein JH, Korcarz CE, Hurst RT, Lonn E, Kendall CB, Mohler ER, et al. Use of carotid ultrasound to identify subclinical vascular disease and evaluate cardiovascular disease risk: A consensus statement from the American Society of Echocardiography carotid intima-media thickness task force endorsed by the Society for Vascular Medicine. *J Am Soc Echocardiogr.* 2008;21(2):93-111.

18. Hsu AR, Chen X. Advances in anatomic, functional, and molecular imaging of angiogenesis. *J Nucl Med.* 2008;49(4):511-4.
19. Willmann JK, Kimura RH, Deshpande N, Lutz AM, Cochran JR, Gambhir SS. Targeted contrast-enhanced ultrasound imaging of tumor angiogenesis with contrast microbubbles conjugated to integrin-binding knottin peptides. *J Nucl Med.* 2010;51(3):433-40.
20. Hoogi A, Adam D, Hoffman A, Kerner H, Reisner S, Gaitini D. Carotid plaque vulnerability: Quantification of neovascularization on contrast-enhanced ultrasound with histopathologic correlation. *AJR Am J Roentgenol.* 2011;196(2):431-6.
21. Giannarelli C, Ibanez B, Cimmino G, Garcia Ruiz JM, Fata F, Bianchini E, et al. Contrast-Enhanced Ultrasound Imaging Detects Intraplaque Neovascularization in an Experimental Model of Atherosclerosis. *J Am Coll Cardiol Img.* 2010;3(12):1256-64.
22. Fleiner M, Kummer M, Mirlacher M, Sauter G, Cathomas G, Krapf R, et al. Arterial neovascularization and inflammation in vulnerable patients: Early and late signs of symptomatic atherosclerosis. *Circulation.* 2004;110(18):2843-50.
23. Giannoni MF, Vicenzini E, Citone M, Ricciardi MC, Irace L, Laurito A, et al. Contrast carotid ultrasound for the detection of unstable plaques with neoangiogenesis: A pilot study. *Eur J Vasc Endovasc Surg.* 2009;37(6):722-7.
24. Coli S, Magnoni M, Sangiorgi G, Marrocco-Trischitta MM, Melisurgo G, Mauriello A, et al. Contrast-enhanced ultrasound imaging of intraplaque neovascularization in carotid arteries: Correlation with histology and plaque echogenicity. *J Am Coll Cardiol.* 2008;52(3):223-30.
25. Shah F, Balan P, Weinberg M, Reddy V, Neems R, Feinstein M, et al. Contrast-enhanced ultrasound imaging of atherosclerotic carotid plaque neovascularization: A new surrogate marker of atherosclerosis? *Vasc Med.* 2007;12(4):291-7.
26. van Ooijen PMA, Ho K, Dorgelo J, Oudkerk M. Coronary artery imaging with multidetector CT: visualization issues. *Radiographics.* 2003;23(6):e16.
27. Suri J, Liu K, Reden L, Laxminarayan S. A review on MR vascular image processing: skeleton versus nonskeleton approaches: part II. *IEEE Trans Inf Technol Biomed.* 2002;6(4):338-50.
28. Anderson CM, Saloner D, Tsuruda JS, Shapeero LG, Lee RE. Artifacts in maximum-intensity-projection display of MR angiograms. *AJR Am J Roentgenol.* 1990;154(3):623-9.
29. ten Kate GL, Renaud GGJ, Akkus Z, van den Oord SCH, ten Cate FJ, Shamdasani V, et al. Far-wall pseudoenhancement during contrast-enhanced ultrasound of the carotid arteries: Clinical description and in vitro reproduction *Ultrasound Med Biol.* 2012;38(4):593-600.
30. Chahal NS, Lim TK, Jain P, Chambers JC, Kooner JS, Senior R. Does subclinical atherosclerosis burden identify the increased risk of cardiovascular disease mortality among United Kingdom Indian Asians? A population study. *Am Heart J.* 2011;162(3):460-6.
31. Akkus Z, Bosch JG, Renaud G, Hoogi A, ten Kate GL, van den Oord S, et al. Motion compensation method for quantification of neovascularization in carotid atherosclerotic plaques with contrast enhanced ultrasound (CEUS). *Proceedings of SPIE Medical Imaging Conference, San Diego, CA, USA.* 2012:8320.
32. Nevo S, van Stralen M, Vossepoel A, Reiber JHC, de Jong N, van der Steen AFW, et al. Automated tracking of the mitral valve annulus motion in apical echocardiographic images using multidimensional dynamic programming. *Ultrasound Med Biol.* 2007;33(9):1389-99.
33. Rabben SI, Torp AH, Støylen A, Slørdahl S, Bjørnstad K, Haugen BO, et al. Semiautomatic contour detection in ultrasound M-mode images. *Ultrasound Med Biol.* 2000;26(2):287-96.
34. Poli R, Valli G. An algorithm for real-time vessel enhancement and detection. *Comput Methods Programs Biomed.* 1997;52(1):1-22.

35. Tozaki T, Kawata Y, Niki N, Ohmatsu H, Moriyama N. 3-D visualization of blood vessels and tumor using thin slice CT images. Nuclear Science Symposium and Medical Imaging Conference, 1994 IEEE Conference Record. 1994;31:1470-4.



PART IV

SUMMARY, DISCUSSION AND PERSPECTIVES





Chapter 10

Summary, Discussion and Perspectives



SUMMARY AND DISCUSSION

Current status of non-invasive imaging of atherosclerosis

The identification of vulnerable plaques, that cause limited stenosis but which composition make it at increased risk of rupture and thrombosis, should improve the prediction of cerebrovascular events. In **Part 1** we review the current knowledge on the use non-invasive imaging for the evaluation of atherosclerosis and identification of vulnerable plaques. **Chapter 2** compares the relative merits of ultrasound, computed tomography (CT) and magnetic resonance imaging (MRI) for the evaluation of atherosclerosis and shows advantages and disadvantages of each technique. MRI provides good soft tissue characterization, but is less available and has relatively long scan times. The ability of MRI to provide good soft tissue characterization makes it an interesting technique for the evaluation of vulnerable plaque components. CT is fast and able to evaluate the coronary arteries, it provides accurate information on calcification and plaque morphology. However, CT lacks in soft tissue characterization, making the evaluation of vulnerable plaque components limited.

Ultrasound provides high resolution, real time images, however has limited penetration depth and images are relatively noisy. The use of conventional ultrasound techniques for the evaluation of vulnerable plaque has thus far provides limited results. Several studies have investigated the addition of contrast enhanced ultrasound (CEUS) to the standard ultrasound evaluation, in order to improve border delineation and the evaluation of intraplaque neovascularization, with promising results in both animal and human studies. In **Chapter 3** we review the current knowledge on the use of CEUS for the identification of the vulnerable plaque, and show that imaging of intraplaque neovascularization may be a good marker of plaque vulnerability.

Contrast enhanced ultrasound for imaging atherosclerosis

In **Part 2** we apply currently available ultrasound techniques in patients. The accuracy of standard ultrasound of the carotid arteries to detect atherosclerotic plaques and plaque morphology is suboptimal. In **Chapter 4** we demonstrate that the addition of CEUS to standard carotid ultrasound results in a significantly increased number of patients found to have subclinical atherosclerosis. Though the use of CEUS significantly increases the number of plaques identified, the plaques present are small and their clinical value is unknown. However, it is known that plaques don't necessarily need to be of large size or cause significant stenosis, to cause symptomatic cardiovascular disease.¹ In contrary vulnerable plaque are thought to cause positive remodeling, maintaining lumen diameter while growing and are at risk of rupture and thrombosis, rather than stenosis. Additionally the atherosclerotic plaques which were only detected with CEUS and not with standard carotid ultrasound were predominantly hypoechoic suggesting a more

vulnerable plaque type.²⁻⁵ Follow-up studies are required to determine the additional predictive value of the absence or presence of subclinical atherosclerosis detected with CEUS.

In **Chapter 5** we show that the improved vessel wall delineation provided by CEUS significantly improves the identification of plaque ulceration. Recent data indicates that carotid plaque ulceration is an important predictor of cerebrovascular events, but standard color Doppler ultrasound (CDUS) is known to have a poor diagnostic accuracy for the detection of carotid plaque ulceration. The addition of CEUS to the examination provided an improved sensitivity and diagnostic accuracy for the assessment of carotid plaque ulceration as compared with CDUS. Accurate detection of plaque ulceration using CEUS could be implemented in clinical practice for the identification of plaques at high risk for causing thrombo-embolic events.

Assessment of these unstable or vulnerable plaques may help to further improve identification of patients who may benefit from carotid surgery. The results demonstrate that CEUS improves vessel wall delineation and concomitantly plaque and ulceration detection. CEUS provides an easily implementable improvement for ultrasound examinations in the absence of ionizing radiation and using safe contrast agents. Further studies are needed to assess whether carotid CEUS might be an effective imaging modality for the selection of patients for more invasive diagnostic procedures or intervention. The challenge for the future will be to develop accurate risk stratification models.

In **Chapter 6** we evaluate the presence of carotid atherosclerosis in with heterozygous familial hypercholesterolemia (FH) and its association with coronary artery disease. Patients with FH were found to have a high prevalence of both carotid and coronary artery disease despite the absence of symptoms. No association was found between the carotid intima-media thickness and coronary artery disease, while there was an association between carotid plaque and coronary artery disease. The absence of carotid plaque excluded the presence of obstructive coronary artery disease, however the presence of carotid plaque and carotid plaque burden are no reliable indicators of obstructive coronary artery disease.

Technical innovations in contrast enhanced ultrasound

In **Part 3** we investigate limitations and new technical development in CEUS. In **Chapter 7** we describe enhancement in close proximity to the far wall, parallel to the main lumen that is present during all CEUS examinations of carotid arteries. We identify this as significant far wall pseudoenhancement created by the currently available CEUS pulse sequences and might be misidentified as contrast enhancement. Currently used techniques for contrast-enhanced ultrasound imaging require linear propagation to detect nonlinear scattering of contrast agent microbubbles. Waveform distortion due to nonlinear propagation impairs their ability to distinguish microbubbles from tissue. As

a result, tissue can be misclassified as contrast agent, and contrast agent concentration can be overestimated. Therefore, these artifacts can significantly impair the quality of medical diagnoses. To corroborate the hypothesis that this is a pseudoenhancement artifact it was recreated in a tissue-mimicking material phantom, using the same ultrasound system, settings and contrast agent as used in the patient study. The phantom study showed that pseudoenhancement may be present during vascular CEUS and that the degree of pseudoenhancement is influenced by the size and concentration of the microbubbles. During vascular CEUS studies, identification of the artifact is important to prevent misinterpretation of enhancement in and near the far wall.

Chapter 8 provides a possible solution for the pseudoenhancement artifact, by utilizing microbubble specific physical properties. We show that the use of counter propagation could create artifact free images. Contrary to biological tissue, the lipid-coated gas microbubbles used as a contrast agent allow the interaction of two acoustic waves propagating in opposite directions (counter-propagation). Using pulse schemes based on that principle we were able to create an in vitro image that is free from nonlinear propagation artifacts (pseudoenhancement). We show that the new pulse sequence can be implemented in a clinically available ultrasound scanner and that it reduces pseudoenhancement in vitro and thus could improve the accuracy for contrast detection.

In **Chapter 9** we propose a semi-automatic algorithm for quantification of intraplaque neovascularization (IPN). IPN is an increasingly studied marker of the vulnerable atherosclerotic plaque. CEUS is an attractive imaging technique for the assessment of IPN. However, visual analysis of IPN may result in substantial intrareader and interreader variability. We show that semi-automated quantification software improves the assessment of carotid IPN by providing objective and reproducible information. We show that our method can successfully quantify features that are linked to vulnerability of the carotid plaque.

PERSPECTIVES

Possible clinical implications

Screening for subclinical atherosclerosis

The implementation of CEUS in clinical practice could provide several improvements over the current diagnostic modalities. First of all CEUS improves the identification of subclinical atherosclerosis by detecting small, early atherosclerotic lesions. This would allow the detection of the disease processes leading to the development of symptomatic cardiovascular disease at an earlier stage, allowing for early intervention. Additionally the association between coronary and carotid atherosclerosis could in the future help

in the selection of patients eligible for computed tomography coronary angiography or invasive coronary angiography. Improved screening and prediction of future cardiovascular disease could allow for earlier and more personalized treatment selection.

Selection of patients for carotid surgery

Secondly the current treatment guidelines for patient after ischemic stroke or transient ischemic attack state that surgical carotid endarterectomy (CEA) is highly beneficial in patients with a >70% stenosis in the ipsilateral carotid artery and is beneficial in patients with a 50-70% stenosis with a low surgical risk or additional risk factors. The addition of CEUS determined plaque vulnerability could improve selection for surgical treatment. Patients with a 50-70% stenosis and overt intraplaque neovascularization of plaque ulceration might be at increased risk of plaque rupture and therefore would benefit from invasive CEA. While reverse patients with a >70% and a stable plaque phenotype might be better off with medical treatment only. Currently the decision for carotid endarterectomy is based on the presence of a significant stenosis and the presence of symptomatic cardiovascular disease. Future studies are needed to evaluate whether this decision might be expanded to include the presence of ulceration and intravascular neovascularization.

Monitoring treatment response

CEUS could be used for the evaluation of treatment effect. Previous studies have suggested that CEUS can identify a reduction in intraplaque after statin treatment.⁶ Currently no randomized controlled trial has been executed investigating this claim. However, animal studies have shown that statin treatment reduces intraplaque neovascularization⁷ and it can be hypothesized that if an accurate non-invasive measurement of intraplaque neovascularization is available this could be used as a measure of treatment response.

Furthermore, the availability of an accurate measurement of treatment response could provide an endpoint for clinical pharmaceutical trials. Carotid intima media thickness (cIMT) is an FDA accepted intermediate endpoint for pharmacological trials. However, cIMT investigates a process possibly more related to mediasclerosis, rather than atherosclerosis. Furthermore, the wide spread use of statin treatment has reduced baseline cIMT levels to a below population average, making further gain unlikely. CEUS detected reduction of intraplaque neovascularization could provide a more pathophysiology based surrogate endpoint in cardiovascular disease.

Limitations of CEUS

Though ultrasound allows for real time imaging at a superior resolution to other techniques, it also presents a number of inherent limitations due to the use of sound waves for imaging. In general, ultrasound images are relatively noisy and are subject to both

patient and transducer movement. This can hinder image evaluation and particularly automated quantification. Furthermore, the penetration depth of ultrasound is dependent on the frequency and amplitude of the ultrasound wave. In which lower frequency ultrasound provided greater penetration depth but reduced resolution. This trade-off between penetration and resolution that may result in reduced image quality especially in patients whose carotid arteries are at large distance from the transducer, for example obese patients. Additionally, ultrasound waves cannot penetrate through calcifications in the plaque. Calcifications cause shadows that hinder the view on structures behind the calcification, limiting the view especially in heavily calcified plaques. These limitations may be partially overcome by new developments such as 3D ultrasound limiting the problem of probe and patient movement, or may be limited such as narrow shadows by small calcifications. However, for instance heavily calcified plaques are very challenging to be evaluated by ultrasound.

Future developments in CEUS

Molecular imaging

Developments in targeted contrast agents present a prospective for molecular CEUS imaging of intraplaque neovascularization. By using molecular imaging one would be able to not only identify the presence of intraplaque neovascularization but also evaluate the angiogenic activity in the plaque. Studies using targeted microbubbles have shown the possibility to identify cellular adhesion molecules and receptors associated with angiogenesis in atherosclerotic animal models.^{8,9} The first human study evaluating vascular endothelial growth factor receptor targeted microbubbles has recently been performed in patients with prostate cancer, showing promising results for identification of active angiogenesis (clinicaltrials.gov; study no: NCT01253213).¹⁰

Drug delivery

CEUS has been investigated as novel technique for therapeutic drug delivery. Microbubbles can be used to deliver encapsulated drugs that are highly toxic (e.g. chemotherapeutics), not soluble (e.g. lipophilic drugs), or need to be delivered intracellular (e.g. RNA, DNA). The encapsulated drug can be released locally at the target location by the application of a high acoustic pressure ultrasound pulse (within limits of the currently available equipment).¹¹ Additionally, the interaction of microbubbles with ultrasound has been shown to increase of the drug uptake *in vitro*.^{12,13} It is thought that oscillation and implosion of microbubbles creates transient micropores in the cellular membrane (sonoporation) and induces endocytosis.¹⁴ Microbubbles have been used effectively as an *in vivo* drug and gene delivery system in animal studies.^{15,16} The availability of CEUS

mediated drug delivery could provide interesting new treatment options directed at individual plaques.

3D Ultrasound

The current commercially available ultrasound systems are equipped with 2D transducers for carotid imaging. The use of 2D data is subject to operator dependency and out of plane probe motion. Several producers of ultrasound equipment are currently developing vascular 3D matrix probes. The implementation of 3D CEUS will allow acquisition of full volume information of carotid lumen and plaque including intraplaque neovascularization. 3D carotid ultrasound will probably also improve inter-observer and intra-observer variability.

REFERENCES

1. Golledge J, Greenhalgh RM, Davies AH. The symptomatic carotid plaque. *Stroke*. 2000;31(3):774-81.
2. Bluth EI, Kay D, Merritt CR, Sullivan M, Farr G, Mills NL, et al. Sonographic characterization of carotid plaque: detection of hemorrhage. *AJR Am J Roentgenol*. 1986;146(5):1061-5.
3. Reilly LM, Lusby RJ, Hughes L, Ferrell LD, Stoney RJ, Ehrenfeld WK. Carotid plaque histology using real-time ultrasonography. Clinical and therapeutic implications. *Am J Surg*. 1983;146(2):188-93.
4. Grønholdt ML, Nordestgaard BG, Bentzon J, Wiebe BM, Zhou J, Falk E, et al. Macrophages are associated with lipid-rich carotid artery plaques, echolucency on B-mode imaging, and elevated plasma lipid levels. *J Vasc Surg*. 2002;35(1):137-45.
5. Droste DW, Karl M, Bohle RM, Kaps M. Comparison of ultrasonic and histopathological features of carotid artery stenosis. *Neurol Res*. 1997;19(4):380-4.
6. Feinstein SB. Contrast ultrasound imaging of the carotid artery vasa vasorum and atherosclerotic plaque neovascularization. *J Am Coll Cardiol*. 2006;48(2):236-43.
7. Wilson SH, Herrmann J, Lerman LO, Holmes DR, Napoli C, Ritman EL, et al. Simvastatin Preserves the Structure of Coronary Adventitial Vasa Vasorum in Experimental Hypercholesterolemia Independent of Lipid Lowering. *Circulation*. 2002;105(4):415-8.
8. Kaufmann BA, Sanders JM, Davis C, Xie A, Aldred P, Sarembock IJ, et al. Molecular imaging of inflammation in atherosclerosis with targeted ultrasound detection of vascular cell adhesion molecule-1. *Circulation*. 2007;116(3):276-84.
9. Decano J, Moran A, Ruiz-Opazo N, Herrera V. Molecular imaging of vasa vasorum neovascularization via DEspR-targeted contrast-enhanced ultrasound micro-imaging in transgenic atherosclerosis rat model. *Mol Imaging Biol*. 2011;13(6):1096-106.
10. Smeenge M, Mischi M, Laguna Pes M, de la Rosette J, Wijkstra H. Novel contrast-enhanced ultrasound imaging in prostate cancer. *World J Urol*. 2011;29(5):581-7.
11. Frinking PJA, Bouakaz A, de Jong N, Ten Cate FJ, Keating S. Effect of ultrasound on the release of micro-encapsulated drugs. *Ultrasonics*. 1998;36(1-5):709-12.
12. van Wamel A, Kooiman K, Hartevelde M, Emmer M, ten Cate FJ, Versluis M, et al. Vibrating microbubbles poking individual cells: Drug transfer into cells via sonoporation. *J Control Release*. 2006;112(2):149-55.
13. Meijering BDM, Juffermans LJM, van Wamel A, Henning RH, Zuhorn IS, Emmer M, et al. Ultrasound and microbubble-targeted delivery of macromolecules is regulated by induction of endocytosis and pore formation. *Circ Res*. 2009;104(5):679-87.
14. Dijkmans PA, Juffermans LJM, Musters RJP, van Wamel A, ten Cate FJ, van Gilst W, et al. Microbubbles and ultrasound: From diagnosis to therapy. *Eur J Echocardiogr*. 2004;5(4):245-6.
15. Kobulnik J, Kuliszewski MA, Stewart DJ, Lindner JR, Leong-Poi H. Comparison of gene delivery techniques for therapeutic angiogenesis: Ultrasound-mediated destruction of carrier microbubbles versus direct intramuscular injection. *J Am Coll Cardiol*. 2009;54(18):1735-42.
16. Suzuki JI, Ogawa M, Takayama K, Taniyama Y, Morishita R, Hirata Y, et al. Ultrasound-microbubble-mediated intercellular adhesion molecule-1 small interfering ribonucleic acid transfection attenuates neointimal formation after arterial injury in mice. *J Am Coll Cardiol*. 2010;55(9):904-13.



Nederlandse Samenvatting



NEDERLANDSE SAMENVATTING

Stand van zaken in beeldvormend onderzoek van atherosclerose

Het detecteren van kwetsbare plaques, die geen significante vernauwing van het bloedvat veroorzaken, maar door hun samenstelling een hoog risico hebben op scheuren en tromboseren, zou de voorspelling van een acuut hart of herseninfarcten kunnen verbeteren. In **Deel 1** behandelen we de huidige kennis op het gebied van niet-invasieve beeldvorming voor het afbeelden van kwetsbare plaques. **Hoofdstuk 2** vergelijkt echo, computed tomography (CT) en magnetic resonance imaging (MRI) voor de evaluatie van hart en vaatziekten en laat zien dat elke techniek zijn voor- en nadelen heeft. MRI heeft een hoog onderscheidend vermogen voor zachte weefsels, welke geassocieerd zijn met plaque kwetsbaarheid. Echter MRI is beperkt beschikbaar en heeft relatief lange scantijden. CT heeft zeer korte scantijden en is de enige techniek momenteel beschikbaar voor het beoordelen van de kransslagaderen rond het hart. CT biedt accurate informatie over de aanwezigheid van plaques, verkalkingen in de plaque en plaque morfologie. Echter CT is slechts beperkt in staat onderscheid te maken tussen verschillende zachte weefsels, waardoor de waarde voor de evaluatie van de kwetsbare plaque beperkt is.

Echo biedt hoge resolutie afbeeldingen in real time, echter de beperkte penetratie diepte en relatief lage signaal-ruisverhouding beperken de kwaliteit van echobeelden. Tot op heden laten studies met echo ook beperkte resultaten zien voor de identificatie van kwetsbare plaques. Enkele studies hebben gekeken naar de toevoeging van contrast echo (CEUS) bij de standaard echo onderzoek, om daarmee een beter onderscheid te maken tussen vaatwand en lumen en te kijken naar vaatnieuwvorming in de plaque. Zowel dier- als humane studies hebben hiermee veel belovende resultaten laten zien. In **Hoofdstuk 3** behandelen we de huidige kennis op het gebied van CEUS voor het identificeren van kwetsbare plaques en laten zien dat aanwezigheid van vaatnieuwvorming in de plaque mogelijk een goede maat is voor plaque kwetsbaarheid.

Contrast echo voor afbeelding van atherosclerose

In **Deel 2** passen we de op dit moment in de kliniek beschikbare echo technieken toe op patiënten. Het is bekend dat de nauwkeurigheid van conventionele echo technieken voor het identificeren van plaques niet optimaal is. In **Hoofdstuk 4** laten we zien dat de toevoeging van CEUS bij standaard echo onderzoek een significante stijging veroorzaakt in het aantal patiënten geïdentificeerd met subklinische plaques in de arteria carotis. De klinische waarde van deze plaques is echter onbekend. De afmeting van de extra gevonden plaques is klein, maar het is bekend dat symptomatische plaques niet noodzakelijk grote plaques zijn, of een significante stenose veroorzaken.¹ Juist van kwetsbare plaques wordt gedacht dat ze bij groeien de vaatwand naar buiten verplaatsen waardoor de lumen diameter behouden blijft. Deze plaques kunnen wel schuren

en trombose veroorzaken, maar veroorzaken geen stenose. In onze studie waren de gevonden plaques bovendien voornamelijk hypoechoisch, wat een meer kwetsbaar plaque type suggereert.²⁻⁵ Follow-up studies zijn nodig om te bepalen wat de toegevoegde waarde is van de aanwezigheid van subklinische plaques waargenomen met CEUS.

In **Hoofdstuk 5** laten we zien dat het gebruik van CEUS het onderscheid tussen vaatwand en lumen verbeterd en daarmee de detectie van plaque ulceraties. Recente data laten zien dat ulceratie van een plaque in de arteria carotis een belangrijke voorspeller is voor herseninfarcten of een transient ischemic attac (TIA). Van standaard echo met kleuren doppler (CDUS) is bekend dat het een matige diagnostische waarde heeft in het detecteren van plaque ulceraties. De toevoeging van CEUS verbeterde de sensitiviteit en nauwkeurigheid waarmee ulceraties werden waargenomen. Nauwkeurige waarneming van ulceraties zou in de kliniek kunnen worden toegevoegd om de voorspelling van hoog risico plaques te verbeteren.

Detectie van kwetsbare plaques in de arteria carotis helpt mogelijk om te voorspellen welke patiënten baat hebben bij carotis chirurgie. De resultaten laten zien dat met CEUS het onderscheid vaatwand-lumen verbeterd, en daarmee de detectie van plaques en plaque ulceraties. CEUS is eenvoudig te implementeren in de huidige echo onderzoeken en gebruikt een relatief veilig contrastmiddel en geen ioniserende röntgen stralen. Verdere studies zijn nodig om te bepalen of CEUS een effectieve modaliteit is voor de selectie van patiënten voor invasieve interventies of diagnostiek. De uitdaging is om op basis van beeldvorming een nauwkeurig risico stratificatie model te vormen.

In **Hoofdstuk 6** evalueren we de aanwezigheid van atherosclerose in de arteria carotis van patiënten met heterozygote familiale hypercholesterolemie (FH) en de associatie met coronair lijden in deze patiënten. We vonden dat patiënten met FH een hoge prevalentie hebben van zowel carotis als coronair ziekten, ondanks de afwezigheid van symptomen. Echter er was geen associatie tussen de carotis intima-media dikte en coronair ziekte. Wel was er een associatie was tussen plaque in de carotis en coronair ziekte. De afwezigheid van plaque in de carotis excludeerde de aanwezigheid van obstructieve plaque in de coronairen. Echter de aanwezigheid van plaque in de carotis en de hoeveelheid plaque in de carotis waren geen betrouwbare maten voor obstructief coronair lijden.

Technische ontwikkelingen in contrast echo

In **Deel 3** onderzoeken we de beperkingen en laatste technische ontwikkelingen in CEUS. In **Hoofdstuk 7** beschrijven we contrast aankleuring parallel aan het lumen welke aanwezig is bij alle patiënten die CEUS onderzoek van de arteria carotis ondergingen. We identificeren dit als pseudoenhancement welke gecreëerd wordt door alle pulse sequenties die op dit moment gebruikt worden in klinisch beschikbare echo apparaten en verward kan worden met echte contrast aankleuring. Voor CEUS gebruiken huidige

echo apparaten puls sequenties waarbij het noodzakelijk is dat de voortgeleiding van de geluidsgolf lineair is, om de non-lineaire verstrooiing van de echo golf door contrastmiddel te detecteren. Vervorming van de golf door non-lineaire voortgeleiding verstoort de mogelijkheid om contrast van weefsel te onderscheiden. Dit resulteert in weefsel dat aankleurt als contrastmiddel in de afwezigheid van contrastmiddel. Tevens kan de concentratie van contrastmiddel in het lumen overschat worden. Deze pseudoenhancement artefacten kunnen de beoordeling van een CEUS onderzoek aanzienlijk beïnvloeden. Om te onderbouwen dat dit pseudoenhancement is werd het artefact nagemaakt in een fantoom, met het zelfde echo apparaat, instellingen en contrastmiddel. De fantoom studie liet zien dat pseudoenhancement aanwezig kan zijn tijdens CEUS en dat de mate van pseudoenhancement afhankelijk is van de afmeting en concentratie van de echo contrast bubbels. Tijdens CEUS studies is het herkennen van pseudoenhancement belangrijk om verkeerde interpretatie van aankleuring in en bij de vaatwand te voorkomen.

Hoofdstuk 8 biedt een mogelijke oplossing voor het pseudoenhancement artefact eerder besproken, door echo contrast specifieke eigenschappen te benutten. We laten zien dat het gebruik van twee in tegengestelde richting bewegende geluidsgolven (counter propagation) het mogelijk is om afbeeldingen te maken vrij van deze artefacten. In tegenstelling tot humaan weefsel, hebben twee in tegengestelde richting verzonden geluidsgolven invloed op elkaar in de aanwezigheid van echo contrast. Door gebruik te maken van opeenvolgende geluidsgolven zo geprogrammeerd om counter propagation te veroorzaken waren we in staat *in vitro* een beeld te maken vrij van pseudoenhancement. We laten zien dat deze geluidsgolven te implementeren zijn in echo apparatuur welke nu al beschikbaar is voor de kliniek en dat ook met deze apparatuur pseudoenhancement vrije beelden worden verkregen *in vitro*. Daarmee zou de nauwkeurigheid voor het detecteren van contrast verbeterd kunnen worden.

In **Hoofdstuk 9** beschrijven we een semigeautomatiseerd algoritme voor de kwantificatie van vaatnieuwvorming in de plaque (IPN). IPN wordt toenemend bestudeerd als marker voor de kwetsbaarheid van een atherosclerotische plaque. CEUS is een aantrekkelijke techniek voor het beoordelen van IPN, echter visuele analyse resulteert in substantiële intra- en interbeoordelaar variatie. We laten zien dat semigeautomatiseerde kwantificatie software in staat is de beoordeling van IPN te verbeteren door objectieve, reproduceerbare informatie te produceren. Tevens laten we zien dat onze methode in staat is om eigenschappen geassocieerd met de kwetsbaarheid te kwantificeren van een plaque in de arteria carotis.

REFERENTIES

1. Golledge J, Greenhalgh RM, Davies AH. The symptomatic carotid plaque. *Stroke*. 2000;31(3):774-81.
2. Bluth EI, Kay D, Merritt CR, Sullivan M, Farr G, Mills NL, et al. Sonographic characterization of carotid plaque: detection of hemorrhage. *AJR Am J Roentgenol*. 1986;146(5):1061-5.
3. Reilly LM, Lusby RJ, Hughes L, Ferrell LD, Stoney RJ, Ehrenfeld WK. Carotid plaque histology using real-time ultrasonography. Clinical and therapeutic implications. *Am J Surg*. 1983;146(2):188-93.
4. Grønholdt ML, Nordestgaard BG, Bentzon J, Wiebe BM, Zhou J, Falk E, et al. Macrophages are associated with lipid-rich carotid artery plaques, echolucency on B-mode imaging, and elevated plasma lipid levels. *J Vasc Surg*. 2002;35(1):137-45.
5. Droste DW, Karl M, Bohle RM, Kaps M. Comparison of ultrasonic and histopathological features of carotid artery stenosis. *Neurol Res*. 1997;19(4):380-4.



Curriculum Vitae



CURRICULUM VITAE

Gerrit Luit ten Kate werd geboren op 4 juli 1982 te Uithoorn. In 2000 behaalde hij zijn VWO diploma aan het Eerst Christelijk Lyceum te Haarlem. Daarna studeerde Luit Bewegingswetenschappen aan de Rijksuniversiteit Groningen alwaar hij in 2005 zijn doctoraal verkreeg. Aansluitend studeerde hij studie Geneeskunde aan de Universiteit Leiden en behaalde in februari 2009 zijn artsexamen. Vanaf 2009 werkte Luit als arts-onderzoeker aan zijn promotie bij de sector Farmacologie, Vasculaire en Metabole geneeskunde van de afdeling Inwendige Geneeskunde van het Erasmus Medisch Centrum in Rotterdam. Sinds 1 juli 2012 is hij werkzaam als arts-assistent in opleiding tot internist in het IJsselland ziekenhuis, Capelle aan den IJssel (opleiders: Prof.dr. J.L.C.M. van Saase, en dr. H.E. van der Wiel).



Publications and PhD Portfolio



PUBLICATIONS

Akkus Z, Hoogi A, Renaud G, van den Oord SC, **ten Kate GL**, Schinkel AF, Adam D, de Jong N, van der Steen AF, Bosch JG. New Quantification Methods for Carotid Intra-plaque Neovascularization Using Contrast-Enhanced Ultrasound. *Ultrasound Med Biol*. 2013;Epub ahead of print

ten Kate GL, van Dijk AC, van den Oord SC, Hussain B, Verhagen HJ, Sijbrands EJ, van der Steen AF, van der Lugt A, Schinkel AF. Usefulness of contrast-enhanced ultrasound for detection of carotid plaque ulceration in patients with symptomatic carotid atherosclerosis. *Am J Cardiol*. 2013;112(2):292-298

ten Kate GL, ten Kate GJ, van den Oord SC, Dedic A, Dharampal AS, Nieman K, de Feyter PJ, Sijbrands EJ, van der Steen AF, Schinkel AF. Carotid plaque burden as a measure of subclinical coronary artery disease in patients with heterozygous familial hypercholesterolemia. *Am J Cardiol*. 2013;111(9):1305-1310

van den Oord SC, Sijbrands EJ, **ten Kate GL**, van Klaveren D, van Domburg RT, van der Steen AF, Schinkel AF. Carotid intima-media thickness for cardiovascular risk assessment: systematic review and meta-analysis. *Atherosclerosis*. 2013;228(1):1-11.

van den Oord SC, **ten Kate GL**, Sijbrands EJ, van der Steen AF, Schinkel AF. Effect of carotid plaque screening using contrast-enhanced ultrasound on cardiovascular risk stratification. *Am J Cardiol*. 2013;111(5):754-759

ten Kate GL, van den Oord SC, Sijbrands EJ, ten Cate FJ, van der Lugt A, de Jong N, Bosch JG, van der Steen AF, Schinkel AF. Current status and future developments of contrast-enhanced ultrasound of carotid atherosclerosis. *J Vasc Surg*. 2013;57(2):539-546

Hoogi A, Akkus Z, van den Oord SC, **ten Kate GL**, Schinkel AF, Bosch JG, de Jong N, Adam D, van der Steen AF. Quantitative analysis of ultrasound contrast flow behavior in carotid plaque neovasculation. *Ultrasound Med Biol*. 2012;38(12):2072-2083.

Renaud G, Bosch JG, **ten Kate GL**, Shamdasani V, Entreklin R, de Jong N, van der Steen AF. Counter-propagating wave interaction for contrast-enhanced ultrasound imaging. *Phys Med Biol*. 2012;57(21):L9-18.

van den Oord SC, **ten Kate GL**, Akkus Z, Renaud G, Sijbrands EJ, ten Cate FJ, van der Lugt A, Bosch JG, de Jong N, van der Steen AF, Schinkel AF. Assessment of subclinical

atherosclerosis using contrast-enhanced ultrasound. *Eur Heart J Cardiovasc Imaging*. 2013;14(1):56-61

ten Kate GL, Renaud GG, Akkus Z, van den Oord SC, ten Cate FJ, Shamdasani V, Entrekin RR, Sijbrands EJ, de Jong N, Bosch JG, Schinkel AF, van der Steen AF. Far-Wall Pseudoenhancement During Contrast-Enhanced Ultrasound of the Carotid Arteries: Clinical Description and in Vitro Reproduction. *Ultrasound Med Biol*. 2012;38(4):593-600

Carvalho DD, Klein S, Akkus Z, **ten Kate GL**, Schinkel AF, Bosch JG, van der Lugt A, Niesen WJ. Estimating 3D lumen centerlines of carotid arteries in free-hand acquisition ultrasound. *Int J Comput Assist Radiol Surg*. 2012;7(2):207-215

Schinkel AF, Staub D, **ten Kate GL**, van den Oord SC, ten Cate FJ, Sijbrands EJ, Feinstein SB. More on advances in imaging angiogenesis and inflammation in atherosclerosis. *Thromb Haemost*. 2011;105(5):920-921 (Letter)

ten Kate GL, Sijbrands EJ, Staub D, Coll B, ten Cate FJ, Feinstein SB, Schinkel AF. Noninvasive imaging of the vulnerable atherosclerotic plaque. *Curr Probl Cardiol*. 2010;35(11):556-591

ten Kate GL, Sijbrands EJ, Valkema R, ten Cate FJ, Feinstein SB, van der Steen AF, Daemen MJ, Schinkel AF. Molecular imaging of inflammation and intraplaque vasa vasorum: a step forward to identification of vulnerable plaques? *J Nucl Cardiol*. 2010;17(5):897-912

Schinkel AF, Elhendy A, van Domburg RT, Biagini E, Rizzello V, Veltman CE, **ten Kate GL**, Sijbrands EJ, Akkerhuis KM, Geleijnse ML, ten Cate FJ, Simoons ML, Bax JJ, Poldermans D. Prognostic significance of QRS duration in patients with suspected coronary artery disease referred for noninvasive evaluation of myocardial ischemia. *Am J Cardiol*. 2009;104:1490-1493

ten Kate GL, Kleibeuker JH, Nagengast FM, Craanen M, Cats A, Menko FH, Vasen HF. Is surveillance of the small bowel indicated for Lynch syndrome families? *Gut*. 2007(9);56:1198-1201

PHD PORTFOLIO

Carotid Artery Contrast Enhanced Ultrasound

G.L. ten Kate

Erasmus MC Department: Internal medicine
 Research school: Cardiovascular Research School Erasmus University Rotterdam (COEUR)
 PhD Period: April 2009 – June 2012
 Promotors: E.J.G. Sijbrands, A.F.W. van der Steen
 Supervisor: A.F.L. Schinkel

PhD Training

Year

Courses and Lectures (24,7 ECTS)

| | |
|---|-----------|
| MolMed Biomedical research techniques..... | 2009 |
| Geavanceerde beeldvormende technieken voor dokters..... | 2009 |
| The 4th animal imaging workshop by AIME..... | 2010 |
| Workshop Photoshop and Illustrator CS4..... | 2010 |
| AIME translational imaging, from animal to man..... | 2011 |
| English biomedical writing and Communications..... | 2011 |
| Biostatistical methods 1: basic principles..... | 2011 |
| COEUR Courses and research seminars (8,7 ECTS)..... | 2009-2012 |
| Various Lectures (1.3 ECTS)..... | 2009-2011 |

Teaching (1.5 ECTS)

| | |
|-----------------------------------|------------------|
| Junior Med School: Lecturing..... | 2009, 2010, 2011 |
|-----------------------------------|------------------|

Conferences (5,5 ECTS)

| | |
|--|--------------|
| Diabetes platform, Rotterdam..... | 2009 |
| Wetenschapsdagen Interne geneeskunde, Antwerpen..... | 2010, 2011* |
| European symposium on ultrasound contrast imaging, Rotterdam..... | 2010, 2011 |
| The Annual Advances in Contrast Ultrasound, Chicago..... | 2010, 2011** |
| Nederlandse vereniging tegen de kwakzalverij jaarcongres, Amsterdam..... | 2011 |

*Poster presentation ** Oral presentation



Dankwoord



DANKWOORD

Tot slot wil ik hierbij de vele mensen bedanken die direct of indirect hebben bijgedragen aan het tot stand komen van dit proefschrift.

Allereerst mijn promotoren Prof.dr. E.J.G. Sijbrands en Prof.dr.ir. A.F.W. van der Steen. Beste Eric, dank voor de mogelijkheden die je me geboden hebt en je altijd positieve houding, welke ongetwijfeld heeft bijgedragen aan dat ik hier vandaag sta. Ton, pas in de laatste fase werd duidelijk dat ook jij mijn promotor zou zijn, maar zonder jouw steun was het nooit afgekomen. Bedankt voor je begeleiding en adviezen.

Mijn copromotor Arend Schinkel, dank voor de begeleiding die je over de jaren gegeven hebt en de stimulans voor de laatste push.

De leden van de leescommissie, Prof.dr. P.J. de Feyter, Prof.dr. A. van der Lugt en Prof.dr. M.J.A.P. Daemen, wil ik bedanken voor hun inspanningen en natuurlijk hun positieve beoordeling van dit proefschrift.

De overige commissieleden, Prof.dr.ir. N. de Jong, Dr. F.J. ten Cate en Prof.dr. D.W.J. Dippeel, wil ik bedanken voor hun aanwezigheid bij mijn verdediging en hun bereidheid met mij van gedachten te wisselen over dit proefschrift.

Dan kom ik bij mijn paranimfen, Nils van der Lubbe en Stijn van den Oord, hartelijk dank dat jullie naast mij willen staan vandaag. Nelis, vele jaren heb je aangehoord als ik het weer eens ergens niet mee eens. Elke keer was jij daarbij de stem van redelijkheid die mij behoede voor misstappen. Nog altijd mis ik het drankje aan het einde van de dag om wat frustraties te uiten. Veel succes met opleiding en hoop dat we ook snel jouw promotie kunnen vieren. Beste Stijn, we waren met zijn tweeën bij de "Vasa Study". Zodoende hebben we intensief samengewerkt. Dat was niet altijd gemakkelijk, maar altijd zijn we er weer goed uit gekomen. Ik hoop snel ook op jouw promotie en opleiding tot cardioloog te kunnen drinken.

Uiteraard wil ik alle collega's van de verschillende afdelingen waarmee ik de afgelopen jaren heb samengewerkt bedanken.

My colleagues from the Department of Biomedical Engineering Zeynettin, Hans, Guillaume, Varya, Assaf and the Bio-imaging Group, Stefan, Arna and Diego. Thank you all for the technical knowhow you have provided. I hope my clinical insights were equally helpful in your projects. True translational medicine remains difficult since the gap between

what the clinician wants and what technician is able to provide is mainly determined by the amount of time available, and time is the one thing always in short supply.

Anouk van Dijk, Kim van Gaalen en Heleen van Beusekom bedankt voor jullie hulp bij de inclusie van de CVA patiënten en de verwerking van de carotis endarterectomiën. Het materiaal is verzameld, helaas zal ik de uitkomsten er van niet van dichtbij mee maken.

Gert Jan ten Kate bedankt voor de hulp met de data van de CT-Coronairen. Veel mail heb ik voor je mogen ontvangen.

To all coauthors of the papers used in this thesis which have not been named thus far, I want to thank you for your help, support and critical comments.

Ook zijn er natuurlijk mensen te bedanken die niet in directe zin hebben bijgedragen aan het tot stand komen van dit proefschrift, maar die wel het dagelijks werk wel lichter maakte. Ook zonder jullie was dit boekje er nooit gekomen.

De Bd-289: Sjaam, Thijs, Bassie, mr. Sardonis en natuurlijk Jos Geelhoed, de domotica was niet best, maar de sfeer des te beter. Van Euthanasieman tot de Haanmevrouw, ze zijn niet snel te vergeten. Helaas is de Bd-289 nu ontmanteld en zijn we gedwongen samen te komen op locaties zonder TL verlichting en het continue achtergrondkoor van vier -80 vriezers. Ik wens jullie succes met je verdere opleiding en hoop jullie in de toekomst nog vaak te zien.

De Bd-zuipkeet: Anton, Akis, Arthur, Frank, Hisko, Koen, Lodi, Luuk, Manne, Matej, Marcel, Pieter, Joep, Eric, en soms ook Els. Vele avonden (en middagen) hebben we doorgebracht in de Zuipkeet, Boudewijn, Ballentent of zoals vanavond in Locus Publicus. Vele smaken bier en whisky zijn er langs gekomen, maar helaas komt de dan toch de tijd voor ieder om verder te trekken. Het goede hieraan is dat er nieuwe plekken op de wereld bijkomen voor een Zuipkeet op locatie.

Matej, we'll see each other again in Prague for the inaugural party of The Baudelaire Institute of Applied Narcotics. You showed me that there are more stereotypes about East-Europeans than I could have ever thought of.

En aan alle fietsende promovendi, het voorjaar komt er weer aan, de fiets kan weer uit de stalling!

Tot slot mijn ouders, die mij altijd onvoorwaardelijk gesteund hebben.

